Circulating Tumor Cell Chip in Breast Cancer for Theragnosis based on Surface-Enhanced Raman Spectroscopy

2014년

서강대학교 대학원
바이오융합기술협동과정
Md. Khaled Hossain

Circulating Tumor Cell Chip in Breast Cancer for Theragnosis based on Surface-Enhanced Raman Spectroscopy

2014년

서강대학교 대학원
바이오융합기술협동과정
Md. Khaled Hossain

Circulating Tumor Cell Chip in Breast Cancer for Theragnosis based on Surface-Enhanced Raman Spectroscopy

지도교수 최 정 우

이 논문을 공학박사 학위논문으로 제출함

2014년 12월 4일

서강대학교 대학원

바이오융합기술협동과정

Md. Khaled Hossain

논 문 인 준 서

Md. Khaled Hossain 의 공학박사 학위논문을 인준함

2014 년 12 월 4 일

주심　신　관　우

부심　최　정　우

부심　김　현　철

부심　김　영　기

부심　정　건　영

Acknowledgements

All the praises are due to Almighty Allah, who empowers me to complete the thesis.

I would like to express my deepest gratitude, indebtedness, profound regards and sincere appreciation to my thesis advisor, Professor Jeong-Woo Choi, for his guidance and assistance he has provided me throughout this work. Without his guidance and support, this work has not been possible. Also sincere thanks to Prof. Byung-Keun Oh for his constant help and appreciation in the entire work. Constructive suggestions and valuable advices on the research by the defense committee members are gratefully acknowledged.

I would like to thank my lab manager (Mr. Si-Youl Yoo, Mr. Hyeon-Yeol Cho, and Mr. Jinho Yoon) and team leader (Dr.Tae-Hyung Kim, Mr. Hyeon-Yeol Cho) for their help in several circumstances throughout the study period. I am also grateful to all members of the Nanobioelectronics lab (Dr. Jin-Hoo Lee, Dr. Taek Lee, Dr. Yong-Ho Chung, Mr. Woon-Jun Lee, Mrs. Chen Qi, Mrs. Sun-Kyung Kim, Mr. Sang-Uk Kim, Mr. Kyeong-Jun Kim, Mr. Young Sik Kim, Mr. Sang-Yul Lee, Mr. Mohsen Mohammandniaei, Mrs. Hye-Jun Shin Mr. Stanislav Kang, and former Eun-Jae Chae, Se Mi Kang, Jee Hyun Choi, Eun-Bi Koo, and Nanobiotech lab for their helpful work, suggestions and support. I would like to especially thank to Mr. Hyeon-Yeol Cho for his constant help and support. I would like to thank all the members of human network on a chip group for their kind cooperation and help. I would like express my deepest sense of regards to Dr. Ji-Young Lee and other members in the

i

This dissertation is dedicated

To My Parents

And

To My Family

Contents

vii

viii

4. Detection of miR200c Expression in Breast Cancer Cells and Breast SCCs based on surface-enhanced Raman Spectroscopy 131

ABSTRACT OF THE DISSERTATION

Circulating Tumor Cell Chip in Breast Cancer for Theragnosis based on Surface-Enhanced Raman Spectroscopy

Dissertation Director: Professor Jeong-Woo Choi

Circulating tumor cells (CTCs) are emerging biomarkers, especially in case of liquid biopsy, and important indicator for prognosis monitoring in case of personalized anticancer therapy. CTC analysis is a promising diagnostic method for estimating the risk of metastatic relapse and metastatic progression in patient with cancer. The basic problem of CTC study is their extremely low inherent numbers in blood (around one CTC per 10^9 non cancerous hematopoietic cells). Hence, before detection or characterization of CTCs their isolation is important. A subpopulation of CTCs with stem-like behavior are known as stem-like circulating tumor cells (SCTCs). In recent years stem like cancer cells (SCCs) hypothesis has attracted great attention in the field of cancer biology. According to the concept, a minor

1

List of Figures

4

5

7

8

hybrid nanoparticles (MiNPs). (b) Cellular uptaking and formation of nanocluster inside cells.

9

(B-HNPs) and cellular uptaking

10

11

List of Tables

12

Chapter 1

Introduction

1.1.   Cell Chip: A promising tool for *in vitro* analysis

Since the cells are the basic units of any type of living organisms, therefore, it is possible to study some biological phenomena *in vitro* condition using cell chip. Therefore, nowadays cell based chip has become an important tool for *in vitro* analysis. Cell based chip (Figure 1.1) can be applied in many fields, such as drug screening, toxicity assessment, biomedicine etc.

Figure 1.1. A cell chip showing cells immobilized on the glass substrate.

13

1.2. Microfluidic Chip

Microfluidic chips are the devices used in microfluidics in which a micro-channels network has been molded or patterned. Due to various numbers of inlet and outlet ports these microfluidic instruments allow fluids to pass through different channels of different diameter. Microfluidics devices have many advantages, as they can decrease sample and reagent consumption and increase automation, thus minimizing the analysis time. Such devices allow applications in many areas such as medicine, biology, chemistry and physics.

1.3. Circulating Tumor Cells

Circuating tumor cells (CTCs) are cells those enter into the blood vessels from a primary tumor and circluate in the blood stream (Figure 1.1) [1.1]. Tumor cell dissemination through blood circulation is crucial step in tumor progression, and most of the breast cancer-related death caused by blood derived metastases [1.2]. CTCs are emerging biomarkers, especially in case of liquid biopsy, and important indicator for prognosis monitoring in case of personalized anticancer therapy [1.3]. Circulating tumor cell analysis is a promising diagnostic method for estimating the risk of metastatic relapse and

14
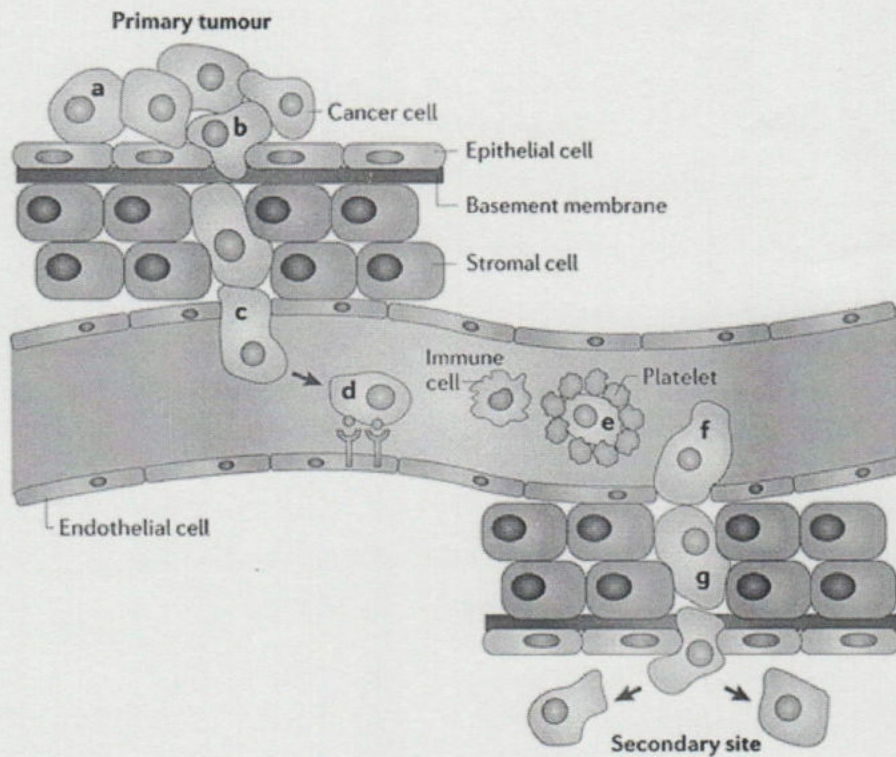
Figure 1.2. Metastasis model showing spreading of tumor cell

metastatic progression in patient with cancer [1.4]. Based on their origin molecular properties of CTCs are different. Molecular characterization of CTCs offers an excellent way for better understanding the biology of metastasis and resistance to established therapies, and novel therapeutic targets may be explored by elucidating the relationship of CTCs to stem-like

15

cancer cells (SCCs) [1.5]. Furthermore, subpopulation of CTCs from same origin also differs in their expression level. The basic problem of CTC study is their extremely low inherent numbers in blood (around one CTC per 10^9 non cancerous hematopoietic cells) [1.6]. Hence, before detection or characterization of CTCs their isolation is important. A sufficient number of studies were conducted previously for capturing and characterization of CTCs and most of the detection techniques were based on fluorescence microscopy [1.7-9]. But the use of fluoirescent dyes has some limitations including photobleaching effect, low number of available fluorescent dyes, and overlapping of fluorescent spectral band during addressing multiple cell surface receptors [1.10].

Raman spectroscopy is a powerful and versatile analytical technique that presents a rapid and non-destructive alternative that could be applied in various research fields including the analysis of living cell biology systems [1.11]. But the basic problem of this technique is its lower spectral intensity. The surface-enhanced Raman scattering (SERS) technique has shown an excellent way for overcoming the low sensitivity problem inherent in conventional Raman spectroscopy. SERS nanotags have several advantages; such as resistance to photobleaching, narrow spectral bands, high spectral

16

specificity, increased intensity, and multiplexing capability [1.12]. In chapter 2 we will describe multiplex Raman hybrid nanoparticles (R-HNPs) for increased isolation efficiency and in situ characterization of the CTCs using surface-enhanced Raman scattering (SERS).

1.4.   Stem-Like Circulating Tumor Cells

Stem-like circulating tumor cells (SCTCs) are a subpopulation of CTCs shares certain properties similar to normal stem cells. In recent years Stem like cancer cells (SCCs) hypothesis has attracted great attention the field of cancer biology [1.13]. According to the concept, tumor consists of a minor component of tumorigenic cells, and a major component of non-tumorigenic cells. The minor population, termed SCCs or tumor initiating cells (TICs), is able to self renew, and generate differentiated progenies to organige a hierarchial cell system in asimilar fashion to normal stem cells. Due to their stemness, the SCCs lead to the generation of more SCCs and ability to differentiate a varirty of cells that are found in malignancy [1.14]. Additionally, there is increasing evidence that SCCs pose a threat in the form of invasion that is resistant to current chemotherapy or radiotherapy. Furthermore, they could play a crucial role in distant metstasis [1.15]. To increase the therapeutic efficacy targeting of SCCs are important. Hence, it is

17

important to characterize the SCCs and distinguish them from tumor cells or CTCs. In chapter 3 we will describe the method of detection, characterization and distinguishing breast SCTCs from breast CTCs based on their surface marker expression level using SERS.

In chapter 4 we will describe the detection of expression of intracellular marker (microRNA) using SERS. MicroRNAs (miRNAs) are endogenous, non-coding RNAs of approximately 22 nucleotides that target various genes either by degrading the mRNA or by repressing the translation [1.16]. Moreover, miRNAs are found to be dysregulated in many cancers, such as breast, prostate, colon and lung [1.17]. Therefore, microRNAs can work as onco-miRNAs or tumor suppressor miRNAs depending on their respective target genes. MicroRNAs are able to modulate the sensitivity of cancer cells to chemotherapeutic drugs and therefore, contribute to the acquisition of chemoresistance [1.18]. miRNAs can regulate epithelial to mesenchymal transition (EMT) by targeting the transcriptional E-Cadherin repressor Zeb1 nad Zeb2. Thus, high level of miRNA determines an epithelial phenotype of cancer cells which is defined by an elevated E-Cadherin expression with low migratory capacity [1.19]. On the other hand, loss of miR-200c may change the tumor cells to mesenchymal-like and chemoresistant phenotype.

18

Therefore, through measuring miRNA expression it is possible to charactertize and distinguishes the epithelial or mesenchymal type of cancer cells, as well as to distinguish chemosensitive or chemoresistant phenotype.In chapter 4 we will introduce new hybrid nanoparticles for distinguishing cancer cell based on miRNA expression.

Cancer causes upto 15% (~ 8 million) of the total death worldwide [1.20]. But, through proper diagnosis and effective treatment it is possible to reduce the cancer related death. For effective chemotherapy therapy targeted drug delivery is important. A lot of nanocarriers have been developed for efficient delivery of therapeutic agents. Nanoparticle based drug delivery has several advantages, particularly at the systemic level including longer circulation half-lives, improved pharmacokinetics and reduced side effects. But the challenges are; preparation of functionalized stable nanoparticles, payload capability, targeted delivery, uptake efficiency by the targeted cells, efficient drug release, as well as prevention of drug efflux. In chapter 5 we will describe a new biohybrid nanoparticle in combination with gold nanoparticle (AuNP), cell penetrating peptide (CPP), polyethylene glycol (PEG), marker specific antibody, and doxorubicin as anticancer agent, which is excellent targeted delivery and increased uptaking of anticancer drugs.

19

1.5. Limitations of Fluorescence Microscopy

The numbers of available fluorescenct dyes are very few, they have photobleaching effect, and they can produce some sorts of cytotoxicity. Furthermore, due to wide spectral range fluorescent spectral bands overlap, when different fluorophores are employed to address multiple cell surface receptor types.

1.6. Raman spectroscopy

Raman spectroscopy is a powerful and versatile analytical technique that presents a rapid and non-destructive alternative that could be applied in various research fields such as, the chemicals and materials analysis field, studying mixture or pure substances, identifying compositions and characterizing chemical structures, as well as for the analysis of living cell biology systems.

1.6.1. Principles of Raman Spectroscopy

Raman spectroscopy was first discovered in 1928, where it was described as the "molecular diffraction of light". The physical concept for the "Raman effect" is the inelastic scattering of a photon. Light that is incident upon a molecule can be reflected, transmitted, absorbed, or scattered. Transmission occurs when the incident light does not interact with the molecule, and passes straight through it. If the energy of a photon of an incident light matches the energy gap between the ground state of a molecule and an electronically excited state, then absorption occurs. Scattering takes place when oscillating and magnetic fields of the incident light cause oscillations of electron distribution within the molecule, that in tern re-emit light in a random direction.

1.6.2.   Limitations of Raman Spectroscopy

It has been stated that, a typical Raman sample can produce one Raman scattered photon from 10^6 to 10^{10} incident photons. Intense sources of light and efficient collection of Raman photons are required for detection of adequate number of Raman photons. The signal to noise ratio increases with the square root of the number of Raman photons to be detected. Due to weak Raman signal intensity the biomedical applications of Raman spectroscopy become limited.

1.7.   Surface-enhanced Raman Scattering (SERS)

Surface-enhanced Raman spectroscopy was first observed in 1974 on pyridines absorbed on Ag electrode roughened by oxidation-reduction cycles. But they attribute the signal enhancement to the big surface area of the electrode. In 1977, it was first reported that the intensity of Raman scattering for a molecule may be dramatically increased when the molecule is placed in very close proximity to colloidal metal nanoparticles or roughened macroscale metal objects with surface variation of 10 to 100 nm scale. Jeanmaire and Van duyne recognized that the large intensity is due to the electromagnetic field effect, while Albrecht and Creighton proposed a charge-transfer effect (chemical enhancement). At present, the enhancement factor in SERS can be as high as 10^9 to 10^{14}, which allows the technique to be sensitive enough to detect single molecule. In these conditions, Raman scattering can exceed the sensitivity of fluorescence, and it has generated great interest in the nanomaterials, spectroscopy and analytical chemistry community.

1.7.1. Principles of Surfcae-enhanced Raman Spectroscopy

SERS is a phenomenon that associated with the enhancement of the electromagnetic field surrounding small metal (or other) objects optically excited near an intense and sharp, dipolar resonance such as a surface-plasmon polarition. In SERS, the target molecule is brought into close proximity to a metallic (typically Ag, Au or Cu) surface with nanoscopically defined features or in solution next to a nanoparticle with a diameter much smaller than the wavelength of the excitation light. When light is incident on the surface or particle, a surface plasmon mode is excited which locally enhances the electromagnetic energy in the vicinity of the target molecule, significantly enhancing the intensity of the inelastically scattered light. The total enhancement to the Raman signal observed in response to this effect (which can be as high as 10^{14} times than that of the unenhanced signal) is commonly attributed to two effects: chemical and electromagnetic.

1.7.2. Mechanism of Surface Enhancement

The exact mechanism of surface enhancement is not clear yet. However, electromagnetic enhancement (EM) and chemical enhancement (CE)

reported in the literature are two widely accepted mechanisms contributing to the SERS effect in ecent years.

1.7.2.1. Electromagnetic Enhancement

The electromagnetic (EM) mechanism has been reported to play a major role of most of the observed features of SERS. The electromagnetic (EM) enhancement occur at the surface of the metallic structures as a consequence of the interaction between laser radiation and electrons on the metal surface for activation of surface plasmons or collective oscillations of conduction band electrons resulting in a larger number of scattered photons. Monochromatic light that is resonant with surface plasmon can induces intense elastic light scattering. The scattered light is characterized by electromagnetic field intensity that is extremely strong at certain portion of space near the metal nanostructure's surface. A molecule present in that space is excited by an enhanced field and produces more intense Raman csattered light than molecules outside the space. The small size of the particles allows the excitation of the metal particle's surface plasmon to be localized. The resultant electromagnetic energy density on the particle is the source of the EM enhancement, the primary contributor to SERS. The size

and shape of the nanostructures change the electric field density on their surface, which in tern change the oscillation frequency of the electrons.

1.7.2.2. Chemical Enhancement

The chemical enhancement (CE) mechanism is much less well understood, but is often attributed to a charge transfer intermediate state which takes place at the strong electron coupling between the analyte and the metal surface. For this reason, CE is also known as charge transfer mechanism. SERS enhancement depends substantially on the chemical structure of the adsorbate, which cannot be accounted by EM mechanism.Basically the chemical enhancement results when molecules chemisorbed directly on the roughened surface, forming an adsorbate metal complex.

1.7.3.   Advantages of SERS Method

SERS phenomenon offers an exciting opportunity to overcome the critical disadvantages of the normal Raman spectroscopy. Therefore, relatively lower laser intensity, longer wavelengths, and rapid signal acquisition time will be possible with SERS. For this reasons, NIR SERS is becoming a useful tool for biological applications.

25

The main analytical advantages of SERS in comparison with other optical detection methods is the inherent molecular specificity which can be obtained, the relatively large sensitivity, and the sharpness of the spectral signals, which can be as little as one nanometer full width at half maximum. This latter advantage is to be compared to conventional fluorescent labels which average about 75 nm or quantum dots which average about 30 nm. The relative sharpness of the spectral SERS signal can facilitate multiplexing since multi-label readouts can be carried out at single excitation wavelength without being limited by spectral overlap.

1.8. Objectives of this Study

1.8.1. *In situ* Characterization of Breast CTCs using Surface-Enhanced Raman Scattering (SERS) method.

Characterization of CTC is important for prognosis monitoring in case of personalized anticancer therapy. In this study we prepared multifunctional conjugated Ranman Hybrid nanoparticles for efficient capturing and insitu characterization of breast CTCs using SERS technique in order to overcome the limitations of fluorescence microscopy.

Distinguishing different subtypes of breast CTCs based on surface marker expression analysis using SERS

Distinguishing breast SCTCs from breast CTCs based on surface marker expression analysis using SERS

Detection of intracellular biomarker (microRNA) in breast CTCs and SCTCs using SERS

Targeted delivery of anticancer drug and *in situ* drug release monitoring

Figure 1.3.   Flow diagram showing objectives of this study.

1.8.2.   Distinguishing Breast CTCs from Breast SCTCs using SERS

SCTCs may be responsible for resistance to chemotherapy and radiation therapy, as well as they are responsible for recurrence of cancer and distant metastasis.For cancer eradication targeting of SCCs is very important. In this study we orepared multifunctional conjugated Ranman Hybrid nanoparticles

for distinguishing breast SCTCs from breast CTCs using SERS technique in order to overcome the limitations of fluorescence microscopy.

1.8.3. Detection of miR200c Expression in Breast Cancer Cells and Breast SCCs using SERS

For effective chemotherapy it is important to know the sensitivity before selecting a drug. In this study we characterize chemosensitive or chemoresistant cancer cells based on their miRNA expression using SERS. A hybrid nanoparticle was synthesized in combination with AuNP, Raman reporter (4-MBA) and complementary half miRNA. This particle can effectively detect the miRNA expression through SERS.

1.8.4. Targeted Chemotherapy

For efficient chemotherapy targeted drug delivery is important. to keep the healthy cells unaffected. In this study we prepared a biohybrid nanoparticle conjugated with AuNPs, doxorubicin, cell penetrating peptides, PEG and antibody that can efficiently target the cancer cells and cause cellular cytotoxicity.

1.9. References

[1.1]   Schroeder, A., Heller, D., A., Winslow, M., M., Dahlman, J., E.,
        Pratt, G., W., Langer, R., Jacks, T. & Anderson, D., G. (2012).
        Treating metastatic cancer with nanotechnology. *Nature Reviews
        Cancer, 2,* 39-50.

[1.2]   Morrison, B. J., Schmidt, C. W., Lakhani, S., R., & Renold, B.,
        A. (2008). Breast cancer stem cells: implication for therapy of
        breast cancer. *Breast Cancer Research*, doi:10.1186/bcr2111.

[1.3]   Gerges, N., Rak, J., Jobado N. (2010). New technologies for the
        detection of circulating tumor cells. *British Medical Bulletins, 94,*
        49-64.

[1.4]   Lin, H., Balik, M., Zheng, H., Datar, Ram & Cote, R., J. (2011).
        Disseminated and circulating tumor cells: Role in effective cancer
        management. *Clinical Reviews in Oncology/Hematology. 77,* 1-
        11.

[1.5]   Toloudi, M., Apostolu, P., Chatziioannou, M., & Papasotiriou,
        (2011). Corelation between cancer stem cells and circulating
        tumor cells and their value. *Case Reports in Oncology, 4,* 44-54.
29

[1.6] Pantel, K., & Alix-Panabieres,C. (2010). Circulating tumor cells in cancer patients: challenges and perspectives. *Trends in Molecular Medicine, 16*, 398-406.

[1.7] Lee, H. J., Oh, J. H. Oh, J. M., Park, J.-M, Lee, J.-G, Kim, M. S., Kim, Y. J., Kang, H. J., Jeong, J., Kim, S. I., Lee, S. S., Choi, J. W. & Huh, N. (2013). Efficient isolation and accurate in situ analysis of Circulating tumor cells using Detachable beads and a high –pore- density filter. *Angewandte Chemie, International Edition 52*, 8337-8340.

[1.8] Lee, H. J., Cho, H.-Y., Oh, J. H., Namkoong, K., Lee, J.-G, Park, J., M., Lee, S. S., Nam, H. & Choi J., W. (2013). Simultaneous capture and *in situ* analysis of circulating tumor cells using multiple hybrid nanoparticles. *Biosensors and Bioelectronics 47*, 508-5 14.

[1.9] He, W., Kularatne, S. A., Kalli, K., R., Prendergast, F., G., Amato, R., J., Klee, G. G., Hartmann L., C., & Low P., S. (2008). Quantification of circulating tumor cells in blood samples from ovarian and prostate cancer patients using tumor specific fluorescene ligands. *International Journal of Cancer. 123*, 1968-
30

[1.15] Gangopadhyay, S., Nandy, A., Hor, P. & Mukhopadhyay, A. (2013). Breast cancer stem cells: A novel therapeutic target. *Clinical Breast Cancer. 13,* 7–15.

[1.16] Engels, B. M. & Hutvagner, G. (2006). Principles and effect of microRNA-mediated post-transcriptional gene regulation. *Oncogene. 25,* 6163-6169.

[1.17] Kopp, F., Oak, P. S., Wagner, E. & Roidl, A. (2012). miR-200c sensitizes breast cancer cells to doxorubicin treatment by decreasing TrkB and Bmi1 expression. *PLOS ONE. 7,* e50469.

[1.18] Kutanzi, K. R., Yurchenko O. V., Beland, F. A., Checkhun, V. F. & Pogribny, I. P. (2011). MicroRNA mediated drug resistance in breast cancer. *Clinical Epigenetics. 2,* 171-185.

[1.19] Hurteau, G. J., Carlson, J, A., Roos, E & Brock, G. J. (2009). Stable expression of miR-200c alone is sufficient to regulate TCF8 (ZEB1) and restore E-cadherin expression. *Cell Cycle. 8,* 2064-2069.

[1.20] Kumeria, T., Kurkuri, M. D., Diener, K. R., Parkinson, L. & Losic, D (2012). Label-free reflectrometric interference

32

microchip biosensor based on nanoporous alumina for detection of circulating tumor cells. *Biosensors and Bioelectronics.* 35, 167-173.

Chapter 2

In-situ Characterization of Circulating Tumor Cells using Hybrid Nanoparticles based on Surface-enhanced Raman Spectroscopy

2.1. Introduction

Cancer accounts for up to 15% (~ 8 million) of the total deaths worldwide [2.1], most as a result of metastatic disease. In case of cancer metastasis tumour cells spread to other organs from the primary organ through blood or lymph. This type of tumour cells is known as circulating tumour cells. Therefore, the metastatic cancer can be diagnosed through the detection of CTCs in the peripheral blood. Early detection and characterization of CTCs has great clinical importance, especially in terms of cancer prognosis and personalization of anti- cancer therapy [2.2-3].

Characterization of CTCs using biomarkers has provided pharmacodynamic information for targeted cancer therapy. Among the mechanisms of

monoclonal antibody-based therapies, antigen-dependent cellular cytotoxicity (ADCC) is one of the important methods [2.4]. For applying ADCC for the treatment of cancer patients, sub-typing of cancer cells is essential. In the last few years, many techniques are used for the detection, enumeration and isolation of CTCs including graphene oxide nanosheet [2.5], photoacoustic detection [2.6], microchip technology [2.7], isolation using detachable beads [2.8], dielectrophoretic device [2.9], silicon substrate [2.10], micromachine [2.11], cytometry [2.12], electrical biosensor [2.13] etc. Conventionally CTCs are characterized by labelling the cell surface antigens with fluorescent dyes [2.14-15]. In fluorescence microscopy the specific surface markers are usually labelled with antibodies and fluorophores. However, the use of fluorescent dyes is frequently limited by several factors. Fluorescent molecules exhibit photobleaching [2.16], there are relatively few suitable fluorescent dye molecules and fluorescence spectral bands overlap [2.17], when different fluorophores are employed to address multiple cell surface receptor typ [2.16]. These factors limit the multiplexing capability of fluorescent dyes conjugated for cell surface marker detection. Therefore, there is still a need for highly sensitive and specific cell detection methods which show a high multiplexing capability and high reproducibility.

35
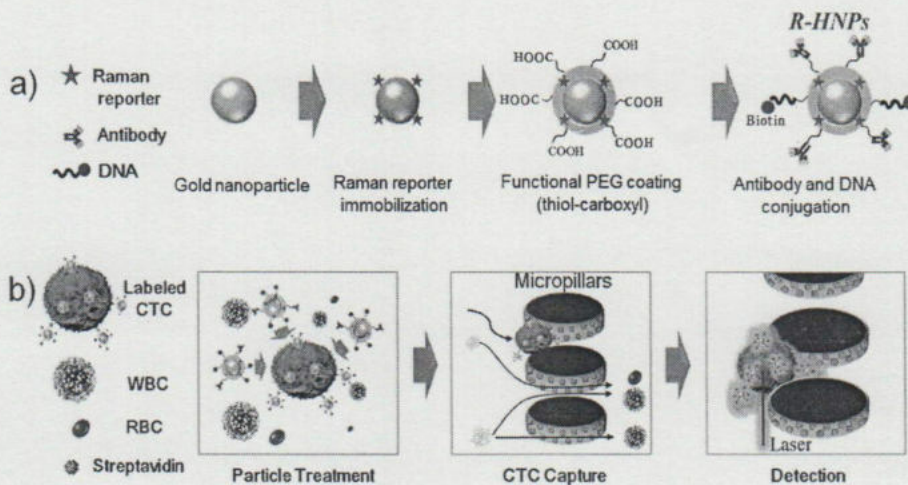
Figure 2.1. a) Schematic diagram for synthesis of Raman hybrid nanoparticles (R-HNPs). b) Labelling of CTCs with R-HNPs, capturing on the microfluidic chip and characterization using SERS.

2.2. Materials and Methods

2.2.1. Reagents

Gold colloids were obtained from BB International-UK. Thiophenol (TP), nile blue A (NBA), 1-naphthalenethiol (NPT), 4-mercaptopyridine (MPy), 2-quinolinethiol (QTH), ethyl dimethylaminopropyl carbodiimide (EDC), N-hydroxy sulfosuccinimide, 2-(N-Morpholino) ethanesulfonic acid hydrate, 3-aminopropyltriethoxysilane, glutaraldehyde, streptavidin, formaldehyde and phosphate buffered saline (PBS) (pH 7.4, 10 mM from Sigma Aldrich -USA . Mouse monoclonal IgG anti-EpCAM, anti-EGFR, anti-MUC1, anti-HER2 and anti-CD-45 were collected from R & D systems. RPMI-1640 medium was purchased from Fresh media^{TM}, Daegu, South Korea. Fetal bovine serum (FBS), antibiotics (penicillin–streptomycin, 10,000 IU/ml of penicillin sodium, and 10,000 mg/ml of streptomycin sulfate in 0.83% saline), and Trypsin (Trypsin –EDTA solution, 1X) were obtained from Welgene Inc. mPEG-SH (MW 5 kDa), heterofunctional linker HS-PEG-COOH (MW 5 kDa) from creative PEG Works were used. NH_2-DNA and biotin-DNA was collected from Bioneer, Daejon, Korea. Restriction enzyme Alu I was purchased from Sigma Aldrich. Streptavidin conjugated quantum dots (525, 545, 565, 625 and 705 nm emission wavelength) were collected from

Invitrogen (USA). BD Vacutainer® CPT™ cell preparation tubes were collected from BD Franklin Lakes, NJ. Ficoll-Paque plus were purchased from GE Healthcare Inc. Other chemicals were all of analytical grade. All solutions were prepared with double-distilled water, which was purified using a Milli-Q purification system (Branstead) to a specific resistance of 418 MΩ cm.

2.2.2.   Fabrication of Microfluidic Chip

The cell chip (Figure 2.9) was fabricated by silicon-on- glass (SOG) technology to create a precise pillar array structure. Briefly, silicon and glass wafers were attached using anodic methods. Lapping and chemical mechanical polishing was performed on the silicon layer of the chip, resulting in filter height of 50μm. Then photoresist (AZ 4330, Clariant Corp., Muttenz, Switzerland) was patterned and deep reactive-ion etching was performed (15 min). To make a fluidic path, glass wafer was laminated and patterned using a dry film photoresist (Ordyl BF 410, Tokyo Ohka Kogyo, Kawasaki, Japan), followed by sand blasting etching to form in/outlet holes. Finally, the cover glass wafer was aligned and connected with the patterned wafer by anodic bonding. There were three channels in the chip for capturing

39

the suspended cells. Two channels were of 5μ diameter and one channel was of 50μ diameter.

2.2.3. Culturing of Cells

Three Breast cancer cell (BCC) lines (MCF-7, MDA-MB-231, and SK-BR-3) were obtained from ATCC (Manassas, VA). The cells were cultured at 37 °C in RPMI-1640 medium supplemented with 10% heat inactivated fetal bovine serum and 1% antibiotics (streptomycin and penicillin) in a humidified atmosphere of 95% air with 5% CO_2. The cells were grown at in TC-grade Petri dish. At 80% confluence the cells were sub-cultured at a density of 1×10^5 cells/ml on culture plates, and then incubated for 2–3 days.

2.2.4. Preparation of Conjugated Raman Hybrid nanoparticles (R-HNPs) for SERS

In this work we prepared fiver combinations of R-HNPs. Each type of R-HNPs was prepared as described by Ximei Qian *et al.*, 2008 [2.31]. Figure 2.1 shows the illustrations of the step by step conjugation process of the GNP/Raman reporter/PEG/antibody/DNA conjugate. Briefly, SERS active probes were prepared by adding a freshly prepared 1-5 μM Raman reporter

40

solution drop wise to a rapidly mixing gold colloid at a 1:6 reporter solution/ Au colloid volume ratio. Different concentrations of different Raman reporters were used to make similar peak intensities in each case. After 10 min, a 10 μM thiol-PEG solution was added drop wise to the Raman-encoded Au colloids, with a minimum ratio of 30,000 PEG-SH molecules per 60-nm Raman-encoded gold particle to stabilize and minimize particle aggregation under various conditions. 293 μl of 1 μM hetero-functional linker HS-PEG-COOH was added drop wise to 3 ml Raman-encoded Au colloids solution in a polypropylene tube under rapid mixing. After 15 min of mixing, the gold nanoparticles (AuNPs) were exposed to a large volume of PEG-SH (1.6 ml at 10mM) to fill the areas not covered by the hetero-functional PEG, yielding well-shielded and stable particle surfaces. Before covalent ligand conjugation at the carboxylic acid functional groups, the GNPs were purified by three rounds of centrifugation (1,000g) and re-suspension in PBS. To activate the -COOH groups on the particle surface for covalent conjugation, freshly prepared ethyl dimethylaminopropyl carbodiimide (EDC) solution (5 ml) at a concentration of 40mg/ml) and sulfo-NHS (5 ml at 110 mg/ml) were mixed vigorously at 25 °C for 15 min. Excess EDC and sulfo-NHS were separated from the activated nanoparticles by three rounds of centrifugation (1,000g) and re-suspended in PBS. The

41

purified GNPs with activated carboxyl groups were then reacted with the mouse monoclonal antibody (11.2 nmol) and H_2N-dsDNA-biotin (20 nmol) at 25 °C for 2 h, and the reaction mixture was stored at 4 °C for overnight. Excess antibody and DNA was removed by three rounds of centrifugation (1,000g) and re-suspended in PBS.

Five different multifunctional R-HNPs were prepared with fiver different combinations. The fully functionalized hybrid nanoparticles (R-HNPs) were characterized by transmission electron microscopy (TEM), UV-(vis.) spectroscopy, dynamic light scattering and SERS. UV (vis.) spectra were measured using Jasco V-530 UV/VIS spectrophotometer. The TEM images were acquired by using a JEOL transmission electron microscope (JEM1010) with an accelerating voltage of 80 kV.

2.2.5.   StreptavidinCoating on the Glass Chip Surface

Streptavidin was coated on the glass surface following the method described by Lee et al., 2013 [2.14]. Briefly, the cell chips were sequentially rinsed with ethanol and deionized (DI) water and dried at 60°C overnight. The chips were then placed in a plasma chamber (Convance-MP, Femto Science,

42

Gyeonggi-do, Korea) and exposed to oxygen plasma (5 min.) to activate surface silanols for subsequent reaction. The chips were immersed in 10% 3-aminopropyltriethoxysilane solution, thoroughly washed with DI water, and baked at 110°C for 1 h. The silanized chips were exposed to 2% glutaraldehyde solution in 100 mM phosphate buffer (pH 8.0) for 1 h, washed with PBS, and dried with N_2. 10 μM of streptavidin was allowed to react with immobilized glutaraldehyde at room temperature (1 h). After washing with PBS, the chips were covered with 1% bovine serum albumin in PBS (1 h) to block any sites not bound to proteins on the glutaraldehyde modified surface. Finally, the chips were washed with PBS solution and dried with N_2.

2.2.6. Preparation of Cells Suspension

48 hours after sub-culturing (incubation 37 °C, 5% CO_2), the cells were detached from the cell culture dishes by trypsin and washed twice with PBS to remove the trypsin. Then the cell pellet was re-suspended RPMI medium. Then 1.5 ml of 1% bovine serum albumin was added, and the cells were incubated for 1 h. This is the blocking process to reduce nonspecific binding of antibody-conjugated AuNPs.

43

2.2.7. Handling of Healthy Human Blood

All healthy human blood samples (7.5-15 ml) were obtained from Health centre of the Sogang University (Seoul, Korea), and this work was approved by the Institutional Review Board (IRB). The blood samples were collected using BD Vacutainer® CPT™ cell preparation tubes (BD Franklin Lakes, NJ) containing sodium heparin and polyester gel. After gentle mixing, the fresh blood was gently diluted twice with PBS. As CTCs exist in the buffy coat layer, we used a density gradient reagent (Ficoll-Paque plus, GE Healthcare Inc.) to get the buffy coat. In a centrifuge tube 6 ml of Ficoll-Paque plus was taken followed by carefully adding 8 ml of diluted blood without mixing with Ficoll and centrifuged at room temperature for 30 min at 400 g. After centrifugation, the plasma layer was removed carefully from the top and the low density buffy coat cell layer containing lymphocytes, monocytes was collected leaving the Ficoll and RBC sediment in the centrifuge tube. After collection the cells were transferred into a new tube, washed with PBS and fixed with 3.7% forladehyde for 10 min. The cells were then washed with PBS, counted and stored at 4°C for next use.

2.2.8. Labeling of Cells with Conjugated SERS Nanoparticles (R-HNPs)

100 suspended cells of each subtype (MCF-7, SK-BR-3 and MDA-MB-231) were mixed with the fixed white blood cells (WBC) suspension and then incubated with 10 pM conjugated SERS nanoparticles with constant mixing for 30 min at room temperature to label the target cells. Then, the cells were washed three times and re-suspended in 2 ml RPMI medium before capturing the CTCs in microfluidic chip.

2.2.9. Capturing of Labeled Cells on the Streptavidin Coated Glass Chip for Measuring SERS.

The R-HNPs treated cells suspension (containing 100 spiking cells) were infused through the microfluidic channel at a flow rate 10μl/min and incubated at room temperature for 1 hour to immobilize on the chip surface. Then the chip was washed with RPMI medium to remove the debris or unbound cells.

2.2.10. SERS Mapping for Visualization of the Distribution of Surface

45

Markers on the Cells and Their Characterization

NTEGRA spectra (AFM-Raman Spectrometer, NT-MDT, Russia) equipped with a liquid nitrogen-cooled CCD detector and an inverted optical microscope (Olympus IX71) was used for SERS mapping of cells. SERS mapping were recorded using a laser of 785 nm NIR wavelengths with a laser power 3 mW on the sample plane. The SERS data were analyzed using Nova software.

2.2.11. Detachment and Collection of the Cells after Characterization

The cells were detached from the microfluidic chip surfcae after characterization. The restriction endonuclease enzyme Alu I was used to detach the cells. For detachment of the cells, the chip was incubated at 37 °C for 1 hour after enzyme treatment.

2.2.12. Labeling of Cells with Quantum dots (QDs)

For fluorescence microscopic imaging the cells surface markers were labeled with quantum dots (QDs). Different surface markers (EGFR, MUC-1,

EpCAM and HER2) of each cell types were labeled with different streptavidin conjugated QDs (525, 545, 565, and 625 nm emission wavelength). Surface marker specific biotinylated antibodies were used to label the cells with different QDs. In the antibody-QDs conjugates, the antibody and QDs were mixed with a molar ratio of 2.5:1 and incubated in dark condition for 2 hrs at room temperature. Then the conjugates were purified by centrifugation at 3,000g for 10 min and resuspension in PBS. The suspended fixed cells of each subtypes (MCF-7, SK-BR-3 and MDA-MB-231) were mixed with 1 pM of each antibody conjugated QDs and incubated with constant mixing for 30 min at room temperature to label the cells. Then the cells were washed PBS three times and re-suspended in PBS before measuring fluorescence.

2.2.13. Fluorescence Microscopic Examination

The quantum dots labeled suspended cells were transferred into 96 well plates and observed under fluorescent microscope. The fluorescence images were acquired with Nikon ECLIPSE- Ti microscope with 400x magnification. The fluorescence data were analyzed using NIS-Elements-BR-3.2 software.

47

2.3.   Results and Discussion

2.3.1.   Expression Analysis through Fluorescent Microscopy

At first fluorescence microscopic experiments were conducted to detect the expression level of different surface markers in different breast CTCs. But fluorescent dyes have some photobleaching effect (Figure 2.2). Four different quantum dots (QDs) (525nm, 545nm, 565nm, and 625nm) were used to label the surface antigens of the breast CTCs. The 525nm, 545nm, 565nm, and 625nm QDs emit green, lemon, yellow and red colour respectively. The results of fluorescence microscopic experiments are shown in Figure 2.3. The cells used in this study were MCF-7(Luminal subtype), SKBR-3 (HER2 subtype) and MDA-MB-231 (basal subtype) [2.32]. For this study, one more surface marker MUC1 was measured separately by fluorescence microscopy. Three different surface markers (EpCAm, EGFR and HER2 and MUC-1) expression level were detected successfully at a time with three different QDs.

The results are shown in Figure 2.19-2.22. When four different surface markers (EGFR, MUC-1, EpCAM and HER2) were labeled with four different QDs (525, 545, 565 and 625 nm emission wavelength respectively),

48

the fluorescence spectra overlap each other (Figure 2.3). The MUC-1 marker was labeled with 545 nm QDs. 545nm QDs emit lemon colour fluorescence which ranges between green and yellow colour. Therefore, due to labeling of MUC-1 surface marker with 545 nm QDs, the fluorescence intensity of the 525 nm (green) and 565nm (yellow) QDs increased in SK-BR-3 cells (Figure 2.3).

2.3.2. Visualization of the Nanoparticle's Structure through Transmission Electron Microscopy (TEM)

Multi-functional Raman reporter based hybrid nanoparticles (R-HNPs) were fabricated which composed of 60 nm size gold nanoparticles (GNPs) Raman reporters, HS- PEG- COOH, antibody and H_2N-DNA-biotin, (Figure 2.1). Figure 2.4a shows the TEM images of bare AuNP, Raman reporter encoded AuNPs and PEG-antibody conjugated AuNP. The core particle size is of the gold colloid is 60 nm, the PEG coating was clearly observed as a thin white layer of ~5 nm by TEM image.

49
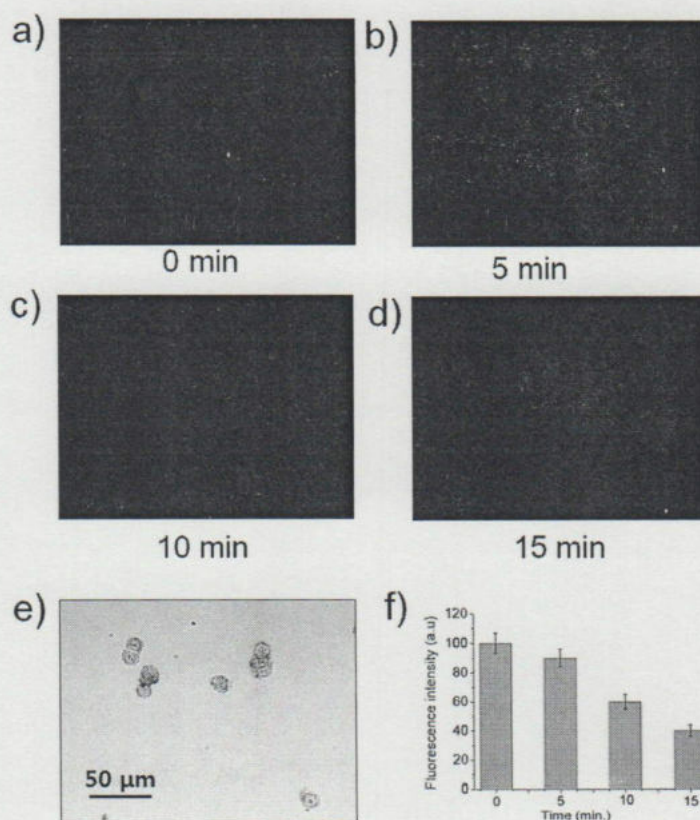
Figure 2.2. Photobleaching property of fluorescent dyes; a), b), c) and d) dark field image of SK-BR-3 cells labelled with quantum dots of 625 nm emission wavelength. The images were taken every 5 min interval in presence of continuous exposure of excitation laser. e) Bright field image of the SK-BR-3 cells. f) Bar graphs showing reduction of fluorescence intensity in every 5 min interval. Error bar indicate standard deviation of three individual experiments.

50

2.3.3. Determination of the Localized Surface Plasmon Absorbance through UV-vis. Spectroscopy

Figure 2.4b demonstrates the UV (vis.) spectra of bare AuNPs, Raman encoded AuNPs and PEG-antibody conjugated AuNPs. The spectrum of the pure GNPs showed a maximum absorption at 530 nm due to Plasmon Resonance [2.31]. The Raman reporter coated AuNPs showed a slight decrease of the maximum absorption peak, which may be due slight aggregation of the GNPs by the Raman reporters. The PEG-conjugated SERS probes showed a somewhat more decrease of the maximum absorption peak and a red shift of ~6 nm. This may be due to PEG coating, and reduction of the concentration of AuNPs during washing steps.

51
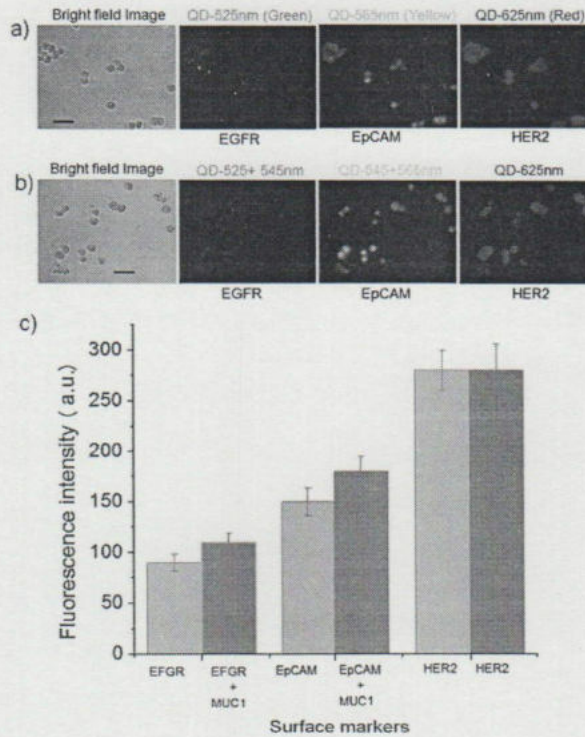
Figure 2.3. Overlapping of fluorescent spectra in case of multiple labeling; a) EGFR, EpCAM and HER2 surface markers of SK-BR-3 cells were labelled with QDs having emission wavelength 525, 565 and 625 nm respectively. b) EGFR, MUC1, EpCAM and HER2 surface markers of SK-BR-3 cells were labelled with QDs having emission wavelength 525, 545, 565 and 625 nm respectively.c) Bar graphs showing comparative intensity of fluorescence spectra between conditions a) and b). Scale bar 50 nm.
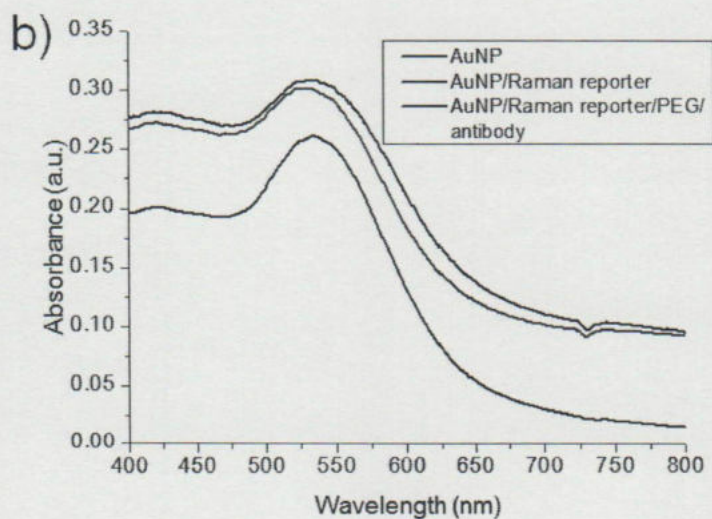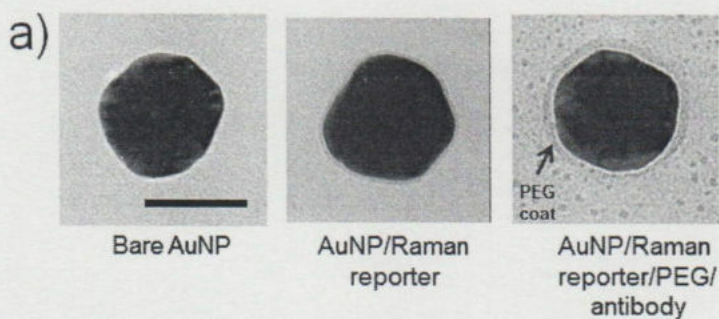
Figure 2.4. Confirmation of conjugation of Raman hybrid nanoparticles through (transmission electron microscopy) TEM, and UV-vis.spectroscopy. a) TEM images of bare AuNP, Raman reporter encoded AuNPs, and Raman reporter, PEG, and antibody conjugated AuNP. b) UV-vis. spectra of bare AuNP, Raman reporter encoded AuNPs, and Raman reporter, PEG, and antibody conjugated AuNP. Scale bar 50 nm.

53

2.3.4. Determination of the Size Distribution through Dynamic light Scattering (DLS)

Figure 2.5 Shows dynamic light scattering (DLS) size data obtained from the bare AuNPs (top left), Raman-encoded (top right), and PEG-stabilized antibody modified AuNPs (bottom). At a core the particle size is 60 nm, the average size is increased to 70 nm after Raman reporter immobilization, whereas the particle's 'wet' hydrodynamic diameter increased by 20 nm after pegylation.
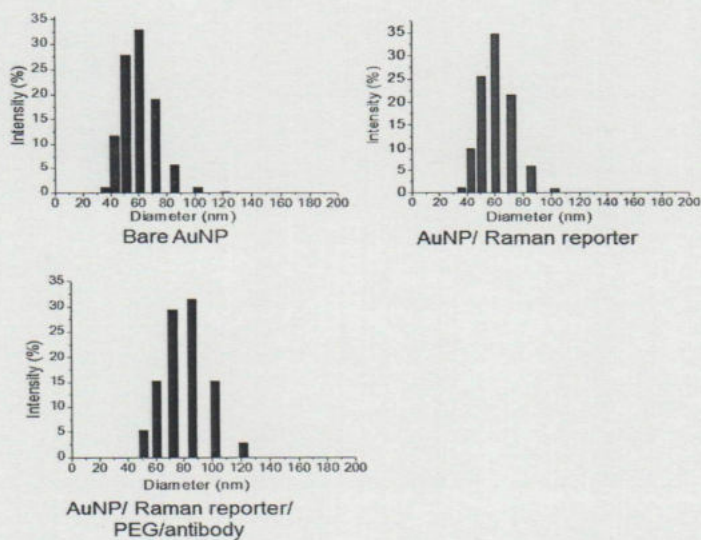
Figure 2.5. Size distribution of the Raman hybrid nanoparticles as measured by dynamic light scattering (DLS).

54

2.3.5. Surface-enhanced Raman spectroscopy (SERS) of Raman Reporter based Hybrid Nanoparticles (R-HNPs)

Figure 2.6 shows the corresponding SERS spectra of the pure Raman reporter and the conjugated naoparticles. The pure Raman reporter molecules showed relatively much stronger SERS signals than the antibody conjugated hybrid nanoparticles (HNPs). The SERS intensity of the Raman reporters gradually decreased with the increase in the coating layer thickness because of the scattering shielding effects [2.33]. Still the final antibody-conjugated HNPs have a strong SERS intensity, and they are suitable to use in cellular SERS imaging studies. The SERS spectrum of thiophenol (TP) showed one dominant peaks at 1575 cm^{-1} (a), which is assigned to the a1 mode of the TP molecule [2.34]. One strong band at 1381 cm^{-1} was observed for the 1-naphthalenethiol (NPT) molecules on the AuNPs (b), which was due to ring stretching of the NPT molecule [2.35]. In case of nile blue A (NBA) there was a strong peak at 1492 cm^{-1} (d), which corresponds to the aromatic ring stretching [2.36]. The SERS spectrum of 2-quinolinethiol (QTH) showed one strong peak at 1369 cm^{-1} (e) which correspons to the aromatic $\upsilon(CC)$ vibration [2.37]. In case of 4-mercaptopyridine (MPy) there is one dominant

55

peaks at 1096 cm^{-1} (c),
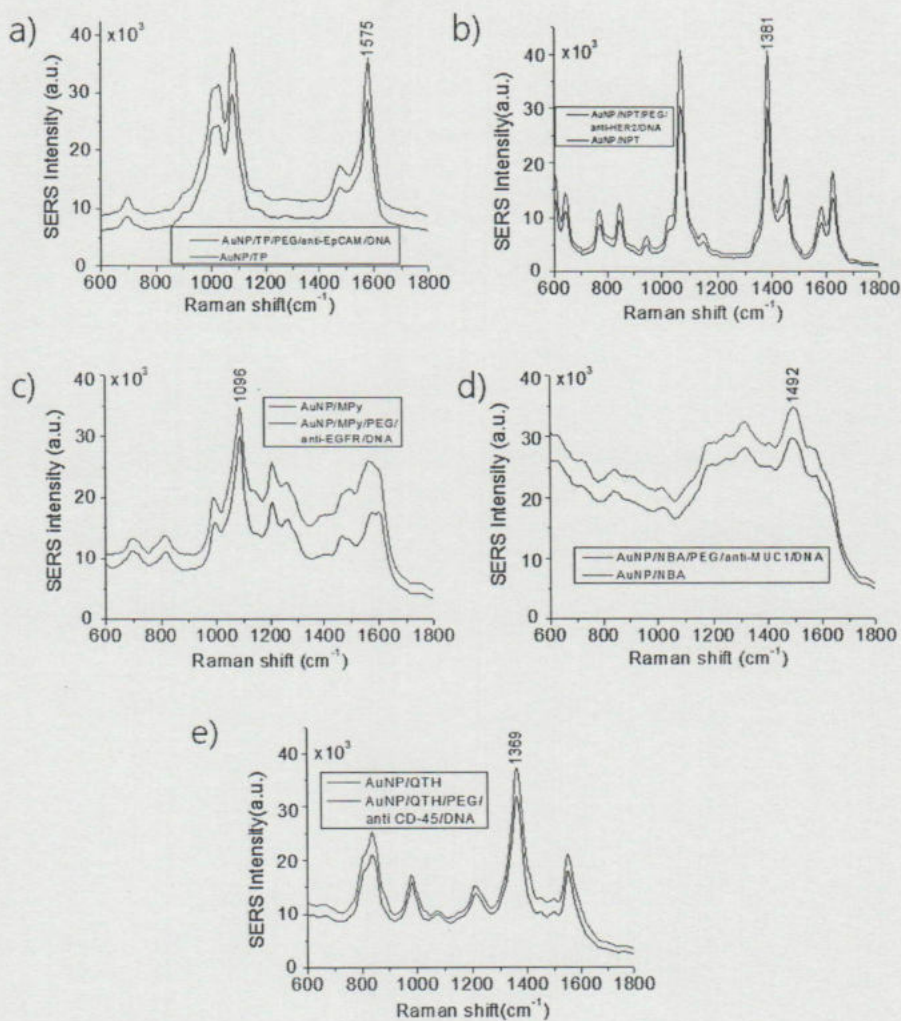
Figure 2.6. SERS Spectra of the Raman Hybrid Nanoparticles (R-HNPs); a)

SERS spectrum of thiophenol (TP) immobilized on AuNP (red curve), and

TP, PEG, anti-Epcam and DNA immobilized on AuNPs (black curve). b)

56

SERS spectrum of 1-naphthalenethiol (NPT) immobilized on AuNP (red curve), and NPT, PEG, anti-HER2 and DNA immobilized on AuNPs (black curve). c) SERS spectrum of 4-mercaptopyridine (MPy) immobilized on AuNP (red curve), and MPy, PEG, anti-EGFR and DNA immobilized on AuNPs (black curve). d) SERS spectrum of Nile blue A (NBA) immobilized on AuNP (red curve), NBA, PEG, anti-MUC1 and DNA immobilized on AuNPs (black curve). e) SERS spectrum of 2-quinolinethiol (QTH) immobilized on AuNP (red curve), and QTH, PEG, anti-CD-45 and DNA immobilized on AuNPs (black curve) which corresponds to the aromatic ring vibration mode [2.38]. The Raman band 1575, 1492, 1381, 1369 and 1096 cm^{-1} of R-HNP-1, R-HNP-2, R-HNP-3, R-HNP-4 and R-HNP-5 were selected to detect the expression level of EpCAM, MUC1, HER2, CD-45 and EGFR respectively.
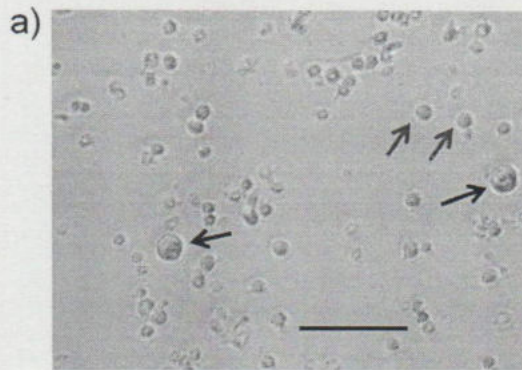
Bright field image
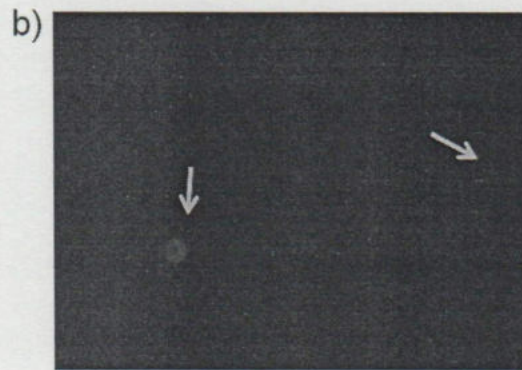
Fluorescent microscopic image

Figure 2.7. Fluorescence labeling of breast CTCs in a mixture of white blood cells (WBCs). a) Bright field image showing white blood cells (small, purple arrow) and SK-BR-3 cells (big, black arrow). b) Fluorescent microscopic image. The HER2 surface markers of the SK-BR-3 (golden arrow) cells were labelled with quantum dots with 625 nm emission wavelength. Scale bar 50 μm.

58
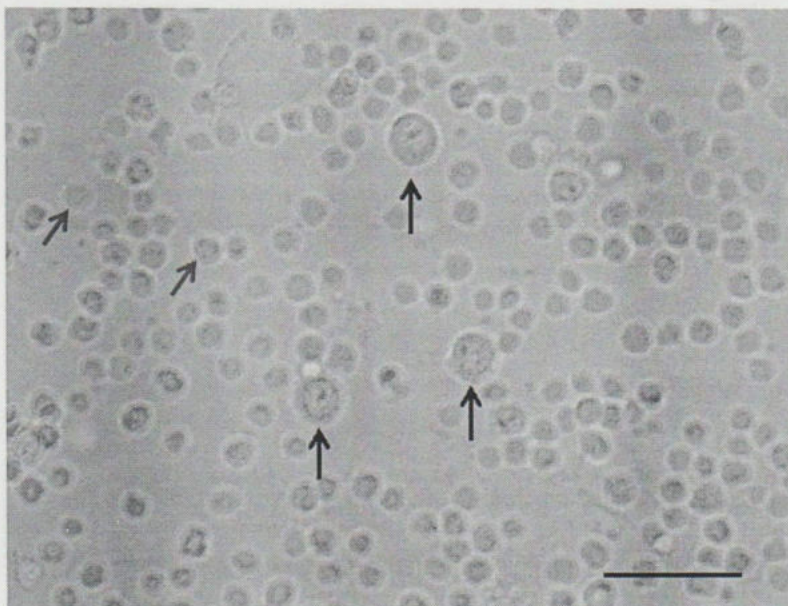
Figure 2.8. Labeling of breast CTCs with R-HNPs in a mixture of white blood cells suspension; Bright field image showing mixed suspension of WBCs (small, purple arrow) and SK-BR-3 cells (big, black arrow). Scale bar 50 μm.

2.3.6. Capturing of CTCs

R-HNPs labelled cells (100 of each type) were infused mixed with normal WBCs suspension (Figure 2.7-8) through the microfluidic channel (5μm gap direction) (Figure 2.9-10) with help of a syringe pump at a flow rate 10 μl/min. During flowing, due to large size of the CTCs (12-18μm), they were easily come in contact on the strepatividin coated surface of the pillars and captured on it. Among three different kind of breast CTCs the SK-BR-3 cells showed highes capturing efficiency, as SK-BR-3 cells show greater expression level of most of the surface markers (EpCAM, EGFR, and HER2). In case of MDA-MB-231 cells, which have relatively low surface protein expression level, but the capture efficiency was still high (89%), this may be due to the larger diameter of MDA-MB-231 cells, allowing for higher chance of contact with the streptavidin-coated pillars (Figure 2.11). The lower capture efficiency in MCF-7 cells may be due to their smaller size. But the bare chip did not capture any CTC (Figure 2.11).

The capturing efficiency was 90%, 89% and 83% in case of SK-BR-3, MDA-MB-231 and MCF-7 cells respectively (Figure 2.12) and the average capture efficiency was 87.33%. After capturing the cells in the microfluidic channel (Figure. 2.9), the chip was washed (50 μm gap direction) with RPMI

60
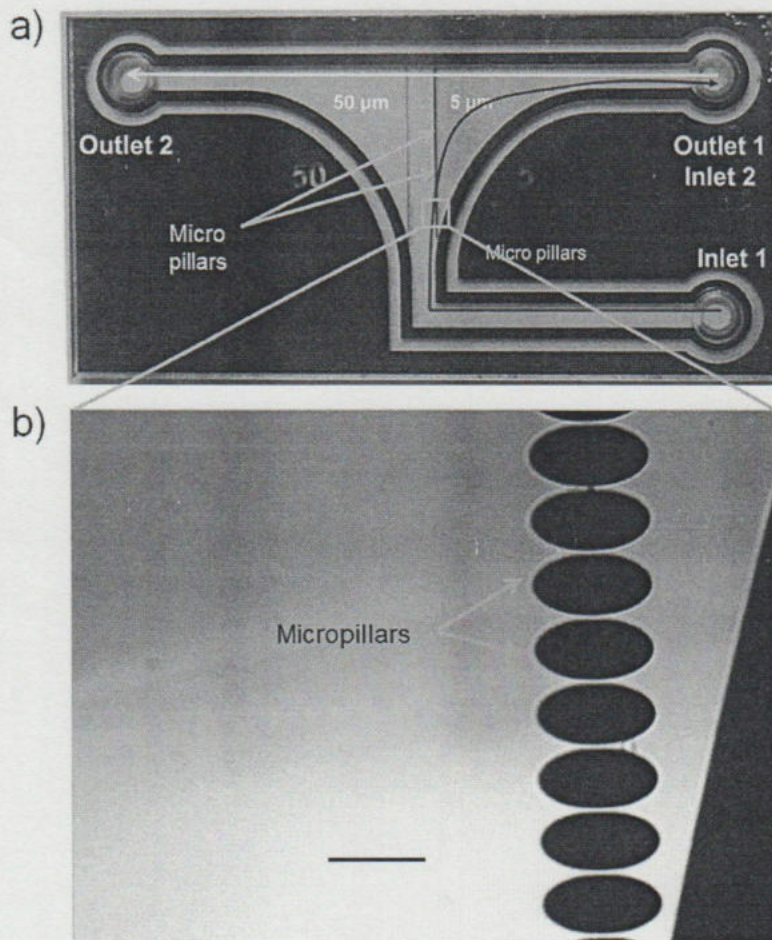
Figure 2.9. Microfluidic chip design. a) Photograpgh of a microfluidic chip showing inlet (red arrow) and outlet (yellow arrow). b) Magnified brightfield image of the golden square box in (a) showing micropillars for capturing CTCs. Scale bar 50 μm.
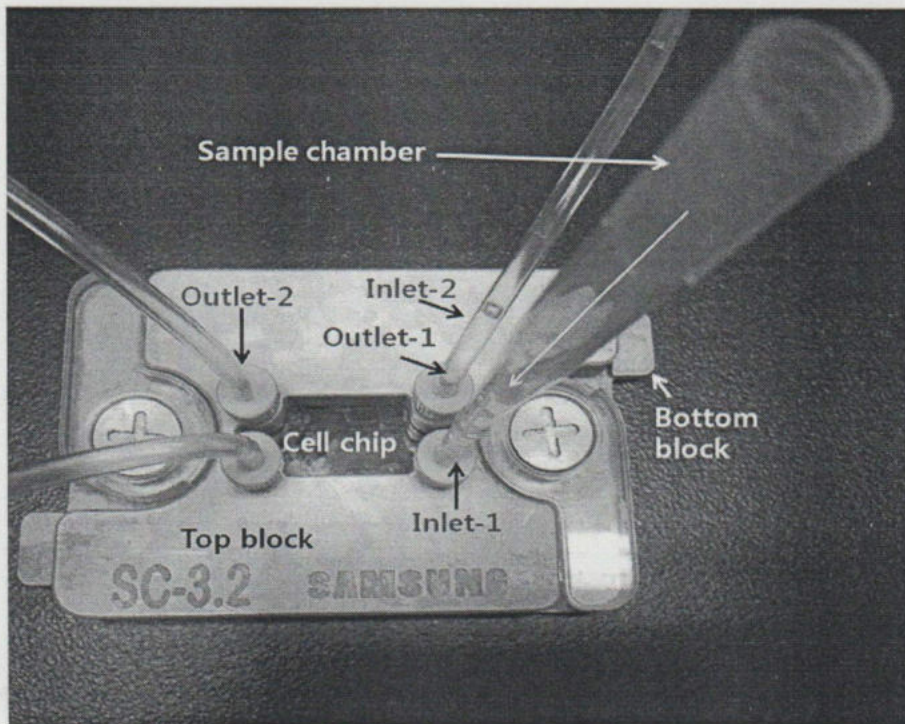
Figure 2.10. Setting of microfluidic chip in metal chip block. Photograph of a microfluidic chip set on metal chip block showing inlets and outlets.
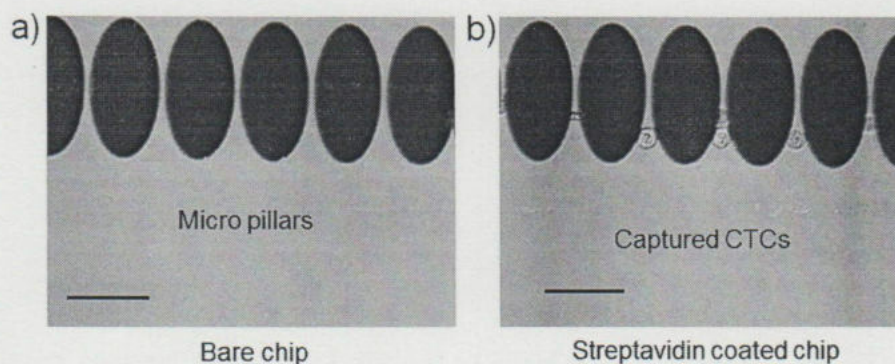
Figure 2.11. Capturing of R-HNP labelled CTCs in microfluidic chip; a) Bare chip, b) Streptavidin coated chip. Scale bar 50 μm.
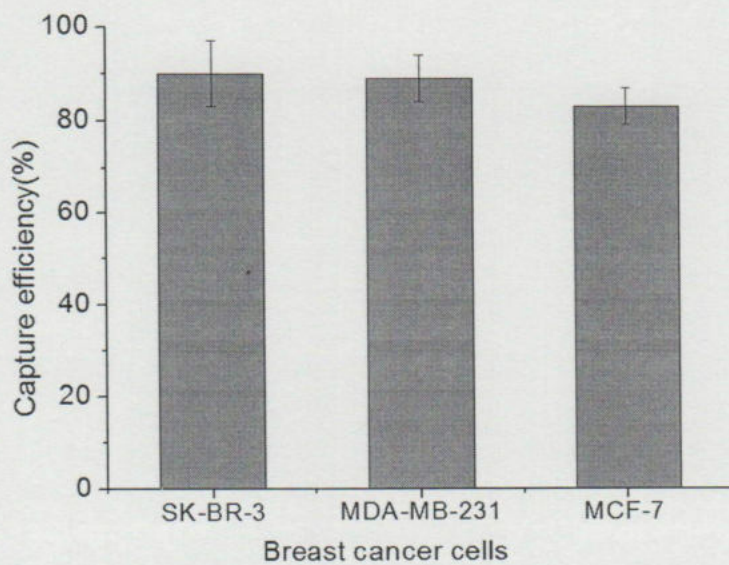
Figure 2.12. CTC capturing efficiency of the microfluidic chip.

media, and then SERS mapping was performed.

2.3.7.   Detection of the Expression Level through SERS Map Imaging

The five different multifunctional R-HNPs were immobilized to each cell type to detect the expression level of EpCAM, MUC1, EGFR, HER2 and CD-45 surface antigens. Attachment of each type of R-HNPs to each cell type depends on the expression level of that type of surface marker on the cell. Therefore, the expression levels were calculated based on the intensity of the selected specific Raman bands of the R-HNPs (Figure 2.6). SERS mapping of the labelled cells was performed to detect the expression level of the surface markers. Figure 2.13-15 shows the surface marker expression level for MCF-7, SK-BR-3, and MDA-MB-231 cells. The vertical scale bar on the right side of each map shows the expression level of the CTCs. The histograms are showing the comparative expression level of each surface marker. The identification accuracy of the captured cells was 97 % in SK-BR-3, 94 % in MCF-7, and 88 % in MDA-MB-231 cells with an average of 93 %.
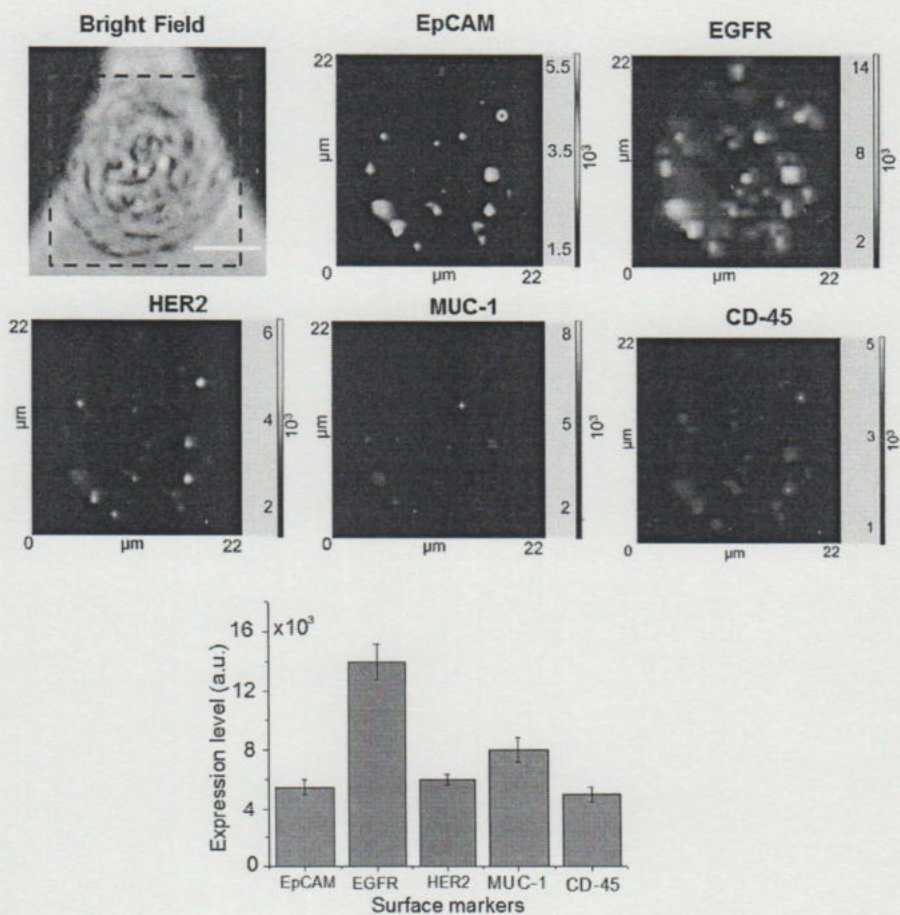
Figure 2.13. Detection of the surface marker expression in MDA-MB-231 cell based on SERS map imaging. Red dashed box is the scanning area. Scale bar 10 μm. Bar graph shows the expression level. Error bar indicates standard deviation of three independent experiments.
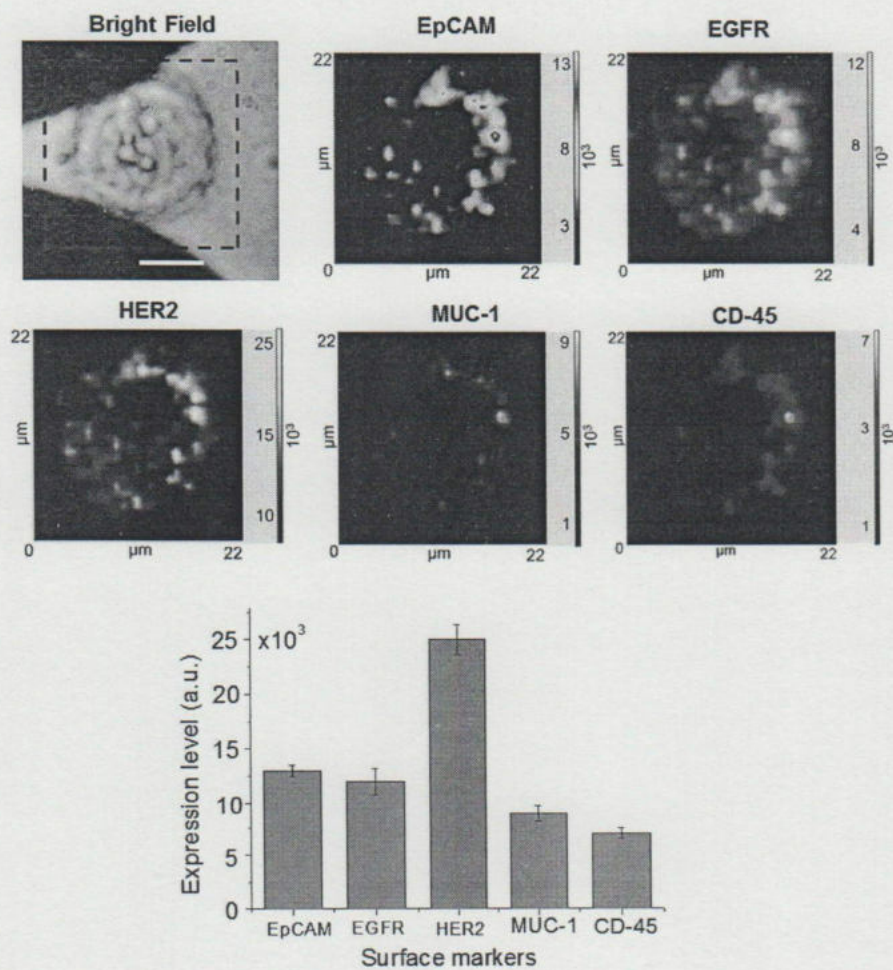
Figure 2.14. Detection of the surface marker expression in SK-BR-3 cells based on SERS map imaging. Red dashed box is the scanning area. Scale bar 10 μm. Bar graph shows the expression level. Error bar indicates standard deviation of three independent experiments.
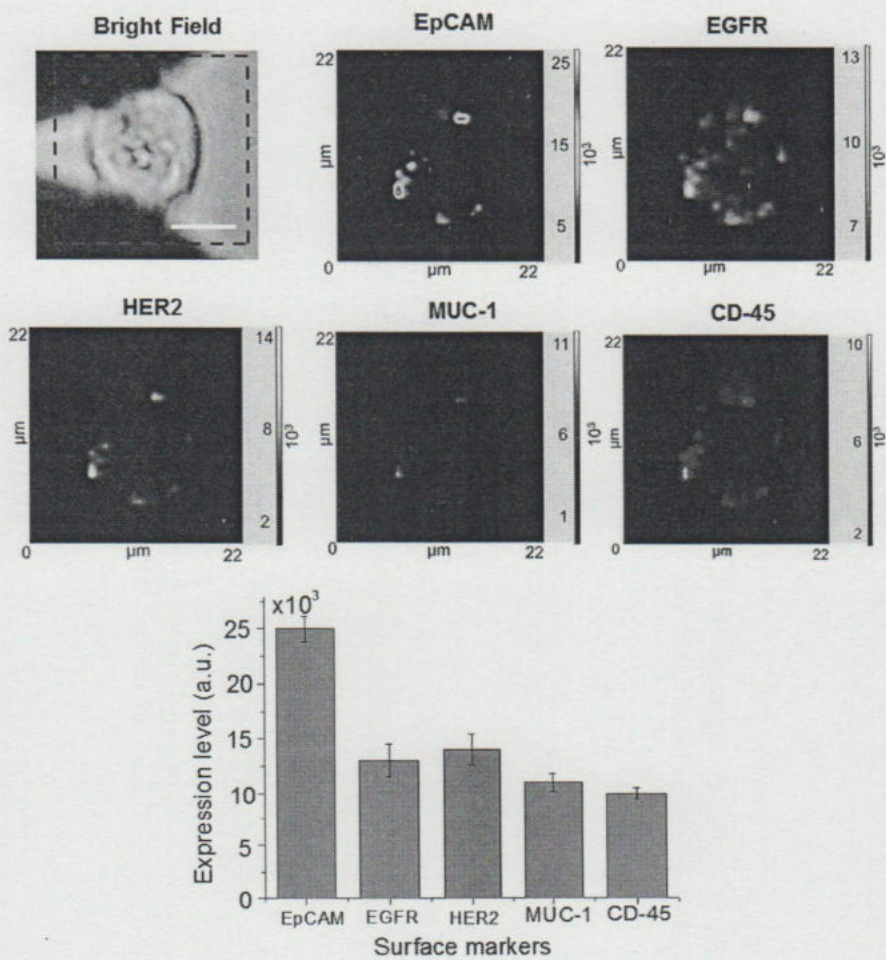
Figure 2.15. Detection of the surface marker expression in MCF-7 cells based on SERS map imaging. Red dashed box is the scanning area. Scale bar 10 μm. Bar graph shows the expression level. Error bar indicates standard deviation of three independent experiments.

2.3.8. Detachment and collection of the cells from chip after characterization

After detection and characterization of the CTCs, the cells were collected from the chip for further experiments. The cells were detached by cleaving the DNA using Restriction enzyme (Figure 2.16). The collected cells were grown in petridish as shown in Figure 2.17.

Capturing of CTCs in the chip

Detachment and collection of the cells after characterization
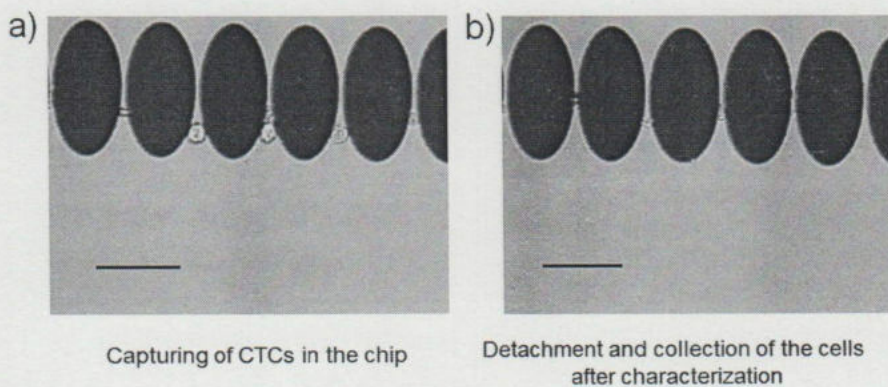
Figure 2.16. Detachment and collection of the captured cells from chip after characterization. Bright filed image of a) capturing of cells in microfluidic chip, b) detachment and collection of the cells from the chip. Scale bar 50 µm.
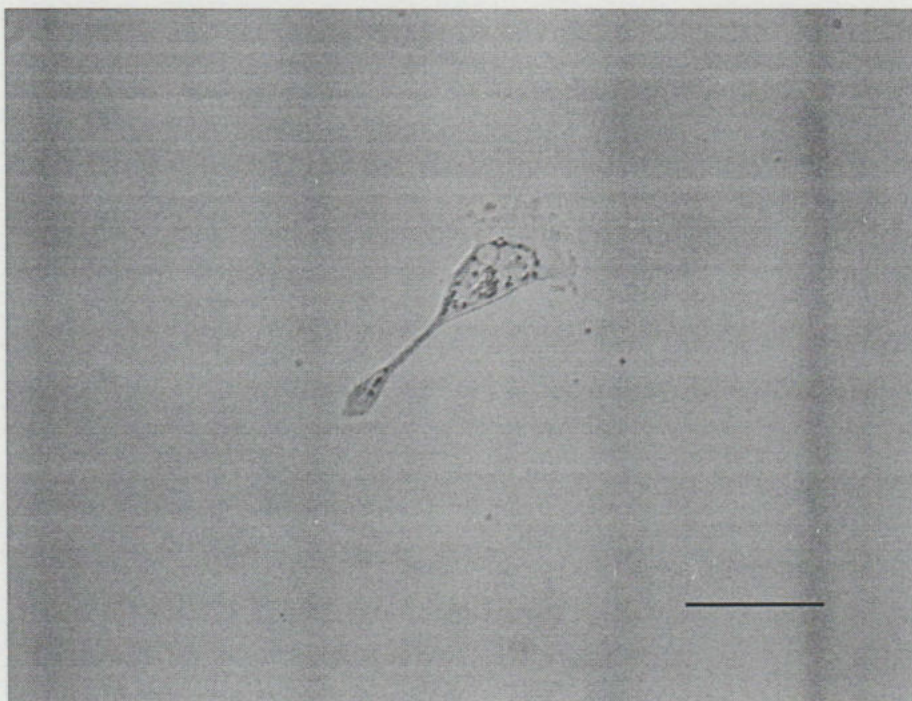
Figure 2.17. Culturing of collected cell after detachment from the chip surface. Bright field image of a SK-BR-3 cell 48 hours after collection and culturing. Scale bar 25 μm.

2.3.9. Detection of the Exression Level through Fluorescence

Figure 2.18-20 shows the surface marker expression level of different breast CTCs as measured by fluorescent microscope. In case SK-BR-3 cells HER2 expression is highest, followed by EGFR and EpCAM. In case MDA-MD-231 cells EGFR expression is highest followed by HER2 and EpCAM. In

69

case MCF-7 cells EpCAM expression is highest followed by HER2 and EGFR. Figure 2.21 shows the CD-45 expression level of different breast CTCs and white blood cells (WBCs).CD-45 expression is highest in WBCs than the breast CTCs.
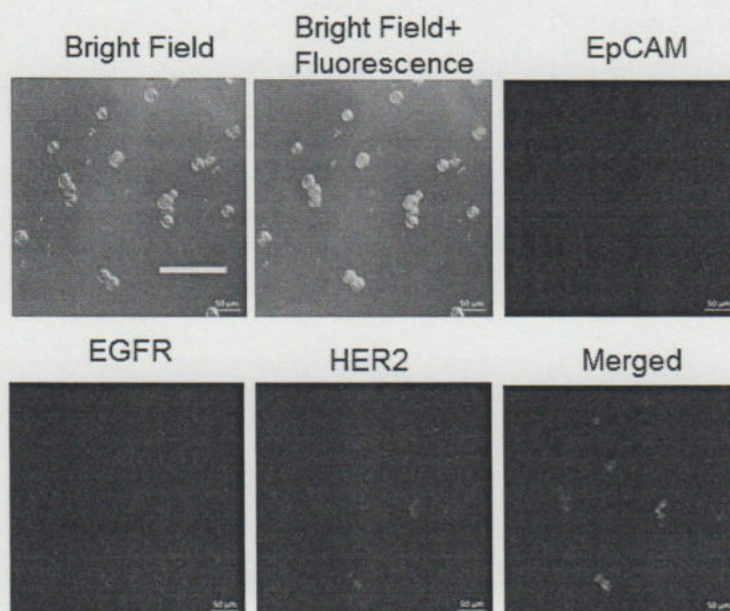
Figure 2.18. Detection of the surface marker expression in SK-BR-3 cells based on fluorescnt microscopy. Three different surface markers (EpCAM, EGFR, and HER2) of the cells were labelled with three different quantum dots of 525, 565 and 625 nm emission wavelength respectively. Scale bar 100 μm.

70
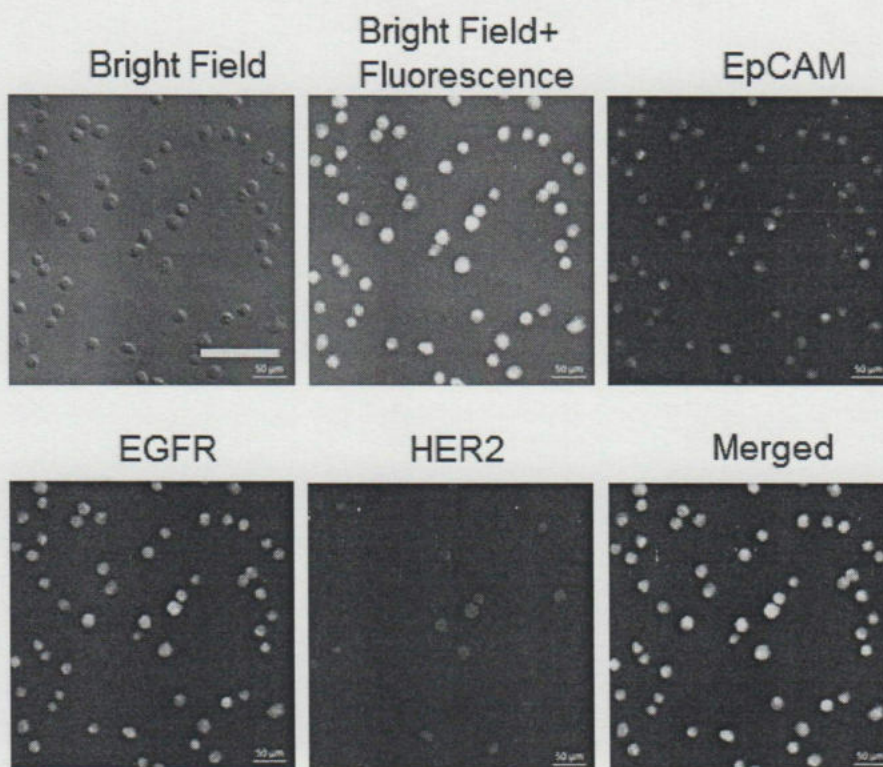
Figure 2.19. Detection of the surface marker expression in MDA-MB-231 cells based on fluorescnt microscopy. Three different surface markers (EpCAM, EGFR, and HER2) of the cells were labelled with three different quantum dots of 525, 565 and 625 nm emission wavelength respectively. Scale bar 100 μm.
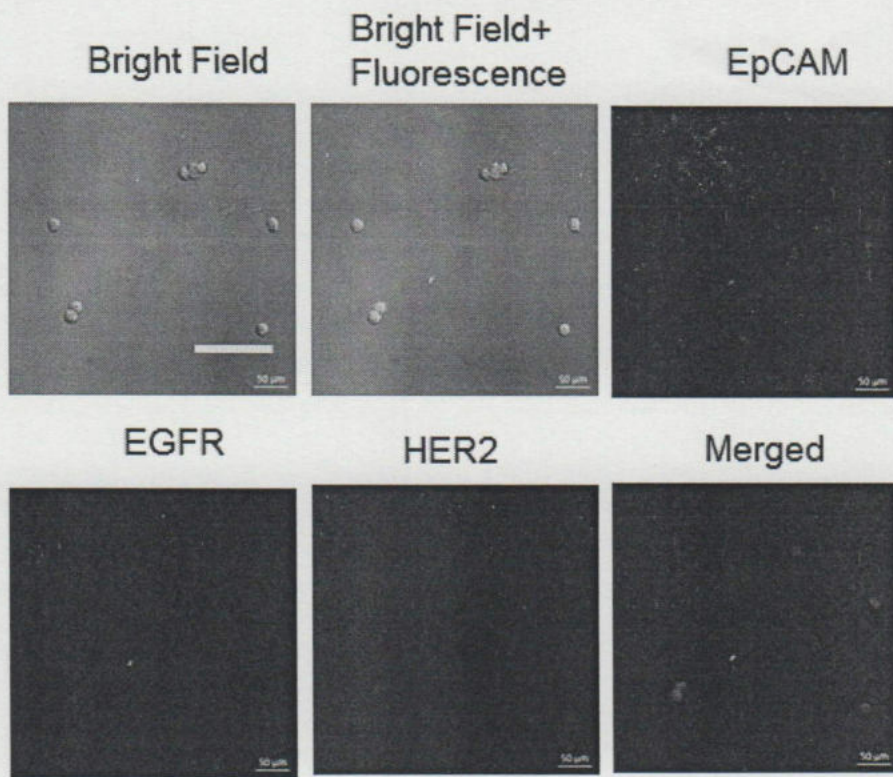
Figure 2.20. Detection of the surface marker expression in MCF-7 cells based on fluorescent microscopy. Three different surface markers (EpCAM, EGFR, and HER2) of the cells were labelled with three different quantum dots of 525, 565 and 625 nm emission wavelength respectively Scale bar 100 μm.
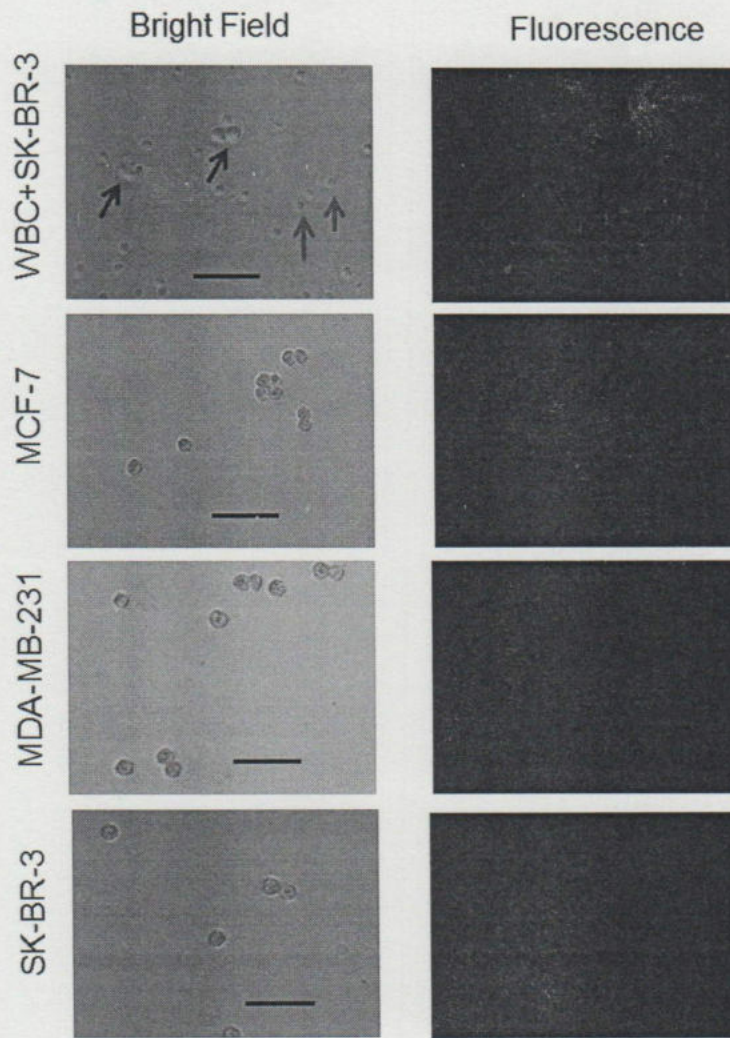
Figure 2.21. Detection of CD-45 surface marker expression on different breast cancer cells and white blood cells (WBC) based on fluorescnt microscopy. Blue arrows-SK-BR-3 cells and red arrows-WBCs. cells.Scale bar 50 μm.

2.3.9. Discussion

Conventially CTCs are detected and characterized by fluorescence microscop. In this study, we also conducted fluorescence microscopic experiments first to detect the expression level of four different surface markers in different breast CTCs. But fluorescent dyes have some photobleaching effect (Figure 2.2), and fluorescent spectra overlap each other (Figure 2.3) when different fluorophores are employed to address multiple cell surface receptor types. In this study three different surface markers (EpCAm, EGFR and HER2)expression level of three different subtypes of breast CTCs (SK-BR-3, MCF-7 and MDA-MB-231) were detected successfully at a time with three different QDs (565nm, 525nm, and 625 nm respectively) (Figure 2.19-21). But when four different surface markers (EGFR, MUC-1, EpCAM and HER2) were labelled with four different QDs (525, 545, 565 and 625nm respectively), the fluorescence spectra overlap each other. Figure 2.3 shows that the fluorescence spectra of 545 nm QDs are overlapped with 525 and 565 nm QDs. These factors limit the multiplexing capability of fluorescent dyes conjugated for cell surface marker detection. Therefore, there is still a need for highly sensitive and specific cell detection methods which show a high multiplexing capability

74

and high reproducibility. In this study we characterized different subtypes of breast CTCs *in situ* using SERS. We prepared multifunctional Raman reporter based hybrid nanoparticles which are capable of simultaneous capturing and *in-situ* characterization of breast CTCs based on SERS (Figure 2.1). The nanoparticles conjugation was characterized by TEM, UV (vis.) spectroscopy and DLS. TEM images of conjugated nanoparticles (Figure 2.4a) exhibit a clear thin white layer of ~5 nm PEG coat. The UV (vis.) spectra of the conjugated nanoparticles (Figure. 2.4b) showed a somewhat decrease of the maximum absorption peak compared with the bare AuNP, which may be due to slight aggregation of the AuNPs or due to the PEG coating. The DLS data demonstrated that the average size of the AuNPs increased in every step of conjugation. The SERS spectra of the conjugated nanoparticles (Figure 2.6) showed comparatively low Raman intensity compared with the bare Raman reporter, which may be due to the scattering shielding effects of the coating layer thickness. Using these R-HNPs the average capture efficiency of the chip was 87.33%

Different subtype of breast CTCs were characterized based on their surface marker expression level. Attachment of each type of R-HNPs to each cell type depends on the expression level of that type of surface marker on the

cell. It is known that, aggregates of nanoparticles induce SERS enhancement because of the large electromagnetic fields at the junctions of the nanoparticles [2.33]. Therefore, hotspots on the cell surfaces were formed depending on their surface antigen expression levels. Where there was more aggregation of R-HNPs, there were more intense SERS spectra. Therefore, the expression levels were calculated based on the intensity of the selected specific Raman bands of the R-HNPs (Figure 2.6). SERS map imaing of the labeled cells were performed to detect the expression level of the surface markers. SERS map images (Figure 2.13-15) shows expression level of the surface antigens of different breast CTCs. The MCF-7 showed highest expression level of EpCAM, the SK-BR-3 cell showed highest expression of HER2 and the MDA-MB-231 cells showed highest expression of EGFR. The average identification accuracy of the captured cells was 93 %.

2.4.   Conclusion

Since fluorescence microscopy has some limitations for multiplex labelling of cells, therefore, SERS may be a unique method for identification and characterization of CTCs. Therefore, this newly developed technique may be

a promising tool for efficient capturing and characterization of CTCs originated from any organ of the body. It can also be applied for multiple labelling of many targeted surface proteins of any cells at a time.

2.5. References

[2.1]   Kumeria, T., Kurkuri, M. D., Diener, K. R., Parkinson, L. & Losic, D. (2012). Label-free reflectrometric interference microchip biosensor based on nanoporous alumina for detection of circulating tumor cells. *Biosensors and Bioelectronics. 35,* 167-173.

[2.2]   Gerges, N., Rak, J. & Jobado, N. (2010). New technologies for the detection of circulating tumour cells. *British Medical Bulletin. 94,* 49-64.

[2.3]   Pantel, K & Alix-Panabieres, C. (2010). Circulating tumour cells in cancer patients: challenges and perspectives. *Trends in Molecular Medicine. 16,* 398-406.

[2.4]   Prang, N., Preithner, K., Brischwein, K., Goster, P., Woppel, A.,

Muller, J., Steiger, C., Peters, M., Baeuerle, P., A. & da Silva A., J. (2005). Cellular and complement-dependent cytotoxicity of Ep-CAM specific monoclonal antibody MT201 against breast cancer cell lines. *British Journal of Cancer. 92,* 342 – 349.

[2.5]   Yoon, H. J., Kim, T., H., Zhang, Z., Azizi, E., Pham, T., M., Paoletti, C., Lin, J., Ramnath, N., Wicha, M., S., Hayes, D., F., Simwone, D., M. & Nagrath, S. (2013) Sensitive capture of circulating tumour cells by functionalized graphene oxide nanosheets. *Nature Nanotechnology. 8,* 735-741 (2013).

[2.6]   Galanzha, E. I., Shashkov, E. V., Kelly, T., Kim, J.-W., Yang, L. & Zharov, V. P. (2009). *In vivo* magnetic enrichment and multiplex photoacoustic detection of circulating tumour cells. *Nature Nanotechnology. 4,* 855 – 860.

[2.7]   Nagrath, S., Sequist, L., V., Maheswararan, S., Bell, D., W., Irimia, D., Ulkaus, L., Smith, M., R., Kwak, E., L., Digumarthy, S., Muzikansky, A., Ryan, P., Balis, U., J., Tompkins, M., R., Haber, D., A. & Toner, M. (2007). Isolation of rare circulating tumour cells in cancer patients by microchip technology. *Nature. 450,* 1235-1239.

78

[2.8] Lee, H., J., Oh, J., H., Park, J., M., Lee, J., G., Kim, M., S., Kim, Y., J., Kang, H., J., Jeong, J., Kim, S., I., Lee, S., S., Choi, J., W., And Huh, N. (2013). Efficient isolation and accurate in situ analysis of circulating tumorcells using detachable beads and a high-pore-density filter. *Angewadte Chemie International Edition.* 52, 8337 –8340.

[2.9] Gupta, V., Jafferji, I., Garza, M., Melnikova, V., O., Hasegawa, D., K., Pethig, R. & Davis D., W. (2012). ApoStream™, a new dielectrophoretic device for antibody independent isolation and recovery of viable cancer cells from blood. *Biomicrofluidics. 6,* 024133.

[2.10] Wang, S., Liu, K., Liu., J., Yu, Z. T. F., Xu, X., Zhao, L., Lee T., Lee, E., K., Reiss, J., Lee, Y., K., Chung, L., W., K., Huang, J., Rettig, M., Seligson, D., Duraiswamy, K., N., Shen, C., K., F. & Tseng, H., R. (2011). Highly efficient capture of circulating tumor cells by using nanostructured silicon substrates with integrated chaotic micromixers. *Angewadte Chemie International Edition.*. 50, 3084-3088.

[2.11] Balasubramanian, S., Kagan, D., Hu, C., M., J., Campuzano, S., Lobo-Castanon, M., S., Lim, N., Kang, D., Y., Zimmerman, M.,

79

Zhang, L. & Wang, J. (2011) Micromachine-enabled capture and isolation of cancer cells in complex media. *Angewadte Chemie International Edition. 50,* 4161-4164.

[2.12] Lazar, D. C. *et al.* (2012). Cytometric comparisons between circulating tumor cells from prostate cancer patients and the prostate-tumor-derived LNCaP cell line. *Physical Biology. 9,* 016002.

[2.13] Chung, Y. –K. *et al.* (2011). An electrical biosensor for the detection of circulating tumor cells. *Biosensor and Bioelectronics. 26,* 2520-2526.

[2.14] Lee, H. J. *et al.* (2013). Simultaneous capture and in situ analysis of circulating tumor cells using multiple hybrid nanoparticles. *Biosensor and Bioelectronics. 47,* 508-514.

[2.15] He, W. *et al.* (2008). Quantitation of circulating tumor cells in blood samples from ovarian and prostate cancer patients using tumor-specific fluorescent ligands. *International Journal of Cancer. 123,* 1968 – 1973

[2.16] Nguyen, C., T., Nguyen, J., T, Rutledge, S., Zhang, J., Wang, Chen

& Walker G.,C. (2010). Detection of chronic lymphocytic leukemia cell surface markers using surface enhanced Raman scattering gold nanoparticles.*Cancer Letters. 292*, 91 -97.

[2.17]   Weissleder, R. (2001). A clearer vision for in vivo imaging. *Nature Biotechnology. 19,* 316-317.

[2.18]   Reinhard, B. M., Siu, M., Agarwal, H., Alivisatos, A. P. & Liphardt. (2005). Calibration of dynamic molecular rulers based on plasmon coupling between gold nanoparticles. *Nano Letters. 5,* 2246- 2252.

[2.19]   Sonnichsen, C. &   Alivisatos, A. P. (2005). Gold nanorods as novel nonbleaching plasmon-based orientation sensors for polarized single-particle microscopy. *Nano Letters. 5,* 301-304.

[2.20]   Aslan, K., Lakowicz, J. R. & Geddes, C. D. (2005). Plasmon light scattering in biology and medicine: new sensing approaches, visions and perspectives. *Current Opinion in Chemical Biology. 9,* 538-544.

[2.21]   Sokolov, K. *et al.* (2003). Real-time vital optical imaging of precancer using anti-epidermal growth factor receptor antibodies conjugated to gold nanoparticles. *Cancer Research. 63,* 1999-2004.

[2.22]   Doering, W. E., Piotti, M. E., Nata, M. J. & Freeman, R. G. (2007). SERS as a foundation for nanoscale optically detected biological labels. *Advancd Materials. 19,* 3100-3108.

[2.23]   Yonzon, C. R., Haynes, L., Zhang, X., Walsh, J.T., Jr., & R. Van Duyne, R.P. (2004). A glucose biosensor based on surface-enhanced Raman scattering: improved partition layer, temporal stability, reversibility, and resistance to serum protein interference. *Analytical Chemistry. 76,* 78-85.

[2.24]   Qian, X. M., Zhou, X. & Nie, S. (2008). Surface-enhanced Raman nanoparticle beacons based on bioconjugated gold nanocrystals and long range plasmonic coupling. *Journal of American Chemical Society. 130,* 14934–14935.

[2.25]   Keren, S. *et al.* (2008). Noninvasive molecular imaging of small living subjects using Raman spectroscopy. *Proceedings of the National Academy of Science. U. S. A. 105,* 5844–5849.

[2.26]   Kneipp, J., Kneipp, H., Wittig, B. & Kneipp, K. (2010). Novel optical nanosensors for probing and imaging live cells. *Nanomedicine: Nanotechnology, Biology and Medicine. 6,* 214–226.

[2.27] Matschulat, A., Drescher, D. & Kneipp, J. (2010). Surface-enhanced Raman scattering hybrid nanoprobe multiplexing and imaging in biological systems. *ACS Nano. 4,* 3259–3269.

[2.28] Doering, W. E. & Nie, S. (2002). Single-molecule and single-nanoparticle SERS: examining the roles of surface active sites and chemical enhancement. *Journal of Physical Chemistry B. 106,* 311-317.

[2.29] Kneipp, J., Kneipp, H. & Kneipp, K. (2008). SERS—a single-molecule and nanoscale tool for bioanalytics. *Chemical Society Review. 37,* 1052–1060.

[2.30] Yang, J. *et al.* (2012). Distinguishing breast cancer cells using surface enhanced Raman scattering. *Analytical and Bioanalytical Chemistry. 402,* 1093-1100.

[2.31] Qian, X. *et al.* (2008). In vivo tumor targeting and spectroscopic detection with surface-enhanced Raman nanoparticle tags. *Nature Biotechnology. 26,* 83-90.

[2.32] Peng, J. & Jordan, V.C. (2010). Expression of estrogen receptor alpha with a Tet-off adenoviral system induces G0/G1 cell cycle

83

arrest in SKBr3 breast cancer cells. *International Journal of Oncology. 36,* 451-458.

[2.33]   Park, H. *et al.* (2009). SERS imaging of HER2-overexpressed MCF7 cells using antibody-conjugated gold nanorods. *Physical Chemistry Chemical Physics. 11,* 7444–7449.

[2.34]   Carron, K. T. & Hurley, L. G. (1991). Axial and azimuthal angle determination with surface-enhanced Raman spectroscopy: thiophenol on copper, silver, and gold metal surfaces. *Journal of Physical Chemistry. 95,* 9979-9984.

[2.35]   Kim, J., H. *et al.* (2006). Nanoparticle Probes with Surface Enhanced Raman Spectroscopic Tags for Cellular cancer targeting.. *Analytical Chemistry. 78,* 7967-6973.

[2.36]   Cáceres, R. C., Martín, B. S. & Barbero, A. F. (2011). Surface-enhanced Raman scattering sensors based on hybrid nanoparticles. *Microsensors.* DOI: 10.5772/18735.

[2.37]   Dey, P. *et al.* (2013). SERS–based detection of barcoded gold nanoparticle assemblies from within animal tissue. *Journal of Raman Spectroscopy. 44,* 1659-1665.

[2.38] Song, W. *et al.* (2007). Surface-enhanced Raman scattering of 4-mercaptopyridine on the surface of TiO_2 nanofibers coated with Ag nanoparticles. *Journal of Physical Chemistry C. 111*, 12786-12791.

Chapter 3

Distinguishing Breast Stem-like Cancer Cells from Breast Circulating Tumor Cells based on Surface-enhanced Raman Spectroscopy

3.1.   Introduction

Recent studies have suggested that, cancer is not only a homogenous mass of rapidly proliferating cells, but it is mass of heterogeneous cancer cells with respect to proliferation and differentiation [3.1]. It has been found that, in several malignancies, a small population of cells is responsible for initiation and maintenance cancer. Those cells are known as stem-like cancer cells (SCCs) [3.2]. Like normal stem cells (NSCs) SCCs are to self- renew and to give rise to a variety of proliferating and differentiated cells that make up the big tumor. Residing in a "stem cell niche" the SCCs maintain them in a stem-like state. SCCs are often remain quiescent and hence may not be affected by the anticancer drugs which are used to target the highly proliferative cells. As a consequence the SCCs can play a crucial role in

86

recurrence after treatment and metastasis [3.3]. Therefore, it is important to find and characterize SCCs in cancer patient for successful cancer therapy. Despite the progress in diagnosis and treatment of breast cancer it is still a leading cause of cancer related deaths among women, with approximately 40% relapse and 60-70% of these recurrences are being due to distant metastasis [3.4]. In case of metastatic cancer tumor cells enter into the blood stream and circulate through the general blood circulation then they are termed as circulating tumor cells (CTCs). SCCs may also enter the general circulation through Epithelial-mesenchymal transition (EMT) pathway and they are termed as stem-like CTCs (SCTCs). Detection of CTCs in the peripheral blood of patient is important for prognosis monitoring in case of personalized cancer therapy [3.5-6]. Since the SCCs reside the stem-cell niche, therefore, it is better to find the SCTCs in the peripheral blood for selecting effective anticancer drugs.

Previously SCTCs were distinguished from CTCs using immunofluorescence technique [3.7], but the limitation of the technique is the photobleaching property of the fluorophores. Furthermore fluorescence spectra overlap each other when more than 4 fluorophores are used to label the cell surface markers simultenously [3.8]. Therefore, there is still a need

87

for highly sensitive and specific cell detection methods which show a high multiplexing capability and high reproducibility.

Gold nanoprobes have been considered as a good alternative because of their non- cytotoxicity, water solubility, long-term stability and good biocompatibility [3.9-12]. The surface- enhanced Raman scattering (SERS) technique opens up a new application era of Raman spectroscopy, because these kinds of nanoparticles have shown promise in overcoming the low sensitivity problem inherent in conventional Raman spectroscopy [3.13-14]. SERS nanotags have several advantages, such as resistance to photobleaching, narrow spectral bands, high spectral specificity, and multiplexing capabilities [3.15-21]. In this study, we prepared multifunctional Raman reporter based SERS nanotags (SNTs) to distinguish breast SCCs from breast CTCs *in-situ* using SERS (Figure 3.1). The cells were characterized based on their surface marker expression level.
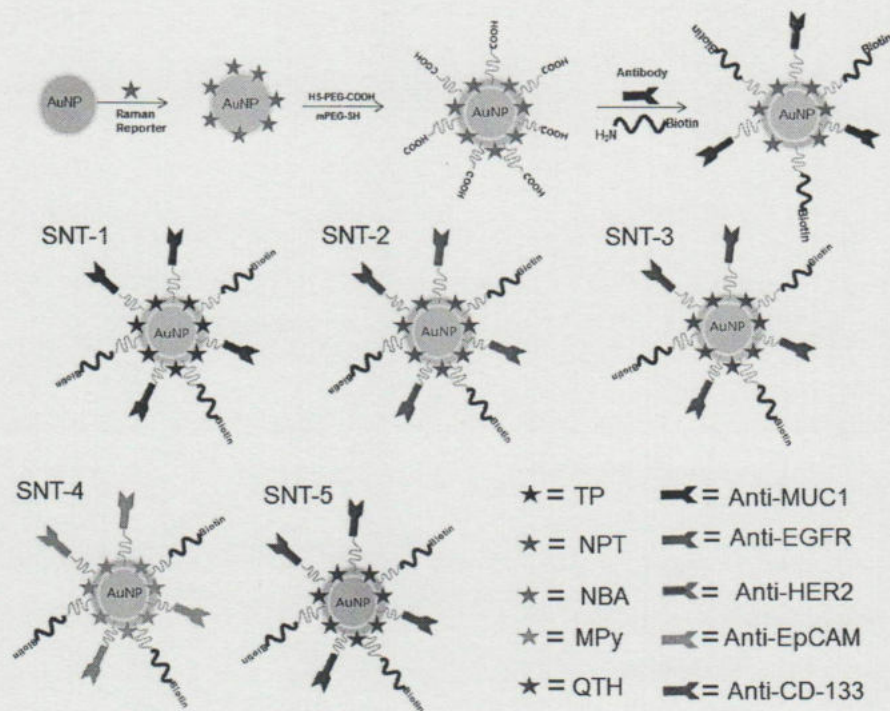
Figure 3.1. Schematic diagram for conjugation of 5 SERS nanotags (SNTs)

3.2. Materials and Methods

3.2.1. Materials

Gold colloids were obtained from BB International-UK. Thiophenol (TP), nile blue A (NBA), 1-naphthalenethiol (NPT), 4-mercaptopyridine (MPy), 2-quinolinethiol (QTH), ethyl dimethylaminopropyl carbodiimide (EDC), N-

hydroxy sulfosuccinimide, 2-(N-Morpholino) ethanesulfonic acid hydrate, 3-aminopropyltriethoxysilane, glutaraldehyde, streptavidin, formaldehyde and phosphate buffered saline (PBS) (pH 7.4, 10 mM from Sigma Aldrich -USA . Mouse monoclonal IgG anti-EpCAM, anti-EGFR, anti-HER2 and anti-CD-133 were collected from R & D systems. RPMI-1640 medium was purchased from Fresh media^{TM}, Daegu, South Korea. Human breast cancer stem cell culture undifferentiation media was purchased from Celprogen, Torrance, CA. Fetal bovine serum (FBS), antibiotics (penicillin–streptomycin, 10,000 IU/ml of penicillin sodium, and 10,000 mg/ml of streptomycin sulfate in 0.83% saline), and Trypsin (Trypsin –EDTA solution, 1X) were obtained from Welgene Inc. mPEG-SH (MW 5 kDa), heterofunctional linker HS-PEG-COOH (MW 5 kDa) from creative PEG Works were used. NH_2-DNA and biotin-DNA was collected from Bioneer, Daejon, Korea. Restriction enzyme Alu I was purchased from Sigma Aldrich.. Streptavidin conjugated quantum dots (525, 545, 565, 625 and 705 nm emission wavelength) were collected from Invitrogen (USA). BD Vacutainer® CPT™ cell preparation tubes were collected from BD Franklin Lakes, NJ. Ficoll-Paque plus were purchased from GE Healthcare Inc. Other chemicals were all of analytical grade. All solutions were prepared with double-distilled water, which was purified using a Milli-Q purification system (Branstead) to a specific

90

resistance of 418 MΩ cm.

3.2.2.   Fabrication of Microfluidic Chip

The cell chip was fabricated by silicon-on- glass (SOG) technology as described in chapter 2.

3.2.3.   Streptavidin Coating on the Glass Chip Surface

Streptavidin was coated on the glass surface following the method described in chapter 2.

3.2.4. Preparation of Conjugated SERS nanotags (SNTs)

In this work we prepared five different combinations of SNTs. Each type of SNT was prepared as described by Ximei Qian *et al.*, 2008 [3.22]. Figure 3.1 shows the illustrations of the step by step conjugation process of the GNP/Raman reporter/PEG/antibody/DNA conjugate. Briefly, SERS active probes were prepared by adding a freshly prepared 1-5 µM Raman reporter solution drop wise to a rapidly mixing gold colloid at a 1:6 reporter solution/ Au colloid volume ratio. Different concentrations of different Raman

91

reporters were used to make similar peak intensities in each case. After 10 min, a 10 μM thiol-PEG solution was added drop wise to the Raman-encoded Au colloids, with a minimum ratio of 30,000 PEG-SH molecules per 60-nm Raman-encoded gold particle to stabilize and minimize particle aggregation under various conditions. 293 μl of 1 μM hetero-functional linker HS-PEG-COOH was added drop wise to 3 ml Raman-encoded Au colloids solution in a polypropylene tube under rapid mixing. After 15 min of mixing, the gold nanoparticles (AuNPs) were exposed to a large volume of PEG-SH (1.6 ml at 10mM) to fill the areas not covered by the hetero-functional PEG, yielding well-shielded and stable particle surfaces. Before covalent ligand conjugation at the carboxylic acid functional groups, the GNPs were purified by three rounds of centrifugation (1,000g) and re-suspension in PBS. To activate the -COOH groups on the particle surface for covalent conjugation, freshly prepared ethyl dimethylaminopropyl carbodiimide (EDC) solution (5 ml) at a concentration of 40mg/ml) and sulfo-NHS (5 ml at 110 mg/ml) were mixed vigorously at 25 °C for 15 min. Excess EDC and sulfo-NHS were separated from the activated nanoparticles by three rounds of centrifugation (1,000g) and re-suspended in PBS. The purified GNPs with activated carboxyl groups were then reacted with the mouse monoclonal antibody (11.2 nmol) and H_2N-dsDNA-biotin (20 nmol)

92

at 25 °C for 2 h, and the reaction mixture was stored at 4 °C for overnight. Excess antibody and DNA was removed by three rounds of centrifugation (1,000g) and re-suspended in PBS.

Five different multifunctional SNTs were prepared with fiver different combinations. The fully functionalized SERS nanotags (SNTs) were characterized by transmission electron microscopy (TEM), UV-(vis.) spectroscopy, dynamic light scattering and SERS. UV (vis.) spectra were measured using Jasco V-530 UV/VIS spectrophotometer. The TEM images were acquired by using a JEOL transmission electron microscope (JEM1010) with an accelerating voltage of 80 kV.

3.2.5. Culturing of Cells

Three Breast cancer cell (BCC) lines (MCF-7, MDA-MB-231, and SK-BR-3) and one breast stem-like cancer cell (SCCs) line were obtained from ATCC (Manassas, VA). The BCCc were cultured at 37^0C in RPMI-1640 medium supplemented with 10% heat inactivated fetal bovine serum and 1% antibiotics (streptomycin and penicillin), and breast SCCs were cultured in human breast cancer stem cell undifferetiation media in a humidified

atmosphere of 95% air with 5% CO_2. The cells were grown at in TC-grade Petri dish. At 80% confluence the BCCs cells were sub-cultured at a density of 1×10^5 cells/ml and the breast SCCs 1×10^6 cells/ml on culture plates, and then incubated for 2–3 days.

3.2.6. Preparation of Cells Suspension

48 hours after sub-culturing (incubation 37 $^\circ$C, 5% CO_2), the cells were detached from the cell culture dishes by trypsin and washed twice with PBS to remove the trypsin. Then the cell pellet was re-suspended in respective medium medium. Then 1.5 ml of 1% bovine serum albumin was added, and the cells were incubated for 1 h. This is the blocking process to reduce nonspecific binding of antibody-conjugated AuNPs.

3.2.7. Handling of Healthy Human Blood

All healthy human blood samples (7.5-15 ml) were obtained from Health centre of the Sogang University (Seoul, Korea), and this work was approved by the Institutional Review Board (IRB). The blood samples were collected

94

using BD Vacutainer® CPT™ cell preparation tubes (BD Franklin Lakes, NJ) containing sodium heparin and polyester gel. After gentle mixing, the fresh blood was gently diluted twice with PBS. As CTCs exist in the buffy coat layer, we used a density gradient reagent (Ficoll-Paque plus, GE Healthcare Inc.) to get the buffy coat. In a centrifuge tube 6 ml of Ficoll-Paque plus was taken followed by carefully adding 8 ml of diluted blood without mixing with Ficoll and centrifuged at room temperature for 30 min at 400 g. After centrifugation, the plasma layer was removed carefully from the top and the low density buffy coat cell layer containing lymphocytes, monocytes was collected leaving the Ficoll and RBC sediment in the centrifuge tube. After collection the cells were transferred into a new tube, washed with PBS and fixed with 3.7% forladehyde for 10 min. The cells were then washed with PBS, counted and stored at 4°C for next use.

3.2.8. Labeling of Cells with Conjugated SERS Nanotags

100 suspended cells of each subtype (MCF-7, SK-BR-3 and MDA-MB-231) were mixed with the fixed white blood cells (WBC) suspension and then incubated with 10 pM conjugated SERS nanoparticles with constant mixing

95

for 30 min at room temperature to label the target cells. Then, the cells were washed three times and re-suspended in 2 ml respective medium before capturing the CTCs in microfluidic chip.

3.2.9. Capturing of Labeled Cells on the Streptavidin Coated Glass Chip for Measuring SERS

The SNTs treated cells suspension (containing 100 spiking cells) were infused through the microfluidic channel at a flow rate 10μl/min and incubated at room temperature for 1 hour to immobilize on the chip surface. Then the chip was washed with respective medium to remove the debrish or unbound cells.

3.2.10. SERS Mapping for Visualization of the Distribution of Surface Markers on the Cells and Their Characterization

NTEGRA spectra (AFM-Raman Spectrometer, NT-MDT, Russia) equipped with a liquid nitrogen-cooled CCD detector and an inverted optical microscope (Olympus IX71) was used for SERS mapping of cells. SERS

mapping were recorded using a laser of 785 nm NIR wavelengths with a laser power 3 mW on the sample plane. The SERS data were analyzed using Nova software [44]

3.2.11. Labeling of Cells with Quantum dots (QDs)

For fluorescence microscopic imaging the cells surface markers were labeled with quantum dots (QDs). Different surface markers (EpCAM, EGFR, HER2 and CD-133) of each cell types were labeled with different streptavidin conjugated QDs (525, 565, 625 and 705 nm emission wavelength respectively). Surface marker specific biotinylated antibodies were used to label the cells with different QDs. In the antibody-QDs conjugates, the antibody and QDs were mixed with a molar ratio of 2.5:1 and incubated in dark condition for 2 hrs at room temperature. Then the conjugates were purified by centrifugation at 3,000g for 10 min and resuspension in PBS. The suspended fixed cells of each subtypes (MCF-7, SK-BR-3 and MDA-MB-231) and the breast SCCs were mixed with 1 pM of each antibody conjugated QDs and incubated with constant mixing for 30 min at room temperature to label the cells. Then the cells were washed PBS three times and re-suspended in PBS before measuring fluorescence.

3.2.12. Fluorescence Microscopic Examination

The quantum dots labeled suspended cells were transferred into 96 well plates and observed under fluorescent microscope. The fluorescence images were acquired with Nikon ECLIPSE- Ti microscope with 400x magnification. The fluorescence data were analyzed using NIS-Elements-BR-3.2 software

3.3.   Results and Discussion

3.3.1.   Preparation of Conjugated SERS nanotags (SNTs)

Five different multifunctional SNTss were prepared with fiver different combinations. The fully functionalized SERS nanotags (SNTs) were characterized by transmission electron microscopy (TEM), UV-vis. spectroscopy, dynamic light scattering and SERS. UV-vis. spectra were measured using Jasco V-530 UV/VIS spectrophotometer. The TEM images were acquired by using a JEOL transmission electron microscope (JEM1010) with an accelerating voltage of 80 kV.

3.3.2. Visualization of Nanoparticle's Structure using Transmission Electron Microscopy (TEM)

Multi-functional SERS nanotags (SNTs) were fabricated which composed of 60 nm size gold nanoparticles (AuNPs) Raman reporters, heterofunctional HS-PEG-COOH, antibody and amine terminated biotinylated dsDNA (Figure 3.1). Figure 3.2a shows the TEM images of bare AuNP, Raman reporter encoded AuNPs and PEG–antibody/dsDNA conjugated AuNP. The core particle size is of the gold colloid is 60 nm, the PEG coating was clearly observed as a thin white layer by TEM image.

3.3.3. Determination of the Localized Surface Plasmon Absorbance through UV-vis. Spectroscopy

Figure 3.2b demonstrates the UV-vis. spectra of bare AuNPs, Raman encoded AuNPs and PEG–antibody/dsDNA conjugated AuNP. The spectrum of the pure AuNPs showed a maximum absorption at 530 nm due to Plasmon Resonance [3.22]. The Raman reporter coated AuNPs showed a slight decrease of the maximum absorption peak, which may be
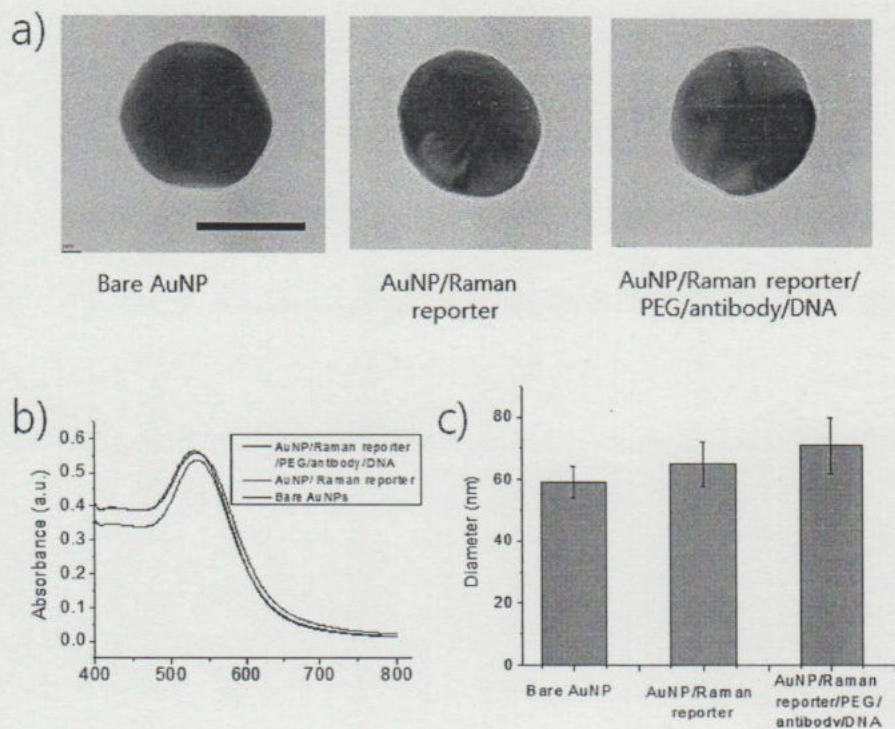
Figure 3.2. Confirmation of conjugation of SERS nanotags (SNTs) through TEM, UV-vis. spectroscopy and DLS. a) TEM images of bare AuNP, Raman reporter encoded AuNPs, and Raman reporter, PEG, antibody and DNA conjugated AuNP. b) UV-vis. spectra of bare AuNP, Raman reporter encoded AuNPs, and Raman reporter, PEG, and antibody conjugated AuNP. Scale bar 50 nm.

100

due slight aggregation of the GNPs by the Raman reporters. The PEG-conjugated SERS probes showed a somewhat more decrease of the maximum absorption peak and a red shift of ~6 nm. This may be due to PEG coating, and reduction of the concentration of AuNPs during washing steps.

3.3.4. Determination of the Size Distribution through Dynamic light Scattering (DLS)

Fig. 3.2c Shows dynamic light scattering (DLS) size data obtained from the bare AuNPs Raman-encoded and PEG-stabilized antibody/dsDNA modified AuNPs as shown in (a). At a core the particle size is 60 nm, the average size is increased to 70 nm after Raman reporter immobilization, whereas the particle's 'wet' hydrodynamic diameter increased by 15 nm after pegylation.

3.3.5. Surface-enhanced Raman spectroscopy (SERS) of SERS Nanotags (SNTs)

Fig. 3.3 shows the corresponding SERS spectra of the pure Raman reporter and the conjugated naoparticles. The pure Raman reporter molecules showed

relatively much stronger SERS signals than the PEG/antibody/dsDNA conjugated SERS nanotags. The SERS intensity of the Raman reporters gradually decreased with the increase in the coating layer thickness because of the scattering shielding effects [3.23]. Still the final antibody-conjugated SNTs have a strong SERS intensity, and they are suitable to use in cellular SERS imaging studies. The SERS spectrum of thiophenol (TP) showed one dominant peaks at 1575 cm^{-1} (Figure 3.3c), which is assigned to the a1 mode of the TP molecule [2.24]. One strong band at 1381 cm^{-1} was observed for the 1-naphthalenethiol (NPT) molecules on the AuNPs (Figure 3.3b), which was due to ring stretching of the NPT molecule [2.25]. In case of nile blue A (NBA) there was a strong peak at 1492 cm^{-1} (Figure 3.3d), which corresponds to the aromatic ring stretching [2.26]. The SERS spectrum of 2-quinolinethiol (QTH) showed one strong peak at 1369 cm^{-1} (Figure 3.3e) which correspons to the aromatic υ(CC) vibration [2.27]. In case of 4-mercaptopyridine (MPy) there is one dominant peaks at 1096 cm^{-1} (Figure 3.3a), which corresponds to the aromatic ring vibration mode [2.28]. The Raman band 1575, 1381, 1492, 1096 and 1369 cm^{-1} of SNT-1, SNT-2, SNT-3, SNT-4 and SNT -5 were selected to detect the expression level of MUC1, EGFR, HER2, EpCAM, and CD-133 respectively.

102
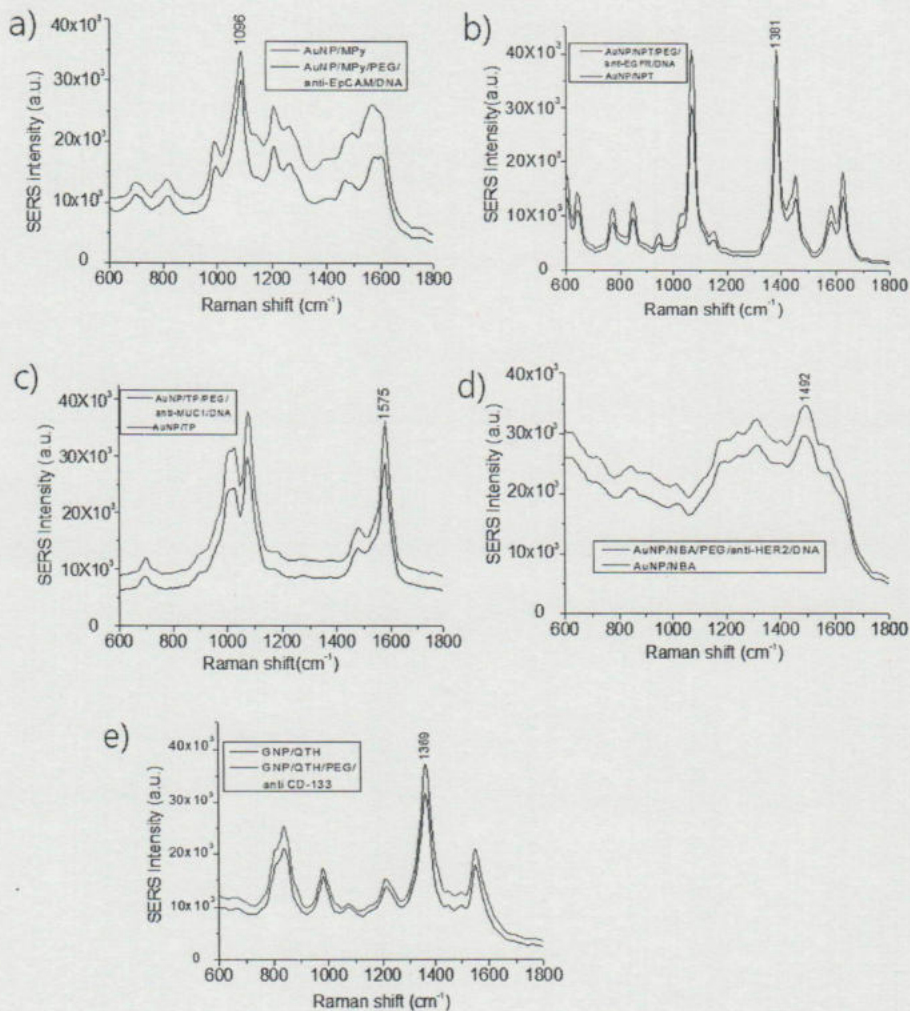
Figure 3.3. SERS Spectra of the SERS nanotags (SNTs). a) SERS spectrum of 4-mercaptopyridine (MPy) immobilized on AuNP (red curve), and MPy, PEG, anti-Epcam and DNA immobilized on AuNPs (black curve). b) SERS spectrum of 1-naphthalenethiol (NPT) immobilized on AuNP (red curve),

and NPT, PEG, anti-HER2 and DNA immobilized on AuNPs (black curve).

c) SERS spectrum of Thiophenol (TP) immobilized on AuNP (red curve), and TP, PEG, anti-MUC1 and DNA immobilized on AuNPs (black curve).

d) SERS spectrum of Nile blue A (NBA) immobilized on AuNP (red curve), and NBA, PEG, anti-HER2 and DNA immobilized on AuNPs (black curve).

e) SERS spectrum of 2-quinolinethiol (QTH) immobilized on AuNP (red curve), and QTH, PEG, anti-CD-45 and DNA immobilized on AuNPs (black curve).
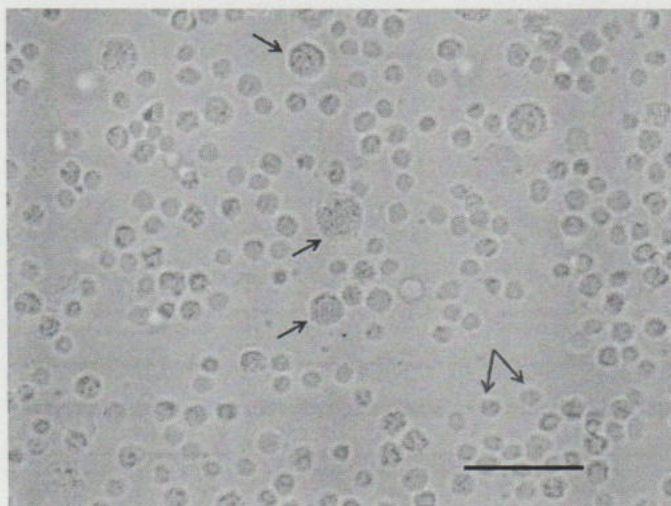
Figure 3.4. Labelling of breast CTCs and breast SCTCs with SERS nanotags in a mixture of white blood cell suspension. Red arrows indicate CTCs or CSCs, and purple arrows indicate White blood cells

104

3.3.6. Capturing of Labeled Cells on the Streptavidin Coated Glass Chip for Measuring SERS

SNTs labelled cells (100 of each type) (Figure 3.4) were infused mixed with normal WBCs suspension through the microfluidic channel with help of a syringe pump at a flow rate 10 μl/min. During flowing, due to large size of the CTCs and SCTCs they were easily come in contact on the strepatividin coated surface of the pillars and captured on it. Among three different kind of breast CTCs the SK-BR-3 cells showed highes capturing efficiency, as SK-BR-3 cells show greater expression level of most of the surface markers (EpCAM, EGFR, and HER2). In case of MDA-MB-231 cells, which have relatively low surface protein expression level, but the capture efficiency was still high (89%), this may be due to the larger diameter of MDA-MB-231 cells, allowing for higher chance of contact with the streptavidin-coated pillars (Figure 3.5). The lower capture efficiency in MCF-7 and breast SCTCs may be due to their smaller size (Figure 3.5).

The capturing efficiency was 91%, 90%, 84% and 75% in case of SK-BR-3, MDA-MB-231 MCF-7 and breast SCTCs respectively (Figure 3.6). After capturing the cells in the microfluidic channel the chip was washed with respective media, and then SERS mapping was performed.
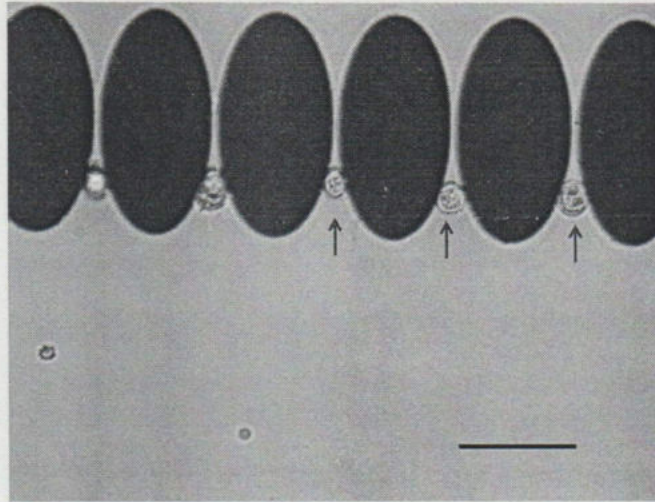
Figure 3.5. Captured breast CTCs or breast SCTCs (red arrows) in microfluidic chip. Scale bar 50 μm.
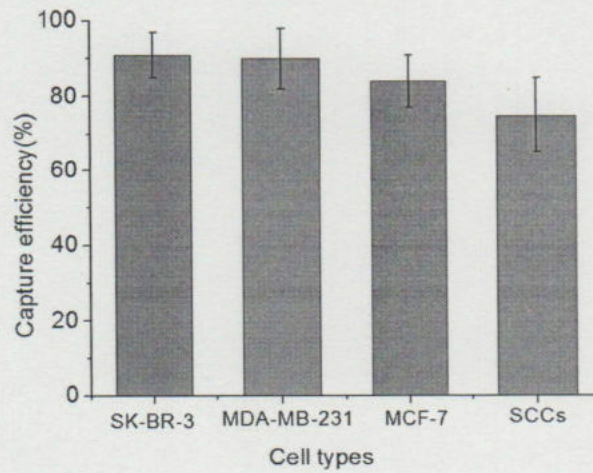
Figure 3.6. Capturing efficiency of breast CTCs and breast SCTCs. Error bars indicate standard deviation of three independent experiments.

3.3.7. SERS Mapping for the Distribution of Surface Markers on the Cells and Their Characterization

NTEGRA spectra (AFM-Raman Spectrometer, NT-MDT, Russia) equipped with a liquid nitrogen-cooled CCD detector and an inverted optical microscope (Olympus IX71) was used for SERS mapping of cells. SERS mapping were recorded using a laser of 785 nm NIR wavelengths with a laser power 3 mW on the sample plane. The SERS data were analyzed using Nova software

The multifunctional SNTs were attached to each cell type to detect the expression level of EpCAM, EGFR, HER2 and CD-133 surface antigens. Attachment of each type of SNTs to each cell type depends on the expression level of that type of surface marker on the cell. Therefore, the expression levels were calculated based on the intensity of the selected specific Raman bands of the SNTs (Figure 3.2). SERS mapping of the labelled cells was performed to detect the expression level of the surface markers. Figure 3.7-10 shows the surface marker expression level for MCF-7, SK-BR-3, and MDA-MB-231 and breast SCTCs. In case MDA-MB-231 cells EGFR expression is highest, followed by MUC1, EpCAM, CD-133 and HER2. In case SK-BR-3 cells HER2 expression is highest, followed by EpCAM,

107

EGFR, MUC1, and CD-133. In case MCF-7 cells EpCAM expression is highest, followed by EGFR, HER2, CD-133 and MUC1. In case breast SCCs CD-133 expression is highest, followed by HER2, EGFR, EpCAM and MUC1. The vertical scale bar on the right side of each map shows the expression level of the cells. The histograms are showing the comparative expression level of each surface marker. On the other hand the non labelled cell did not show any surface marker distribution. The identification accuracy of the captured cells was 96 % in SK-BR-3, 95 % in MCF-7, 90 % in MDA-MB-231 and 89 % in breast SCCs
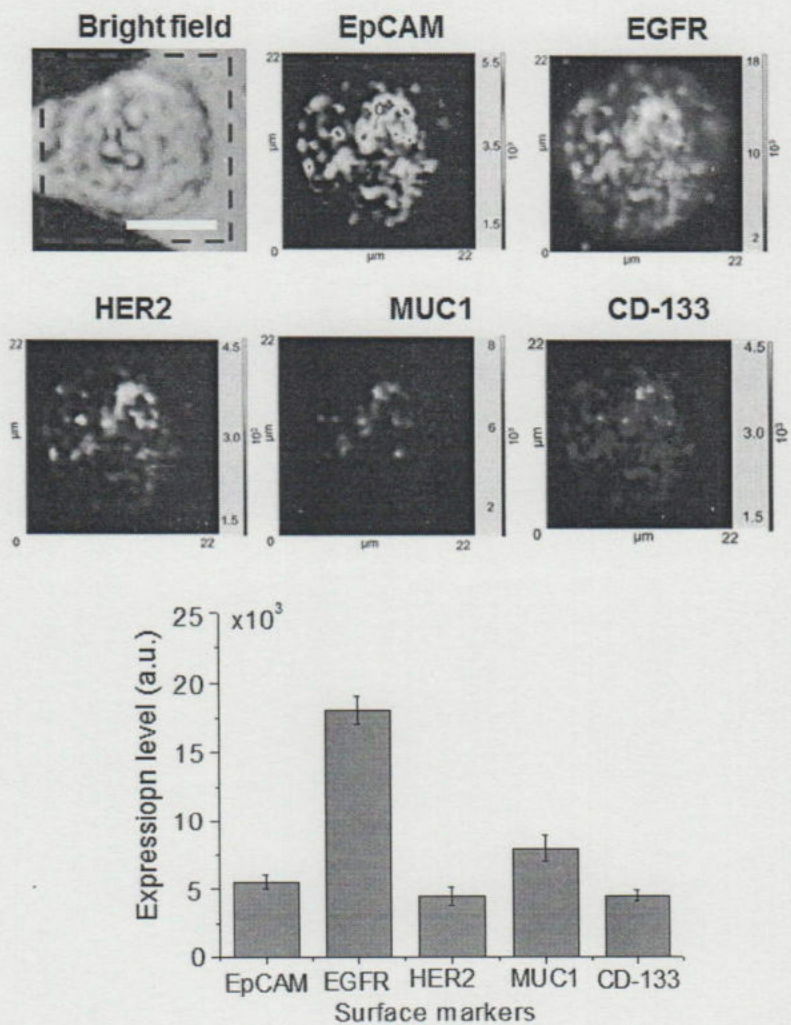
Figure 3.7. Detection of expression level in MDA-MB-231 cells based on SERS map imaging. Scale bar 10 μm. Bar graph shows the expression level of different surface markers. Error bars indicate standard deviation of three independent experiments.

109

Figure 3.8. Detection of expression level in SK-BR-3 cells based on SERS map imaging. Scale bar 10 μm. Bar graph shows the expression level of different surface markers. Error bars indicate standard deviation of three independent experiments.

110
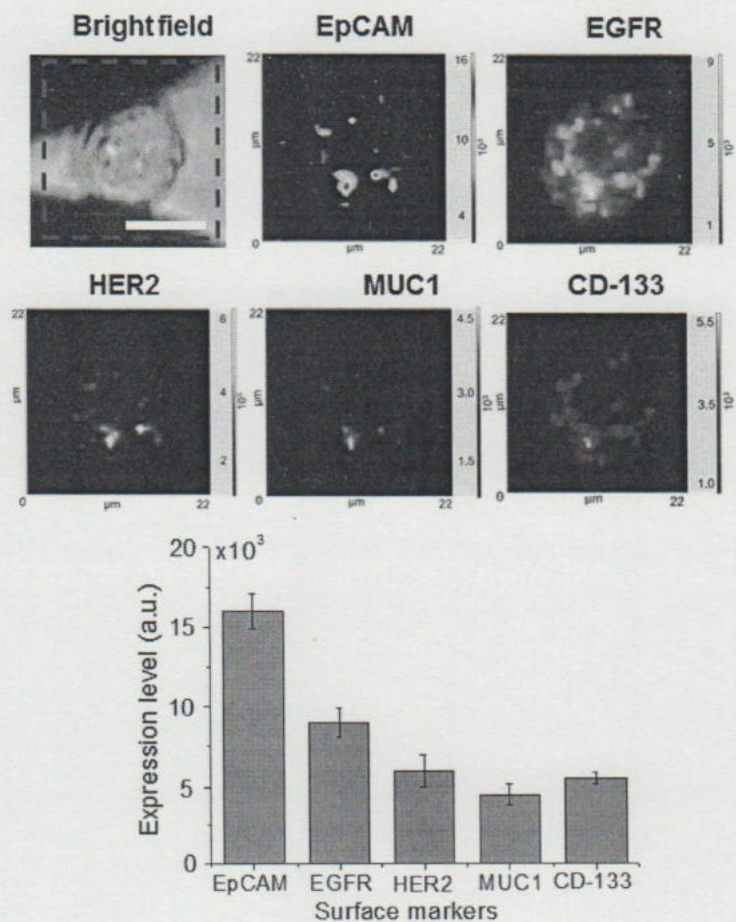
Figure 3.9. Detection of expression level in MCF-7 cells based on SERS map imaging. Scale bar 10 μm. Bar graph shows the expression level of different surface markers. Error bars indicate standard deviation of three independent experiments.

111
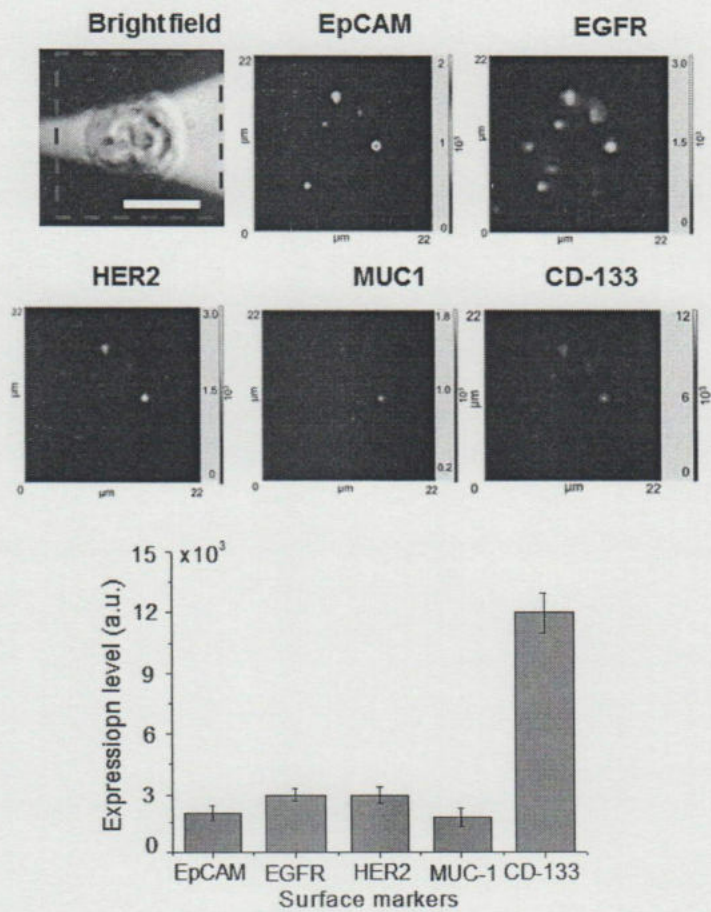
Figure 3.10. Detection of expression level in breast SCCs based on SERS mapping. Scale bar 10 μm. Bar graph shows the expression level of different surface markers. Error bars indicate standard deviation of three independent experiments.

3.3.8. Detachment and collection of the cells from chip surface after characterization

After detection and characterization of the CTCs, the cells were collected from the chip for further experiments. The cells were detached by cleaving the DNA using restriction enzyme. The collected cells were grown in petridish as shown in Fig.3.11.
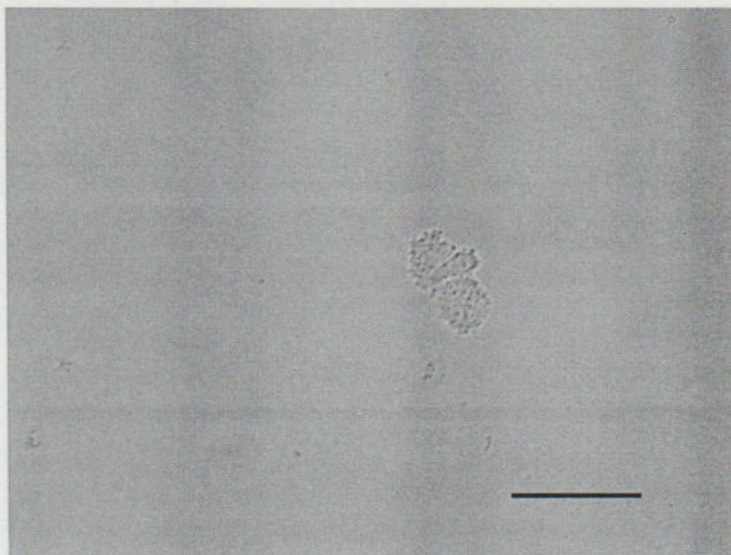
Figure 3.11. Culturing of the collected breast SCCs after characterization. Bright field image of breast SCCs 48 hours after collection and culturing. Scale bar 50 μm.

3.3.9. Detection of Expression Level through Fluorescence

Figure 3.12-15 shows the surface marker expression level of different breast CTCs and SCTCs as measured by fluorescent microscope. In case SK-BR-3 cells (Figure 3.12) HER2 expression is highest, followed by EGFR, EpCAM and CD-133. In case MDA-MD-231 cells (Figure 3.13) EGFR expression is highest followed by HER2, EpCAM and CD-133. In case MCF-7 cells (Figure 3.14) EpCAM expression is highest followed by EGFR., HER2 and CD-133. In case of breast SCTCs cells (Figure 3.15) CD-133 expression is highest followed by HER2, EGFR and EpCAM.

114
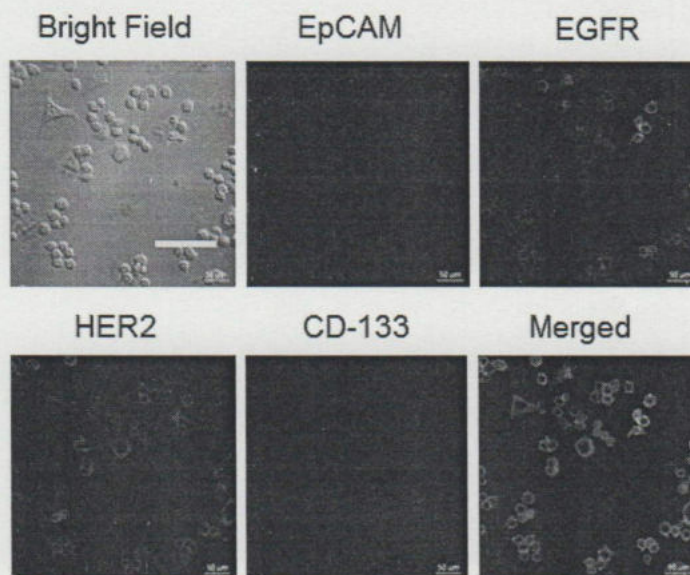
Figure 3.12. Detection of expression level of SK-BR-3 cells based on fluorescence microscopiy. Four surface markers (EpCAM, EGFR, HER2 and CD-133) of the cells were labelled with quantum dots of 525, 565, 625 and 625 nm emission wavelength respectively. Scale bar 100 μm.
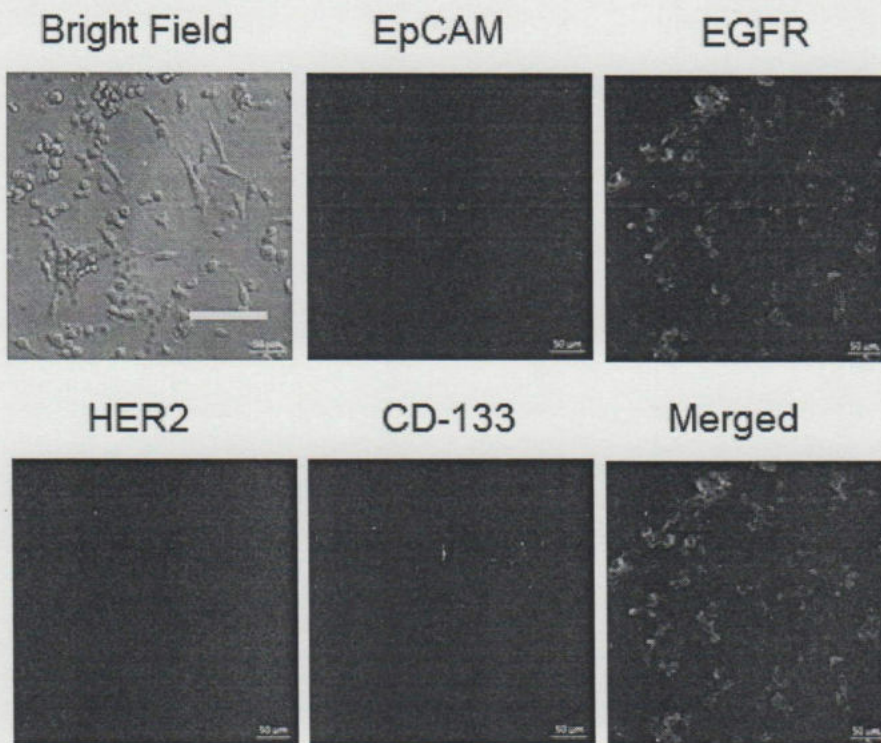
Figure 3.13. Detection of expression level of MDA-MB-231 cells based on fluorescence microscopiy. Scale bar 100 μm. Four surface markers (EpCAM, EGFR, HER2 and CD-133) of the cells were labelled with quantum dots of 525, 565, 625 and 625 nm emission wavelength respectively. Scale bar 100 μm.
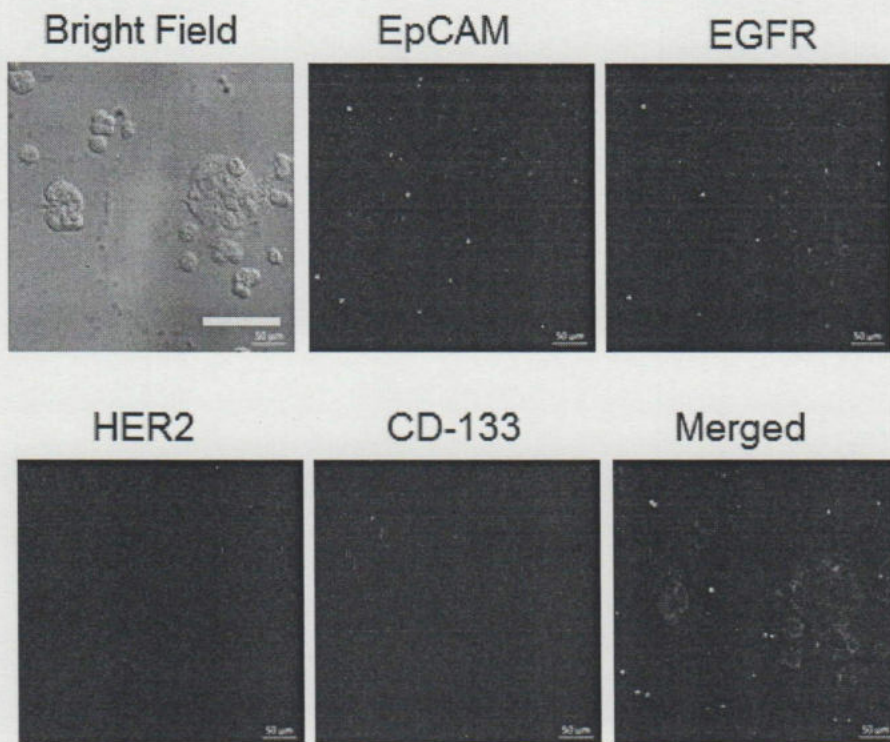
Figure 3.14. Detection of expression level of MCF-7 cells based on fluorescence microscopiy. Scale bar 100 μm. Four surface markers (EpCAM, EGFR, HER2 and CD-133) of the cells were labelled with quantum dots of 525, 565, 625 and 625 nm emission wavelength respectively. Scale bar 100 μm.
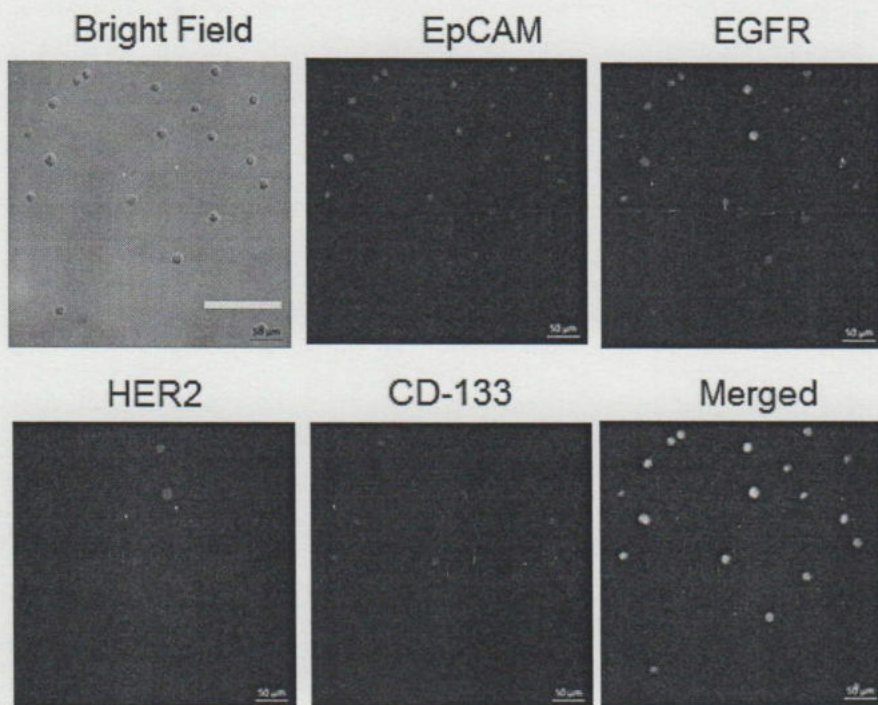
Figure 3.15. Detection of expression level of breast SCCs based on fluorescent microscopy. Four surface markers (EpCAM, EGFR, HER2 and CD-133) of the cells were labelled with quantum dots of 525, 565, 625 and 625 nm emission wavelength respectively. In case of 705 nm emission wavelength quantum dots the red fluorescent color was replaced by a pseudocolor (purple). Scale bar 100 μm.

118
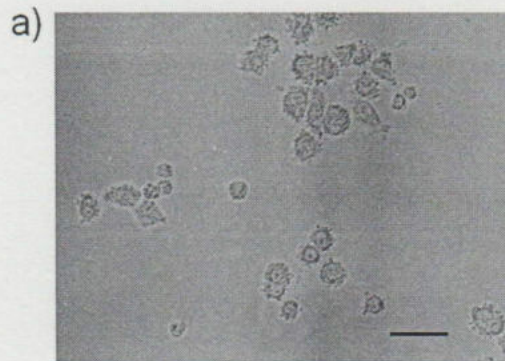
Undifferentiated breast SCCs
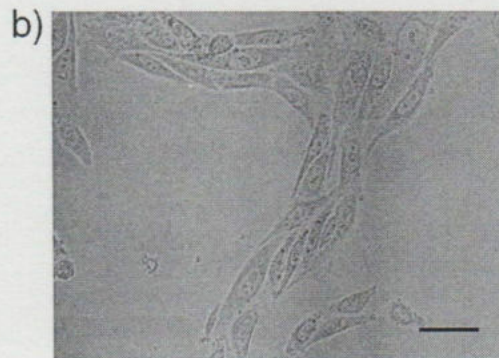
Differentiated breast SCCs

Figure 3.16. Light microscopic images showing morphology of a) undifferentiated and b) differentiated breast SCCs. Scale bar 25 μm.

3.3.10. Morphological differences between undifferentiated and differentiated Breast SCCs

119

Figure 3.16 shows the morphological differences between undifferentiated and differentiated cells. The undifferentiated cells are somewhat round shape, but the differentiated cells are elongated.

3.3.11. Detection of Expression level of undifferentiated Breast SCCs

Figure 3.17 shows the surface marker expression of undifferentiated breast cancer cells. Among five surface markers CD-133 expression is highest followed by EGFR, HER2, EpCAM and MUC1.

3.3.12. Detection of Expression level of differentiated Breast SCCs

Figure 3.18 shows the surface marker expression of differentiated breast cancer cells. Among five surface markers HER2 expression is highest followed by EGFR, CD-133, EpCAM and MUC1.
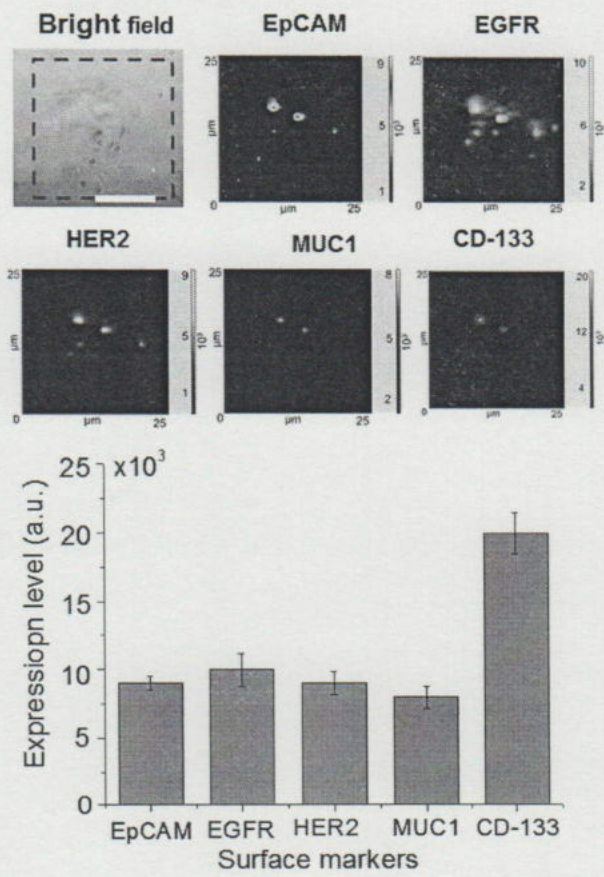
Figure 3.17. Detection of expression level of undifferentiated breast SCCs based on SERS map imaging. Scale bar 10 μm. Bar graph shows the expression level of different surface markers. Error bars indicate standard deviation of three independent experiments.

121
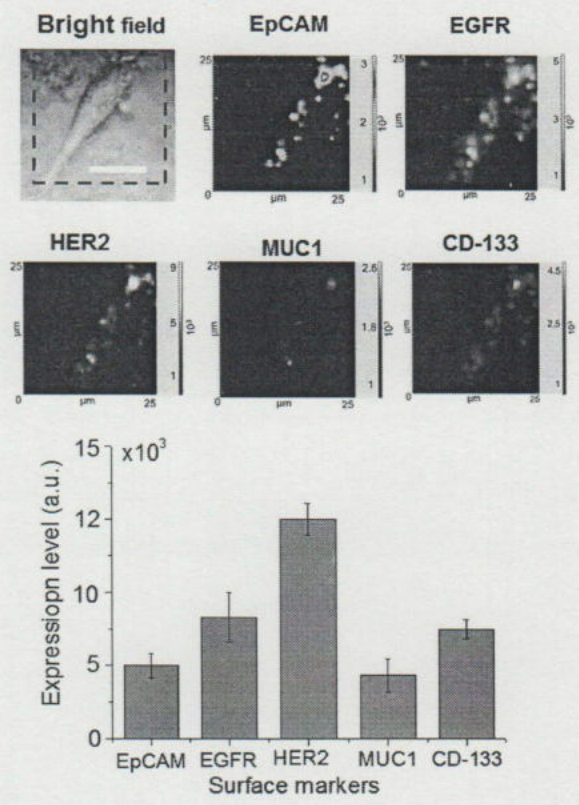
Figure 3.18. Detection of expression level of differentiated breast SCCs based on SERS map imaging. Scale bar 10 μm. Bar graph shows the expression level of different surface markers. Error bars indicate standard deviation of three independent experiments.
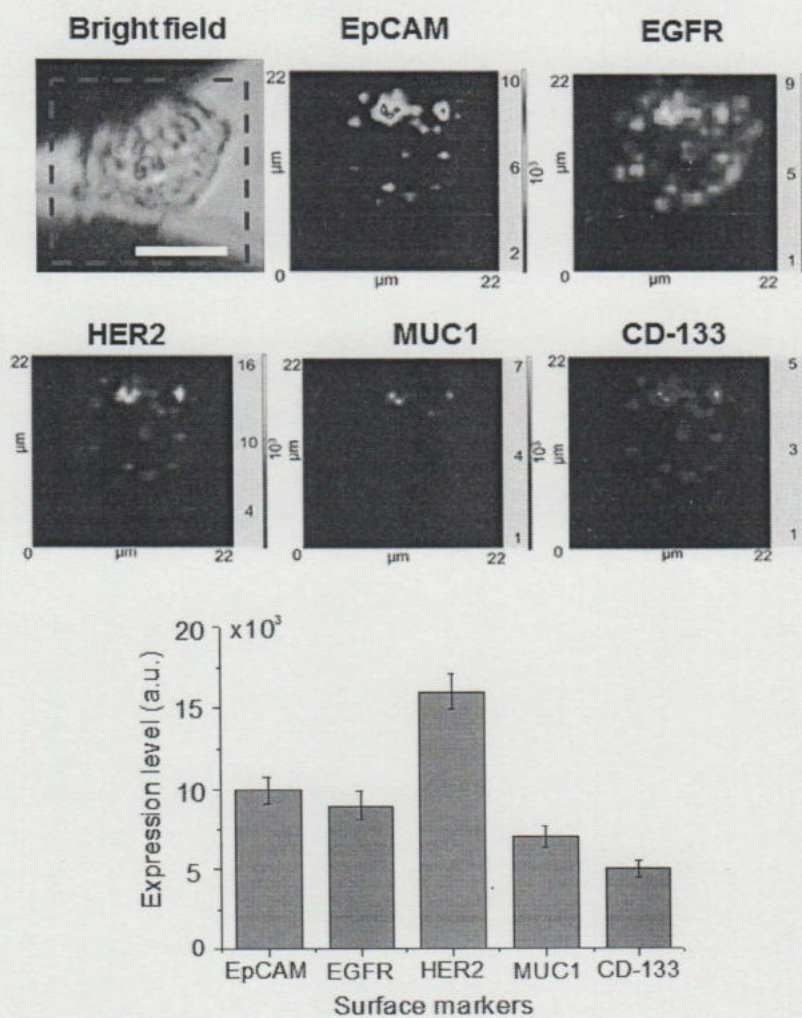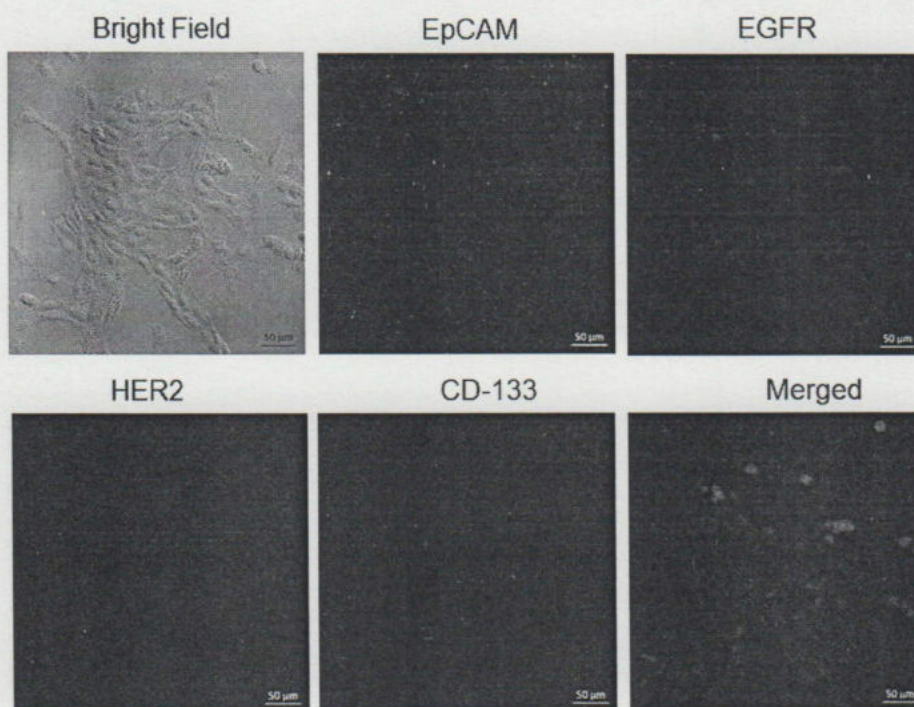
Figure 3.19. Detection of the expression level of differentiated breast SCCs based on fluorescent microscopy. Four surface markers (EpCAM, EGFR, HER2 and CD-133) of the cells were labelled with quantum dots of 525, 565, 625 and 625 nm emission wavelength respectively. In case of 705 nm emission wavelength quantum dots the red fluorescent color was replaced by a pseudocolor (purple). Scale bar 50 μm.

3.4.   Coclusion

Since the numbers of SCTCs are extremely low in the blood, therefore capturing of the SCTCs using multiple antibody may be a unique method of SCTCs detection. Furthermore, due to limitation of fluorescence microscopy for multiplex labelling of cells, SERS may be the best alternative for distinguishing SCTCs from CTCs. The SCTCs were successfully distinguished from the CTCS based on their surface marker expression level using SERS technique. Multifunctional SNTs were fabricated for multiplex labelling of the SCTCs and CTCs. By using the multifunctional SNTs, the SCTCs and the CTCs were captured successfully and different surface marker expression level were detected simultaneously. Therefore, this newly developed technique may be a promising tool for efficient capturing and accurate in situ analysis of the espression level of the the SCTCs and CTCs, and distinguishing them based on it. It can also be applied for multiple labelling of many targeted surface proteins of any cell at a time.

3.5. References

[3.1]   Yi, S. -Y., Hao, Yi.-B., Nan K. –J. & Fan, T. –L. (2013). Cancer stem cell niche: A target for novel cancer therapeutics. *Cancer Treatment Reviews. 39,* 290–296.

[3.2]   Visvader, J. E. & Lindeman, J. E. (2008). Cancer stem cells in solid tumors: accumulating evidence and unresolved questions. *Nature Reviews Cancer. 8*, 755-768.

[3.3]   Trumpp, A. *et al.* (2008). Mechanisms of disease: cancer ctem cells-targeting the evil twin. *Nature Clinical Practice Oncology. 5*, 337-347.

[3.4]   Gangopadhyay, S., Nandy, A., Hor, P. & Mukhopadhyay, A. (2013). Breast cancer stem cells: A novel therapeutic target. *Clinical Breast Cancer. 13,* 7–15.

[3.5]   Gerges, N., Rak, J. & Jobado, N. (2010). New technologies for the detection of circulating tumour cells. *British Medical Bulletin. 94,* 49-64.

[3.6]   Pantel, K & Alix-Panabieres, C. (2010). Circulating tumour

cells in cancer patients: challenges and perspectives. *Trends in Molecular Medicine. 16,* 398-406.

[3.7]   Theodoropoulos, P., A. et al. (2010).   Circulating tumor cells with a putative stem cell photype in peripheral blood of patients with breast cancer. *Cancer Letters. 288,* 99–106.

[3.8]   Nguyen, C., T., Nguyen, J., T, Rutledge, S., Zhang, J., Wang, Chen & Walker G.,C. (2010). Detection of chronic lymphocytic leukemia cell surface markers using surface enhanced Raman scattering gold nanoparticles.*Cancer Letters. 292,* 91 -97.

[3.9]   Reinhard, B. M., Siu, M., Agarwal, H., Alivisatos, A. P. & Liphardt. (2005). Calibration of dynamic molecular rulers based on plasmon coupling between gold nanoparticles. *Nano Letters. 5,* 2246- 2252.

[3.10] Sonnichsen, C. &   Alivisatos, A. P. (2005). Gold nanorods as novel nonbleaching plasmon-based orientation sensors for polarized single-particle microscopy. *Nano Letters. 5,* 301-304.

[3.11] Aslan, K., Lakowicz, J. R. & Geddes, C. D. (2005). Plasmon light scattering in biology and medicine: new sensing approaches, visions

126

and perspectives. *Current Opinion in Chemical Biology. 9,* 538-544.

[3.12] Sokolov, K. *et al.* (2003). Real-time vital optical imaging of precancer using anti-epidermal growth factor receptor antibodies conjugated to gold nanoparticles. *Cancer Research. 63,* 1999-2004.

[3.13] Doering, W. E., Piotti, M. E., Nata, M. J. & Freeman, R. G. (2007). SERS as a foundation for nanoscale optically detected biological labels. *Advancd Materials. 19,* 3100-3108.

[3.14] Yonzon, C. R., Haynes, L., Zhang, X., Walsh, J.T., Jr., & R. Van Duyne, R.P. (2004). A glucose biosensor based on surface-enhanced Raman scattering: improved partition layer, temporal stability, reversibility, and resistance to serum protein interference. *Analytical Chemistry. 76,* 78-85.

[3.15] Qian, X. M., Zhou, X. & Nie, S. (2008). Surface-enhanced Raman nanoparticle beacons based on bioconjugated gold nanocrystals and long range plasmonic coupling. *Journal of American Chemical Society. 130,* 14934–14935.

[3.16] Keren, S. *et al.* (2008). Noninvasive molecular imaging of small living subjects using Raman spectroscopy. *Proceedings of the*

National Academy of Science. U. S. A. 105, 5844–5849.

[3.17] Kneipp, J., Kneipp, H., Wittig, B. & Kneipp, K. (2010). Novel optical nanosensors for probing and imaging live cells. *Nanomedicine: Nanotechnology, Biology and Medicine. 6*, 214–226.

[3.18] Matschulat, A., Drescher, D. & Kneipp, J. (2010). Surface-enhanced Raman scattering hybrid nanoprobe multiplexing and imaging in biological systems. *ACS Nano. 4*, 3259–3269.

[3.19] Doering, W. E. & Nie, S. (2002). Single-molecule and single-nanoparticle SERS: examining the roles of surface active sites and chemical enhancement. *Journal of Physical Chemistry B. 106*, 311-317.

[3.20] Kneipp, J., Kneipp, H. & Kneipp, K. (2008). SERS—a single-molecule and nanoscale tool for bioanalytics. *Chemical Society Review. 37*, 1052–1060.

[3.21] Yang, J. *et al.* (2012). Distinguishing breast cancer cells using surface enhanced Raman scattering. *Analytical and Bioanalytical Chemistry. 402*, 1093-1100.

[3.22] Qian, X. *et al.* (2008). In vivo tumor targeting and spectroscopic detection with surface-enhanced Raman nanoparticle tags. *Nature Biotechnology. 26,* 83-90.

[3.23] Park, H. *et al.* (2009). SERS imaging of HER2-overexpressed MCF7 cells using antibody-conjugated gold nanorods. *Physical Chemistry Chemical Physics. 11,* 7444–7449.

[2.24] Carron, K. T. & Hurley, L. G. (1991). Axial and azimuthal angle determination with surface-enhanced Raman spectroscopy: thiophenol on copper, silver, and gold metal surfaces. *Journal of Physical Chemistry. 95,* 9979-9984.

[2.25]   Kim, J., H. *et al.* (2006). Nanoparticle Probes with Surface Enhanced Raman Spectroscopic Tags for Cellular cancer targeting.. *Analytical Chemistry. 78,* 7967-6973.

[2.26]   Cáceres, R. C., Martín, B. S. & Barbero, A. F. (2011). Surface-enhanced Raman scattering sensors based on hybrid nanoparticles. *Microsensors.* DOI: 10.5772/18735.

[2.27] Dey, P. *et al.* (2013). SERS–based detection of barcoded gold nanoparticle assemblies from within animal tissue. *Journal of*

Raman Spectroscopy. 44, 1659-1665.

[2.28] Song, W. *et al.* (2007). Surface-enhanced Raman scattering of 4-mercaptopyridine on the surface of TiO$_2$ nanofibers coated with Ag nanoparticles. *Journal of Physical Chemistry C. 111,* 12786-12791.

Chapter 4

Detection of miR 200c Expression in Breast Cancer Cells and Breast Stem-like Cancer Cells based on Surface-Enhanced Raman Spectroscopy

4.1. Introduction

Breast cancer is the most common malignant disease in women which causes more than 520,000 deaths worldwide every year [4.1]. Although, early detection and treatment facilities significantly improved due to better understanding the molecular mechanisms, resistance to classical chemotherapeutics is still a great challenge to breast cancer therapy. Even after successful treatment at the early stage of detection, about 40% of all breast cancer patients are suffering a relapse accompanied with metastasis and chemoresistance to classical drugs [4.2]. Hence, an advanced strategy to avoid drug resistance is necessary to improve the efficacy of chemotherapy as well as to improve the clinical outcome of breast cancer patients.

131

MicroRNAs (miRNAs) are a major class of endogenous non-coding small (18-24 nucleotide long) single stranded RNAs found in animals and plants that serve as potent regulators of target gene expression [4.3-5]. The miRNAs can suppress gene expression through incorporation into an active RNA-induced silencing complex. They can bind to the complementary sequences in the 3-untranslated region of mRNAs [4.6-8]. Nowadays miRNAs have become ideal class of biomarkers in many human diseases including a variety of cancers (breast, prostate, colon, lung etc.) [4.9-14]. For this reason, accurate detection of miRNAs is very important for early diagnosis of cancer or other human disease. But, the basic problems of quantitative analysis of miRNAs are their unique small size and low abundance. The traditional microRNA detection methods are northern blotting [4.15], RT-PCR [4.16] and fluorescent microarray [4.17]. Northern blotting is a semi-quantitative method, as well as time and sample-consuming. Moreover, this technique needs miRNA separation and enrichment, which is laborious. RT-PCR generally requires miRNA isolation, purification, and reverse transcription to complementary DNA prior to amplification step. Fluorescent microarray usually suffers from photobleaching, poor reproducibility and inaccuracy. Therefore, it is important to develop a new analytical method for miRNAs detection with

132

high sensitivity and good reliability. Up to present time much effort has been devoted and many detection techniques have been developed for detection of miRNAs, such as fluorescence microscopy [4.8, 4.14], electrochemical method [4.18-20] chemiluminescence, spectrophotometry and mass spectrometry. However, most of these methods suffer from poor reproducibility. Surface-enhanced Raman spectroscopy may be an excellent alternative of the methods mentioned above. SERS nanotags have several advantages; such as high spectral specificity, increased sensitivity.

In this study, we report new miRNA conjugated hybrid nanoparticles (MiNPs) for accurate *in-situ* analysis of miRNA expression in single cell level using SERS method. Each hybrid nanoparticle consists of a colloidal gold nanoparticle (AuNP), a Raman reporter and a thiol group modified half miRNA complementary to the target miRNA (Figure 4.1). The efficiency of the HNPs for detection of the expression level of target miRNA was also described in this report.
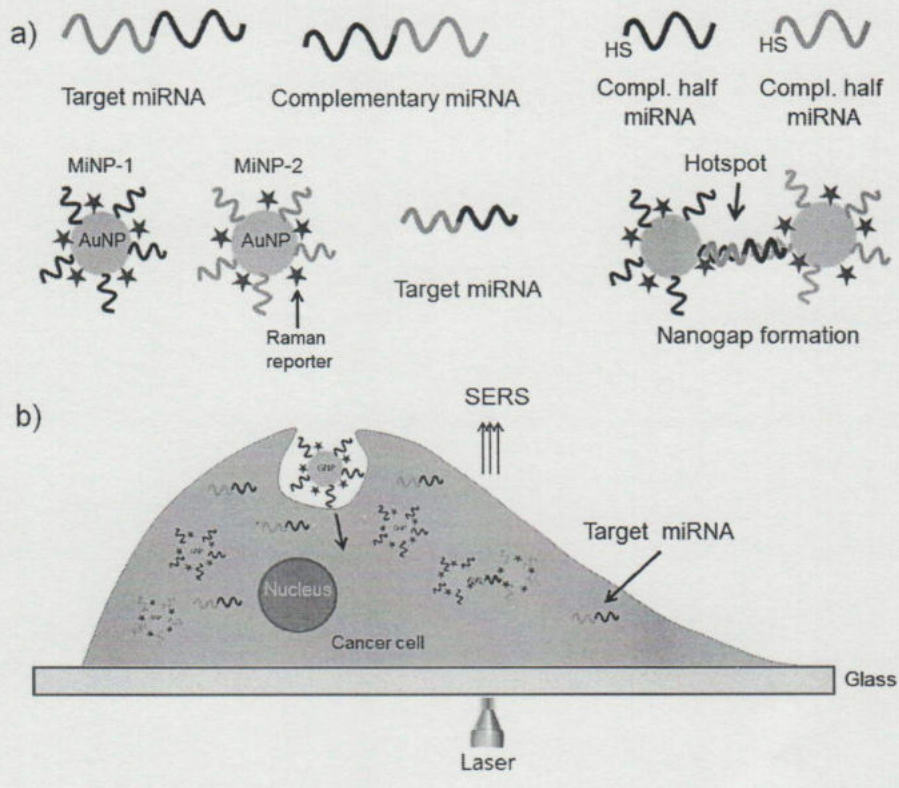
Figure 4.1. a) Schemaitcs for the conjugation of miRNA modified nanoparticles (MiNPs). (b) Cellular uptaking and formation of nanoclusters inside cells.

4.2.   Materials and Methods

4.2.1.   Materials

60 nm diameter colloidal gold nanoparticle (AuNP) solutions were obtained from BB International-UK. RPMI-1640 medium, and breast cancer stem cell medium was purchased from Fresh media™, Daegu, South Korea. Fetal bovine serum (FBS), antibiotics (penicillin–streptomycin, 10,000 IU/ml of penicillin sodium, and 10,000 mg/ml of streptomycin sulfate in 0.83% saline), and Trypsin (Trypsin –EDTA solution, 1X) were obtained from Welgene Inc. 4-mercaptobenzoic acid (4-MBA) and phosphate buffered saline (PBS) (pH 7.4, 10 mM from Sigma Aldrich -USA. Thiolated complementary half miR200c were collected from Bioneer (Daejon, Korea) with the following specific recognition sequences:

3 half-   thiol- 5 ' -CAACTCCATCATTACC-3 '

5 half-   5 ' -CGGCAGTATTAGCAT-3 ' -thiol

4.2.2. Preparation of the miRNA modified Hybrid Nanoparticles (MiNPs)

Stock solutions of miR200c were prepared in deionized water (DW) and kept frozen until use. At first 150 μL (3μM) of 4-mercaptobenzoic acid (4-MBA) solution was added drop wise to 900 μL of rapidly mixing colloidal gold nanoparticles (AuNPs). Subsequently, 100 μL of thiolated half miR200c (100 pmol) was added to the solution and incubated at 4°C for 12 hours for self-assembly of the microRNA and 4-MBA molecule on the AuNP's surface. HNPs were purified by centrifugation (at 1,000g for 10min) to remove excess Raman reporter and DNA. Following the similar way both hybrid nanoparticles (MiNP1 and MiNP2) were prepared. The solutions were stored at 4°C until use.

4.2.3. Confirmation of Nanoparticles Conjugation

For confirmation of conjugation equal volume (50 μL) of MiNP1 and MiNP2 were mixed with 100 μL (10 pmol) mimic of miR200c and 200 μL of 2X PBS, and incubated at room temperature for 2 hours. After incubation the mixture was purified by centrifugation (at 1,000g for 10min) to remove

136

excess DNA. Then the particles conjugation was confirmed by UV-vis. Spectroscopy and transmission electron microscopy (TEM). UV-Vis. spectra were measured using a Jasco V-530 UV/VIS spectrophotometer. The TEM images were acquired by using a JEOL transmission electron microscope (JEM1010) with an accelerating voltage of 80 kV.

4.2.4. Preparation of Cell Chip

Glass substrates (2cm x 2cm) were cleaned by sonication for 15 minutes using 1% Triton-X 100 solution, deionized water (DIW) and ethanol sequentially, and then by basic piranha solution (H_2O_2:NH_3: H_2O, 1:1:5) for 30 min at 80 $^\circ$ C. A polystyrene cell culture unit with the dimension of 1cm x 1cm x 1cm (width x length x height) was attached to the glass surface using polydimethylsiloxane (PDMS).

4.2.5. Culturing of Cancer Cells

The breast cancer cell lines (MCF-7, and SK-BR-3) and breast stem-like cancer cells (SCCs) were obtained from ATCC (Manassas, VA). The breast

cancer cell lines were grown in RPMI 1640 media supplemented with 10% fetal bovine serum (FBS) and 1% Penicillin-Streptomycin, and the breast SCCs were grown in breast cancer stem cell undifferentiation medium. Cells were grown at 37°C and 5% CO_2 in TC-grade Petri dish (BD Biosciences, San Jose, CA). At 80% confluence the cells were transferred to the chip at a density of 2×10^4 cells/ml with a new culture medium, and then incubated for 48 hours.

4.2.6. Treatment of MiNPs to the Cells

20 µl of MiNP1 and MiNP2 were treated to the cells in chip and incubated at 37°C for 24 hours. After incubation the media was removed, fresh media was added and SERS spectra were measured.

4.2.7. Measurement of SERS Spectra

The SERS spectra were measured using Raman NTGRA spectra (NT- MDT, Russia). Before measuring spectra the cells were imaged with SERS mapping with 32x32 point number. The SERS spectra were measured using a 785 nm NIR laser with 3 mW laser powers on the sample plane with one

138

second exposure time. Spectra were measured on ten different spots and an average result was used to make a curve.

4.2.8. Cell Cytotoxicity Assay

The cell cytotoxicity assay was conducted using doxorubicin as anticancer drug. Presence of miR 200c can make the cancer cells more sensitive to doxorubicin. The cytotoxicity of doxorubicin was measured by MTT assay. In brief; the SK-BR-3 and MCF-7 cells were seeded in 96 well plates with a concentration of 20,000 cells per well, and breast SCCs were seeded as 10,000 cells per well, and incubated at $37^{\circ}C$ in a cell culture incubator for 48 hours. The cells were then treated with 1 μM doxorubicin and again incubated for 2 hours at $37^{\circ}C$. After incubation the doxorubicin containing media was removed from each well, fresh media was added, and 20 μl of 3-(4,5 dimethylthiazol-2-yl)-2,5-diphenyl-tetrazolium bromide (MTT) solution (5 mg/ml) was added to each well and incubated at $37^{\circ}C$ for 3 hours. Conversion of MTT into purple formazan by metabolically active cells indicates the extent of cells viability. After incubation the MTT containing media was removed and 200 μl of dimethyl sulfoxide (DMSO) was added to each well to dissolve the crystals of formazan, and the optical density was

139

measured by a universal microplate reader (EL-800, Bio-tek Instrument Incorporation) at 540 nm wavelength. All experiments were performed in triplicates, and the relative cell viability (%) was expressed as a percentage relative to the untreated control cells.

4.3.   Result and Discussion

4.3.1.   Preparation of MicroRNA Modified Hybrid Nanoparticles

MiNPs were prepared in combination with gold nanoparticles (AuNPs), Raman reporter 4-mercaptobenzoic acid (4-MBA), and a half of the complementary miR200c. The conjugation was confirmed by UV-vis. spectroscopy and transmission electron microscopy (TEM). Figure 4.2a shows the TEM images of conjugated nanoparticles. After hybridization of the complementary miRNA with target miRNA the AuNPs become aggregated, but before hybridization the particles remain separately. Figure 4.2b shows the UV-vis. spectra of the conjugated nanoparticlesThe black curve is from bare AuNPs showing highest absorption band at 530 nm, after miRNA conjugation the intensity of the absorption band somewhat decreases (red curve), but after conjugation with target miRNA the intensity of the

140

absorption band significantly decreases, probably due to the aggregation of the AuNPs.

4.3.2   Measurment of SERS Spectra of Hybrid Nanoparticles

Figure 4.2c shows the SERS spectra of the conjugated nanoparticles. The strong Raman band at 1076 1nd 1586 cm^{-1} are due to the ring breathing mode of the 4-MBA molecule [4.21]. The 1076 cm^{-1} Raman band was selected to compare the expression level of the miRNA inside the cells.

4.3.3.   Uptaking of Hybrid Nanoparticles by the Cells

Bright field images in Figure 4.3 shows the nanoparticles uptaking by the cells. After 24 hours of treatment the cells uptake some MiNPs (right pannel). Among the three cell lines the SK-BR-3 cells showing more nanoparticles accumulation inside them compared to the MCF-7 and breast SCCS. This may be due to high content of miR200c in SK-BR-3 cells.

4.3.4. Detection of miRNA Expression in Different Cells using SERS

141

On the basis of the SERS intensity of the SERS nanoprobes accumulated inside cells we detected the expression level of the miR200c inside the cells. The intensity of Raman band at 1076 cm^{-1} was used to detect the expression level. After treatment the SERS nanoprobes are actively uptaken by the cells, and they accumulated by hybridizing with the target miRNA. There will be more HNPs accumulation in those cells which express more miR200c. Before measuring SERS spectra SERS maps were prepared according to the size of the cells. Then SERS spectra were measured on 10 different spots with 1 second exposure time. Then the spectra were averaged to make a curve. Figure 4.4a-c shows the bright field image and 4.4d-f SERS map image of the SK-BR-3, MCF-7 and breast SCC respectively. The measured SERS spectra from the SK-BR-3 (black curve), MCF-7 (red curve) and breast SCCs (blue curve) cells are plotted in Figure 4.4 g. The figure shows that, the intensity of the Raman band at 1076 cm^{-1} in SK-BR-3 cells is higher than that of the MCF-7 or breast breast SCSs. The bar graph in Figure 4.4h shows the comparative expression level of miR200c in SK-BR-3, MCF-7 and breast SCCs. The graph was made on the basis of the intensity of the 1076 cm^{-1} Raman band in measured SERS spectra. Error bar indicates the standard deviation of three independent experiments.
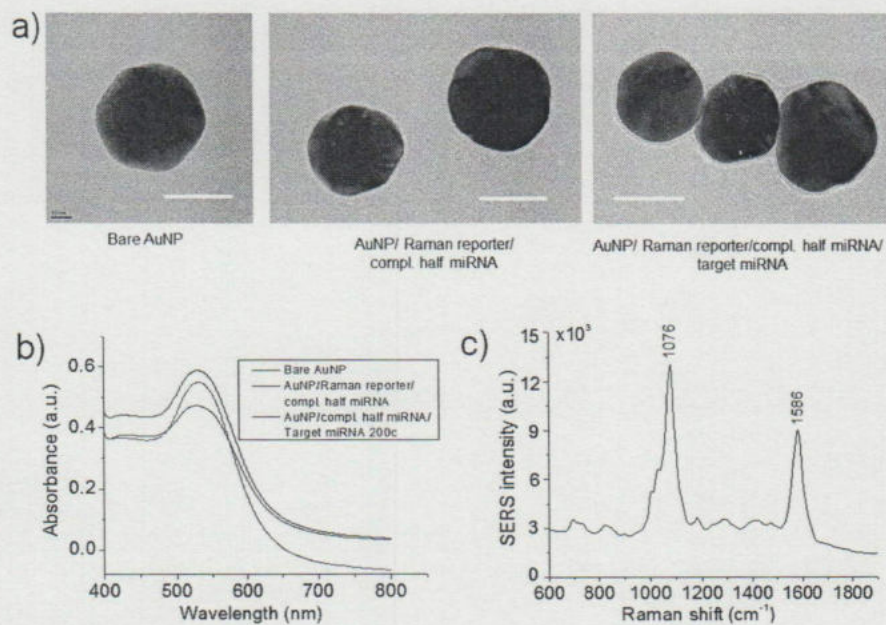
Figure 4.2. a) Confirmation of nanoparticle's conjugation. a) TEM images of step by step conjugation process. b) UV-vis. spectra of the conjugated nanoparticles. c) SERS spectra of the conjugated nanoparticles.
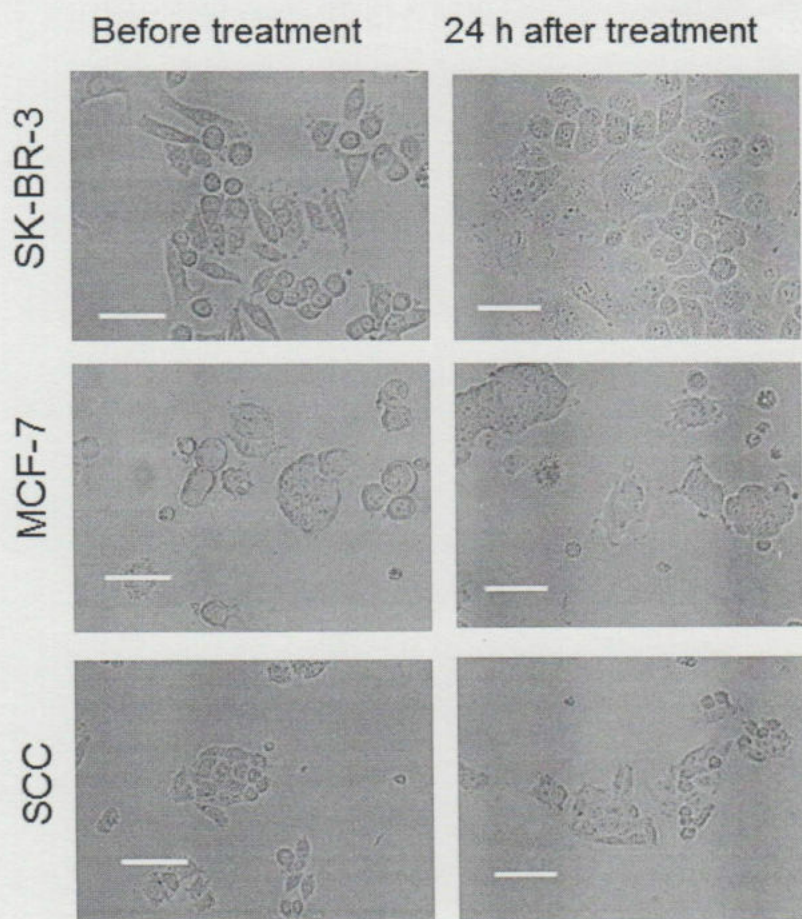
Figure 4.3. Uptaking of conjugated nanoparticles by the cells. Left panel shows the light microscopic images of cells before nanoparticle's treatment. Right panel shows the images of cells after MiNP treatment. Scale bar 20 μm.

144
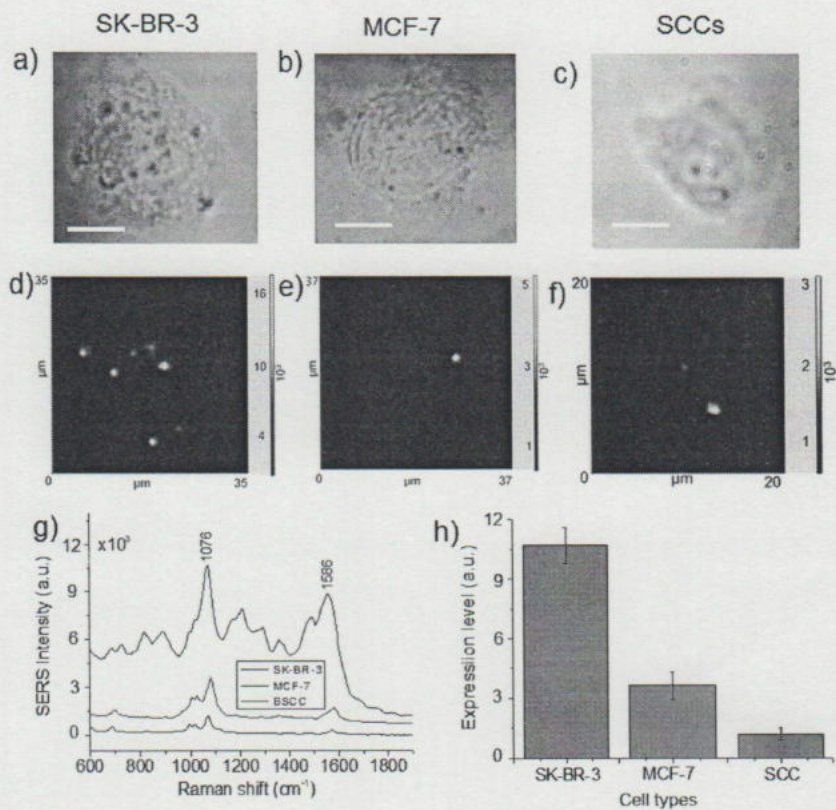
Figure 4.4. Detection of miRNA 200c expression in different cells using SERS. Bright field images of a) SK-BR-3, b) MCF-7 and c) breast SCC. d), e) and f) are the SERS map images of the cells in a), b) and c) respectively. g) SERS sectra measured in the cells. h) Bar graph shows the difference of the miR200c expression level in different cells. Error bar indicates standard deviation oif three independent experiments.

4.3.5. Cell Cytotoxicity Assay

Cytotoxicity of doxorubicin in SK-BR-3, MCF-7 and breast SCCs was measured through MTT assay. Different concentration of doxorubicin was used to treat the cells. The results of MTT assay is presented in Figure 4.5. The bar graph shows that doxorubicin cytotoxicity is higher in SK-BR-3 cells than the MCF-7 or breast SCCs. This may be due to the higher expression of miR200c in SK-Br-3 cells than the MCF-7 or breast SCCs [4.22]
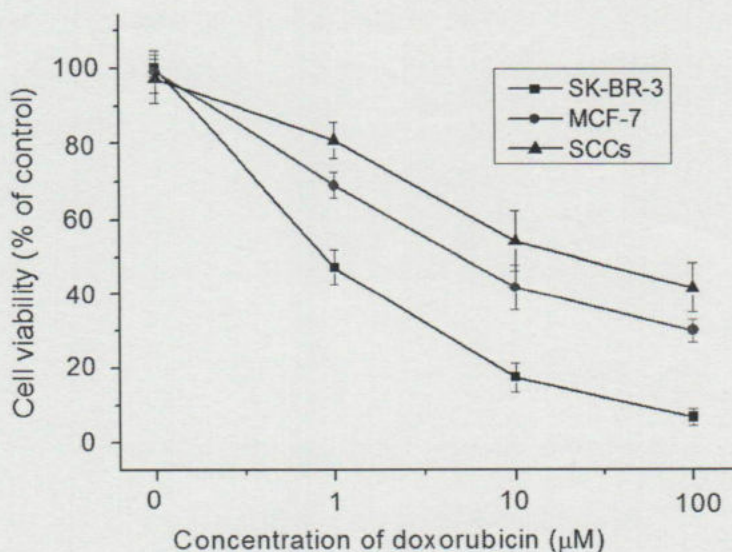
Figure 4.5. Comparison of doxorubicin sensitivity in different cells based on MTT assay. Error bars indicate standard deviation of three independent experiments.

4.4. Conclusion

This study demonstrates the successful synthesis of hybrid nanoparticles (MiNPs), which consist of AuNPs, 4- MBA and complementary half miR200c and applied for *in situ* analysis of miR200c expression without affecting cellular viability. Among the three kinds of cells SK-BR-3 expresses highest quantity of miR200c, MCF-7 moderate and breast SCC express least quantity. We studied doxorubicin's cytotoxicity to three cell lines. Among them SK-BR-3 cells show highest cytotoxixity, MCF-7 moderate and SCC lowest. This result indicates that, miR200c expression is directly proportional to the doxorubicin's cytotoxicity.

4.5. References

[4.1]   Davison, Z., de Blacquiere, G., E., Westley, B., R. & May, F., E., B. (2011). Insulin-like Growtg Factor-Dependent Proliferation and Survival of Triple-Negative Breast Cancer Cells: Implications for therapy. *Neoplasia. 13*, 504-515.

[4.2]   Gangopadhyay, S., Nandy, A., Hor, P. & Mukhopadhyay, A. (2013). Breast cancer stem cells: A novel therapeutic target. *Clinical Breast Cancer. 13,* 7–15.

[4.3]   Zhang, G., J., Chua, J., H., Chee, R., E., Agarwal, A. & Wong, S., M. (2009). Label-free direct detection of miRNAs with silicon nanowire biosensor. *Biosensor and Bioelectronics. 24,* 2504–2508.

[4.4]   Guo, Z. & Peng, Y. (2011). A highly sensitive and specific biosensor for ligation- and PCR-free detection of MicroRNAs. *Biosensor and Bioelectronics. 26,* 3768–3773.

[4.5]   Yin, H., Zhou, Y., Zhang, H., Meng, X. & Ai, S. (2012). Electrochemical detection of microRNA-21 based on graphene, LNA integrated molecular beacon, AuNPs and biotin multifunctional bio bar codes and enzymatic assay system. *Biosensor and Bioelectronics.*

148

33, 247–253.

[4.6]   Li, F., Peng, J., Wang, J., Tang., H., Tan, L., Xie, Q. & Yao, S.
(2014). Carbon nanotube-based label-free electrochemical biosensor
for sensitive detection of miRNA-24. *Biosensor and Bioelectronics.*
54, 158–164.

[4.7]   Shen, W., Deng, H., Ren, Y. & Gao, Z. (2013). A label-free
microRNA biosensor based on DNAzyme-catalyzed and microRNA-
guided formation of a thin insulating polymer film.. *Biosensor and*
Bioelectronics. 44, 171–176.

[4.8]   Ziang, L., Duan, D., Shen, Y. & Li, Z. (2012). Direct microRNA
detection with universal tagged probe and time-resolved fluorescence
technology. *Biosensor and Bioelectronics. 34,* 291–295.

[4.9]   Dong, H., Hao, K., Tian, Y., Jin, S., Lu, H., Zhuo, S., F. & Zhang, X.
(2014). Label-free ultrasensitive microRNA detection based on novel
molecular beacon binding readout and target recycling amplification..
Biosensor and Bioelectronics. 53, 377–383.

[4.10]   Wang, M., Yin, H., Shen, N., Xu, Z., Sun, B. & Ai, S. (2014).
Signal on photoelectrochemical biosensor for microRNA detection

based on Bi_2S_2 nanorods and enzymatic amplification. *Biosensor and Bioelectronics. 53,* 232–237.

[4.11]   Xia, N., Zhang, L., Wang, G., Feng, Q. & Liu, L. (2013). Label-free and sensitive strategy for microRNA detection based on formation of borobnate ester and dual-amplification of gold nanoparticles. *Biosensor and Bioelectronics. 47,* 461–466.

[4.12]   Wang, X., P., Yin, B., C., Wang, P & Ye B., C (2013). Highly sensitive detection of microRNAs based on Isothermal exponential amplification-assisted generation of catalytic G-quadruples DNAzyme. *Biosensor and Bioelectronics. 42,* 131–135.

[4.13]   Driskell, J., D., Seto, A., G., Jones, L., P., Jokela, S., Dluhy, R., R., Zhao, Y., P. & Tripp, R., A. (2008). Rapid microRNA (miRNA) detection and classification via surface-enhanced Raman Spectroscopy. *Biosensor and Bioelectronics. 24,* 917–922.

[4.14]   Ma, C., Liu, S. & Shi, C. (2014). Ultrasensitive detection of microRNAs based on hairpin fluorescence probe assisted isothermal amplification. *Biosensor and Bioelectronics. 58,* 57–60.

[4.15]   Valoczi, A., Hornyik, C., Varga, N., Burgyan, J. Kauppinen, S. &

Havelda, Z. (2004). Sensitive and specific detection of microRNAs by northern blot analysis using LNA-modified oligonucleotide probes. *Nucleic Acid Research. 32*, e175.

[4.16]   Lao, K., Xu, N., L., Yeung, V., Chen, C., LIvak, K., J. & Straus, N., A. (2006). Multiplex RT-PCR for the detection of multiple miRNA species in small samples. *Biochemical and Boiphysical Research Communications. 343*, 85-89.

[4.17]   Thomson, J., M., Parker, J., Perou, C., M. & Hammond, S., M. (2004). A custom microarray platform for analysis of microRNA gene expression. *Nature Methods. 1*, 47-53.

[4.18]   Tran, H., V., Piro, B., Reisberg, s., Nguyen, L., H., Nguyen, T., D., Duc, H., T. & Pham, M., C. (2014). An electrochemical ELISA-like immunosensor for miRNAs detection based on screen-printed gold electrodes modified with reduced graphene oxide, and carbon nanotubes. *Biosensor and Bioelectronics. 62*, 25–30.

[4.19]   Liu, L., Xia, N., Liu, H., Kang, X., Liu, X., Xue, C. & He, X. (2014). Highly sensitive and label-free electrochemical derection of microRNAs based on triple signal amplification of multifunctional

151

gold nanoparticles, enzymes and redox-cycling reaction. *Biosensor and Bioelectronics. 53,* 399–405.

[4.20]   Zhu, W., Su, X., Gao, X., Dai, Z. & Zou, X. (2014). A label-free and PCR-fee electrochemical assay for multiplex microRNA profiles by ligase chain reaction coupling with quantum dots barcodes. *Biosensor and Bioelectronics. 53,* 414–419.

[4.21]   Zong, S., Wang, Z., Yang, J., Wang, C., Xu, S. & Cui, Y. (2012). A SERS and fluorescence dual mode cancer cell targeting probe based on silica coated Au@ Ag core-shell nanorods. *Talanta. 97,* 368–375.

[4.22]   Kopp, F., Oak, P., S., Wagner, E. and Roidl, A. (2012). miR200c sensitizes breast cancer cells to doxorubicin treatment by decreasing TrkB and Bmi1 expression. *PLOS ONE. 7,* e50469.

Chapter 5

In situ Monitoring of Doxorubicin Release inside

Targeted Cancer Cells using Surface-Enhanced

Raman Spectroscopy

5.1. Introduction

Targeted drug delivery is very important in chemotherapy in order to increase therapeutic efficacy and to keep the healthy cells unaffected. A lot of nanocarriers have been designed for the delivery of therapeutic agents [5.1-4], and there are several advantages of nanoparticle based drug delivery, particularly at the systemic level including longer circulation half-lives, improved pharmacokinetics, and reduced side effects [5.5]. Various kinds of inorganic nanoparticles are used in the field of biomedicine including gold nanoparticle (AuNPs) [5.6-10], iron oxide nanoparticles [5.11], carbon nanotubes [5.12], TiO_2 nanoparticles [5.13], graphene oxide nanosheets etc. Among them use of AuNPs have extra advantages due to their size can be easily controlled during synthesis, inertness, their surface can be

153

conveniently functionalized with different types of molecules, water solubility, good biocompatibility, low cytotoxicity, as well as their unique optical and plasmonic properties [5.14]. Considering the properties mentioned above AuNPs have potential application in drug delivery, biosensing, imaging, and chemotherapy [5.15-16]. But the challenges are; preparation of functionalized stable nanoparticles, targeted delivery, uptake efficiency by the targeted cells, as well as efficient drug release [5.17]. For increasing the uptaking efficiency many scientists used cell penetrating peptides (CPPs). The CPPs are short (9-35 mer) cationic and/or amphipathic peptides that are rapidly internalized across the cell membrane, and are able to mediate the translocation of a conjugated cargo (e.g., anti-cancer therapeutics) across the plasma membrane, making the CPPs as an effective and non-toxic carrier of drug delivery [5.18]. Although the exact mechanism of cellular internalization of the CPPs are not clearly understood, but it is clear that CPP can mediate intracellular deliver by both endocytic and non-endocytic (direct trnaslocation) pathways. The basic problem of CPP application is there non-selectivity. The CPPs cannot target specific cells. But for cancer therapy specific targeting is important. This factor limits the CPP's application.

154

In last few years scientists applied many approaches for efficient drug delivery and most of the drug release studies was monitored using fluorescence microscopy. But the drawback of the fluorescence microscopy is the photobleaching effect of fluorophores [5.19]. Therefore, there is still need a suitable technique for effective monitoring of drug delivery.

The surface-enhanced Raman scattering (SERS) technique has shown promise in overcoming the low sensitivity problem inherent in conventional Raman spectroscopy. SERS nanoconjugates have several advantages, such as resistance to photobleaching, narrow spectral bands, and high spectral specificity. In addition, Raman microscopy has unique contributions to the intracellular activity monitoring.

In this study, we report a new biohybrid nanoparticle (B-HNP) in combination with gold nanoparticle (AuNP), cell penetrating peptide (CPP), doxorubicin anticancer drug, polyethylene glycol (PEG) and antibody that is capable for increased delivery of doxorubicin into the targeted cancer cells (Figure 5.1), as well as an excellent *in-situ* drug release monitoring by SERS.

155
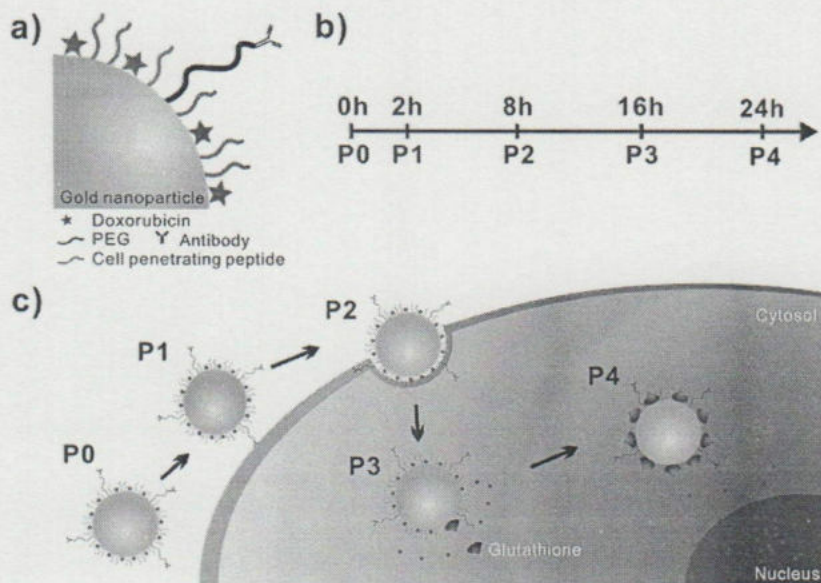
Figure 5.1. Schematic diagram for synthesis of biohybrid nanoparticles (B-HNPs) and cellular uptaking. a) Nanoparticle's conjugation. b) Period of monitoring c) Nanoparticle's uptaking by the cells and release of drug from the nanoparticle's surface.

The CPP modified AuNPs were used to rapid and increased uptaking by the targeted cells. Mouse monoclonal antibody was used in the B-HNP to target specific breast cancer cells. Using SERS technique, the time dependent drug release was monitored efficiently. To observe the effect of intracellular drug

release cell cytotoxicity assay was conducted. To observe the effect of glutathione (GSH) on doxorubicin release from the AuNPs surface, glutathione ethyl ester (GSH-OEt) was added to the cells and doxorubicin release rate was measured using SERS. Our newly developed biohybrid nanoparticles are efficient in increasing uptaking and delivery of drug to the targeted cells, as well as label free *in-situ* monitoring of drug release through SERS, and it can be used for *in-situ* monitoring the effect of other drugs on cells.

5.2   Materials and Methods

5.2.1.   Formation of Biohybrid Nanoparticles (B-HNPs)

At first   20 µl of 1 µM cysteine modified TAT peptide was added to 980 µl of 30 nm AuNPs (2×10^{11} particles/ml), and incubated at 4°C for 24 hours. After incubation the mixture was centrifuged at 13,000 RPM for 10 minutes, the supernatant was discarded to remove the unbound peptides, and the pellet was resuspended in DI water.

In second doxorubicin was dissolved in DI water. Then the doxorubicin was added to the nanoparticles at different concentrations and incubated at room

for 24 hours. Due to the presence of free amine group on the doxorubicin structure, the doxorubicin can be self-assembled on the surface of AuNPs. After incubation the mixture was centrifuged at 13,000 RPM, the supernatant was discarded to remove the unbound materials, and the pellet was resuspended in DI water.

In third step 1 µM heterofunctional PEG (HS-PEG-COOH) was added to the nanoparticles incubated at $4^{\circ}C$ for 24 hours. Due to the presence of thiol group the PEG can be self-assembled on the surface of AuNPs. After incubation the mixture was centrifuged 3 times at 10,000 RPM to remove the unbound antibodies and the pellet was resuspended in PBS.

In the final step, mouse monoclonal anti-HER2 antibody was immobilized to the nanoparticles to a final concentration 10 nm through sufo-NHS chemistry. Briefly to activate the -COOH groups on the particle surface for covalent conjugation, freshly prepared ethyl dimethylaminopropyl carbodiimide (EDC) solution (5 ml) at a concentration of 40mg/ml) and sulfo-NHS (5 ml at 110 mg/ml) were mixed vigorously at 25^{0} C for 15 min. Excess EDC and sulfo-NHS were separated from the activated nanoparticles by three rounds of centrifugation (1,000g) and re-suspended in PBS. The purified GNPs with activated carboxyl groups were then reacted with the mouse monoclonal

158

anti-HER2 antibody (11.2 nmol) at 25^0 C for 2 h, and the reaction mixture was stored at 4^0C for overnight. After incubation the mixture was centrifuged 3 times at 10,000 RPM to remove the unbound antibodies and the pellet was resuspended in PBS

5.2.2. Particle Size and Zeta Potential Analysis

To confirm the conjugation processes, the surface charge and size of the conjugated nanoparticles was measured using a particle size and zeta potential analyser (ELSZ-1000, Otsuka Electronics, Japan). To see the morphology of the conjugated nanoparticles we conducted transmission electron microscopy (TEM). TEM was measured by a JEOL TEM microscope (JEM-2100F) operated at an accelerating voltage of 200 kV.

Breast cancer cell line SK-BR-3 and neuroblastoma cell line SH-SY5Y were obtained from ATCC (Manassas,VA). The cells were cultured at 37°C in RPMI-1640 medium supplemented with 10% heat inactivated fetal bovine serum and 1% antibiotics (streptomycin and penicillin) in a humidified atmosphere of 5% CO_2. The cells were grown at in TC-grade Petri dish. At 80% confluence the cells were transferred to the chip at a density of 1×10^5

cells/ml with a new culture medium, and then incubated for 3 days.

5.2.3. Detection of Penetration Efficacy of Different CPPs

At first SK-BR-3 cells were seeded in a cell chip with a concentration of 2 $\times 10^4$ cells/ml media, and incubated at 37℃ in a cell culture incubator. After 48 hour the cells were treated with FITC modified CPPs at a final concentration of 20 nM, and incubated again at 37℃ for 24 hours. After incubation the media was removed and the cells were fixed with 3.5% formaldehyde. After fixation PBS was added to the cells, and fluorescent intensity of the CPP uptaken cells was measured with a Nikon fluorescent microscope using Elements BR 3.2 software. The images were taken with 400x magnification.

5.2.4. Specific Targeting and Cellular Uptaking of B-HNPs

At first SK-BR-3 and SH-SY5Y cells were seeded in a cell chip with a concentration of 2 $\times 10^4$ cells/ml media, and incubated at 37°C in a cells culture incubator. After 48 hours incubation the cells in the chip were treated with FITC modified GNPs conjugated with TAT and anti-HER2 antibody. After two hours of incubation the nanoparticles containing media was

160

removed, the cells were fixed with 4% formaldehyde, and the cells were observed under a confocal fluorescence microscope. The images were taken with 200x magnification.

5.2.5.   Measurement of Au Content inside Cells

48 hours after seeding the SK–BR-3 cells (with a concentration of 2 x10^4 cells /ml) they were treated with B-HNPs conjugated with CPP, and without CPP, and then again incubated for 2 hours. After incubation the cells were washed five times with PBS, detached from petridishes with trypsin treatment, resuspended in PBS and counted. The samples were digested carefully with *aqua regia* and the Au content was measured with atomic emission spectroscopy (AES).

5.2.6.   Measurement SERS Spectra

At first SK-BR-3 and SH-SY5Y cells were seeded in a cell chip with a concentration of 5,000 cells/ml media, and incubated at 37°C in a cell culture incubator. 48 hours after incubation the cells were treated with BNPs and the

cells were incubated again at 37°C for 2 hours. After incubation the media was removed, fresh media was added and SERS spectra were measured using Raman NTGRA spectra (NT- MDT, Russia). Before measuring spectra the cells were imaged with SERS mapping. The SERS spectra were measured in every 15 min interval using a 785 nm NIR laser with 3 mW laser power on the sample plane.

5.2.7. Cytotoxicity Assay

The cytotoxicity of the conjugated nanoparticles was measured by MTT assay. In brief; the SK-BR-3 cells were seeded in 96 well plates with a concentration of 5000 cells per well, and incubated at 37°C in a cell culture incubator for 48 hours. The cells were then treated with conjugated nanoparticles and again incubated for 2 hours at 37°C. After incubation the nanoparticles containing media was removed from each well, fresh media was added, and 20 µl of 3-(4,5 dimethylthiazol-2-yl)-2,5-diphenyl-tetrazolium bromide (MTT) solution (5 mg/ml) was added to each well and incubated at 37°C for 3 hours. Conversion of MTT into purple formazan by metabolically active cells indicates the extent of cells viability. After incubation the MTT containing media was removed and 200 µl of dimethyl

162

sulfoxide (DMSO) was added to each well to dissolve the crystals of formazan, and the optical density was measured by a universal microplate reader (EL-800, Bio-tek Instrument Incorporation) at 540 nm wavelength. All experiments were performed in triplicates, and the relative cell viability (%) was expressed as a percentage relative to the untreated control cells.

5.3.   Results and Discussion

5.3.1.   Particle Conjugation and Characterization

We prepared the biohybrid nanoparticles (B-HNPs) in conjugation with AuNP, doxorubicin anticancer drug, cell penetrating peptide TAT, polyethylene glycol and anti-HER2 antibody (Figure 5.2). At first, cysteine modified TAT peptide was conjugated to the AuNP's surface. The N-terminal of the CPPs was modified with cysteine, a thiol containing amino acid, for their proper immobilization on the AuNPs surface. The transmission electron microscopy (TEM) image (Figure 5.2a) shows the size of the AuNPs. The particles diameter and zeta potential was measured through dynamic light scattering (DLS) (Figure 5.3-4). After TAT conjugation the average size of the conjugated nanoparticles was increased from 30 nm to 75

163

nm. Figure 5.4 shows that the AuNPs have a negative surface charge as measured by zeta potential (-44 mV), The TAT peptides are positively charged. After TAT peptide conjugation the zeta potential of the conjugated AuNPs were positively increased to -41.72 mV.

In the second step anthracycline antibiotic doxorubicin was immobilized to the 30 nm AuNPs surface. Due to a free amine group in the chemical structure of doxorubicin it can self-assemble on the AuNPs surfaces. The DLS data in Figure 5.4 shows that the doxorubicin are positively charged. After doxorubicin immobilization the average size of the conjugated nanoparticles was increased to 83 nm and the zeta potential was positively increased from -41 mV to -40.07 mV. Since the chemical structure of doxorubicin contain aromatic ring, thus it give some enhanced Raman signals when immobilized on gold surface. Figure 5.2 shows the SERS spectra of doxorubicin after immobilization on AsNPs surfaces, whereas the bare AuNPs do not show such type spectra. The strong Raman band at 1275 cm-1 may be due to stretching vibration (v C-O) of ring A of doxorubicin structure [5.20].

In third step of conjugation we immobilize heterofunctional PEG (HS-PEG-COOH) to the AuNPs surface, to immobilize antibody to the PEG through
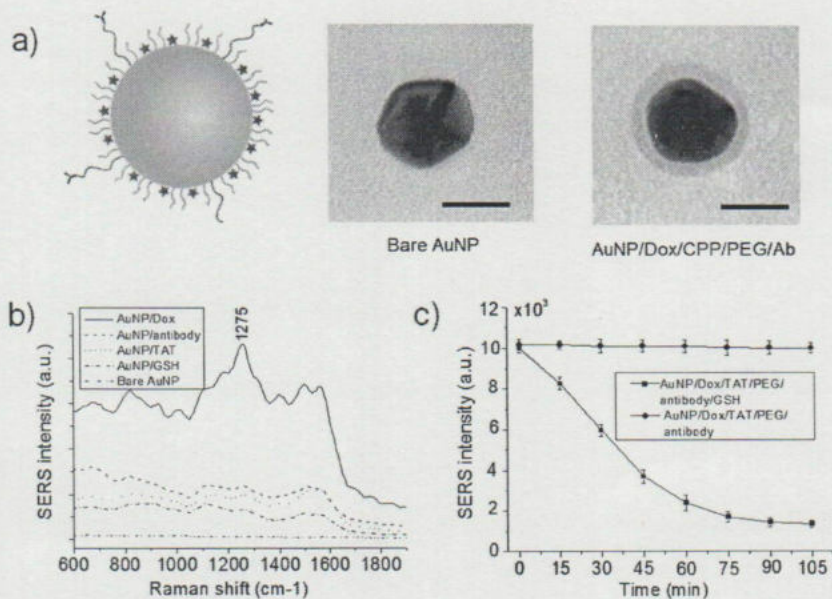
Figure 5.2. Confirmation of nanoparticle's conjugation. a) TEM images. b) SERS spectra of the conjugated nanoparticles. c) Line graph for stability of the B-HNPs. Scale bar 20

sulfo-NHS chemistry. The thiol group of PEG can make strong covalent bond on AuNPs surfaces, and the COOH⁻ group was used to immobilize the antibody. The PEG also helps in stabilizing the conjugated nanoparticles. The DLS data (Figure 5.3) shows that, after PEG immobilization the average size the conjugated nanoparticles increases from 82.8 nm to 92.7 nm and

165

the zeta potential positively increased from -40.72 mV to -13.48 mV due to the positive surface charge of the PEG.

In the final step of conjugation we immobilized mouse monoclonal anti-HER2 antibody to the B-HNPs for specific targeting of SB-BR-3 breast cancer cells. The antibody was immobilized through the COOH⁻ group of PEG using sulfo-NHS chemistry. The DLS data (Figure 5.3) shows that after antibody conjugation the size of the B-HNPs increases from 92.7 nm to 95.6 nm and the zeta potential decreased from -13.48 mV to -26.96 mV due to the negative charge of the antibody.
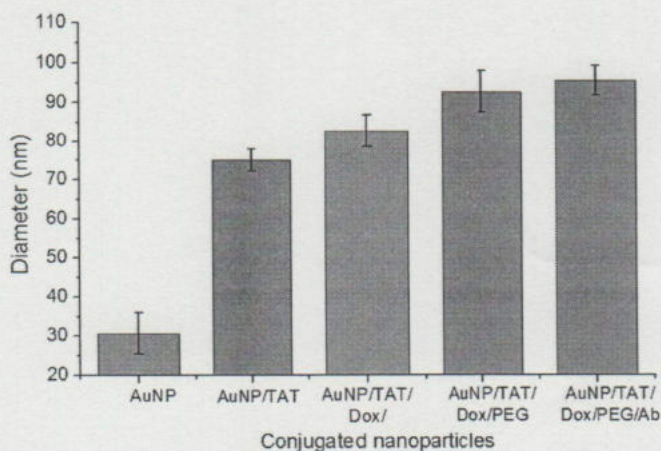
Figure 5.3. Confirmation of nanoparticles conjugation through DLS. Bar graph shows average size of the nanoparticles in every step of conjugation. Error bars indicate standard deviation of three independent measurements.

166

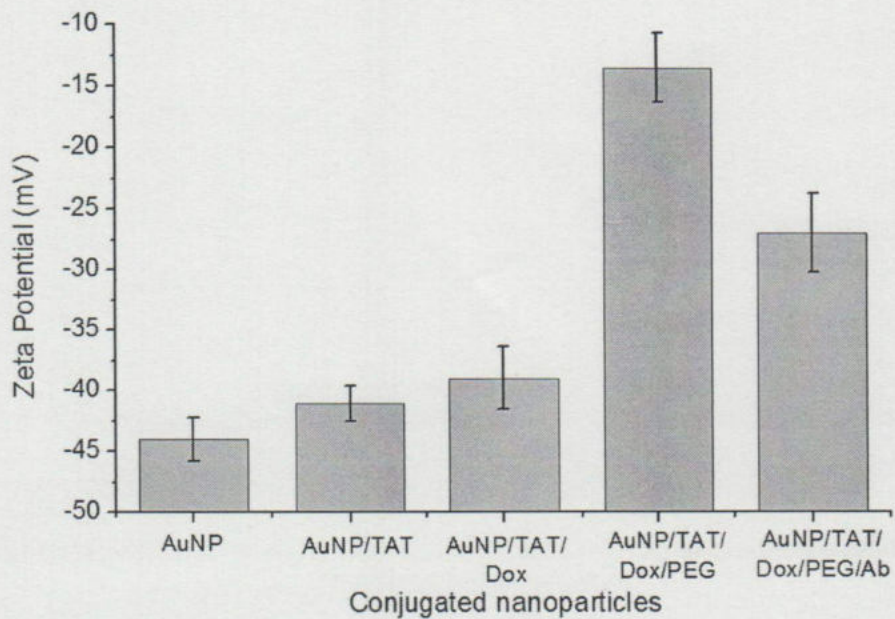**Figure 5.4.** Confirmation of nanoparticles conjugation through zeta potential measurement. Bar graph shows average potential of the nanoparticles in every step of conjugation. Error bars indicate standard deviation of three independent measurements.

5.3.2. Specific Targeting to SK-BR-3 cells

Cancer could be cured if we know to deliver a drug intact to the cytosol of every cancer cell, sparing the healthy cells [5.20]. The circulatory system can deliver a drug to every cell in the body, but our target is cancer cells, not the healthy cells. Therefore, we have to prepare conjugated nanoparticles conjugated with ligand or antibody specific against the cancer cell surface markers. In our experiment we conjugated AuNPs to a mouse monoclonal antibody specific to HER2 overexpressing SKBR-3 breast carcinoma cells for targeted delivery to the SKBR-3 cells. To study the specific targeting we co-cultured HER2 over expressing SK-BR-3 human breast carcinoma cells and HER2 negative SH-SY5Y human neuroblastoma cells. Then we treated the cells with FITC labeled AuNPs conjugated with TAT peptide and anti-HER2 mouse monoclonal antibody. After two hours of particle treatment we remove the particle containing media and fixed the cells. Figure 5.6 show that our conjugated nanoparticles can specifically target the SK-BR-3 cells. The fluorescence image in Figure 5.6a-b shows that the FITC (green color) labeled AuNPs are uptaken by the round SK-BR-3 cells only. We used Hoechst dye to locate the nuclei of the cells (blue color). But the elongated SH-SY5Y cells did not uptake AuNPs. We also conducted SERS experiment

168

Figure 5.5. Specific targeting to cancer cells using biohybrid nanoparticles. a) Bright field image of mixed cultured cells containing SK-BR-3 and SH-SY5Y cells (blue arrow) which were treated with B-HNPs. b) SERS map image showing uptaking of B-HNPs by SK-BR-3 cells only. c) Bright field image of a SH-SY5Y cell treated with B-HNPs. d) SERS map image of the cell in c) showing no B-HNP uptaking. Scale bar 25 μm.

169

to study specific cell targeting. Before measuring SERS we treated the mixed cultured cells with fully functionalized biohybrid nanoparticles. After two hours of treatment we removed the particles containing media and added fresh media. The SERS map image in Figure 5.5a-b shows that only the SK-BR-3 cells uptaken the B-HNPs, but the SH-SY5Y cells did not uptake the conjugated nanoparticles (Figure 5.5c-d).
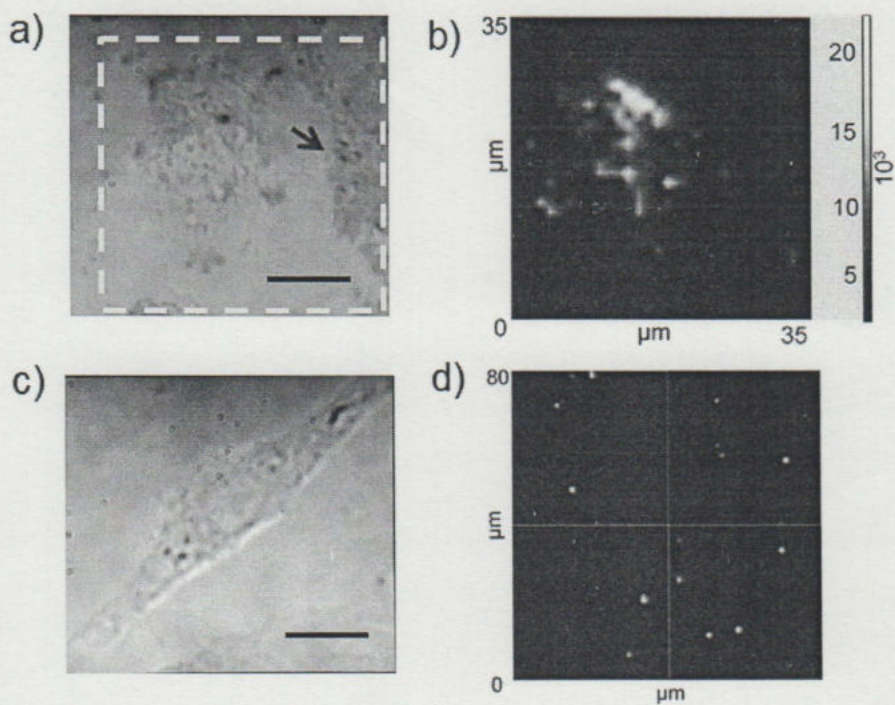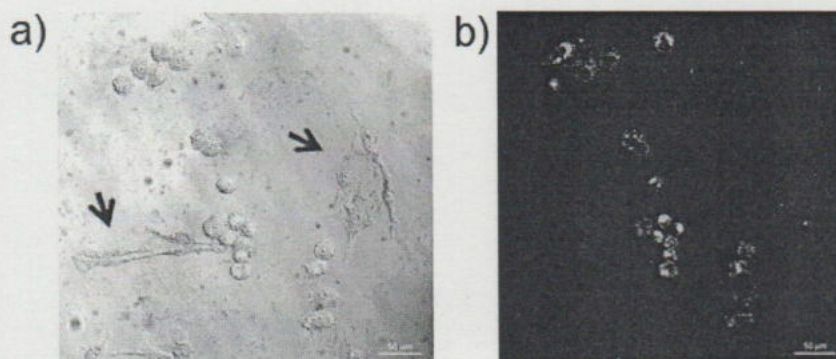

Figure 5.6. Specific targeting to cancer cells using biohybrid nanoparticles. a) Bright field image of mixed cultured cells containing SK-BR-3 and SH-SY5Y cells (blue arrow) which were treated with B-HNPs. b) Fluorescent microscopic image of the cells in a) showing specific uptaking of B-HNPs by the SK-Br-3 cells only. Scale bar 50 μm.

5.3.3. Comparison of Nanoparticles Uptaking by the Cells

We studied the uptaking efficiency of the conjugated nanoparticles (Figure 5.8, and Table 5.1) by the cells. Before measuring we treated the SK-BR-3 cells with B-HNPs conjugated with CPP, and without CPP. Table 5.1. shows that CPP modified B-HNPs uptaking is approximately 170.51 per cells than the B-HNPs not containing CPP, where the uptaking of B-HNP is non-detectable. Before selecting a cell penetrating peptide for preparation of biohybrid nanoparticles we studied the cell penetration efficacy of four different cell penetrating peptides (TAT, Penetration, pVEC and Pep-1) through fluorescence microcroscopy. Among them TAT shows highest penetration efficacy efficacy than others (Figure 5.7).

Type of particles	No. of cells	Quantity of Au (ppm) detected	No. of particles uptaken per cell
AuNPs/Dox/CPP/PEG/Ab	87 x10^4	27 ppm (average)	170.51 (average)
AuNPs/Dox/PEG/Ab	65 x10^4	Non detectable	Non detectable

Table 5.1. Comparison of B-HNPs uptaking by the cells detected by Atomic emission spectroscopy

171
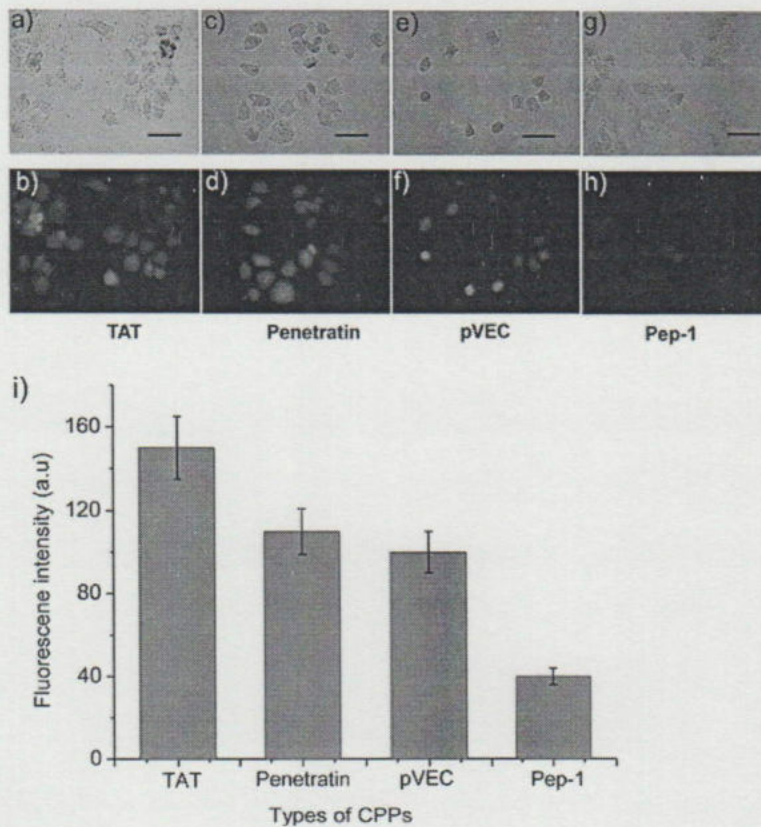
Figure 5.7. Comaprison of cell penetration efficacy of different CPPs. a), c), e) and g) bright field images of SK-BR-3 cells treated with B-HNPs conjugated with different FITC-labelled CPPs. b), d), f) and h) fluorescent microscopic images of the cells in a), c), e) and g) respectively. i) Bar graph showing comparison of penetration efficacy of different CPPs based on their fluorescent intensity. Error bars indicate standard deviation of three independent measurements. Scale bar 50 μm.

172
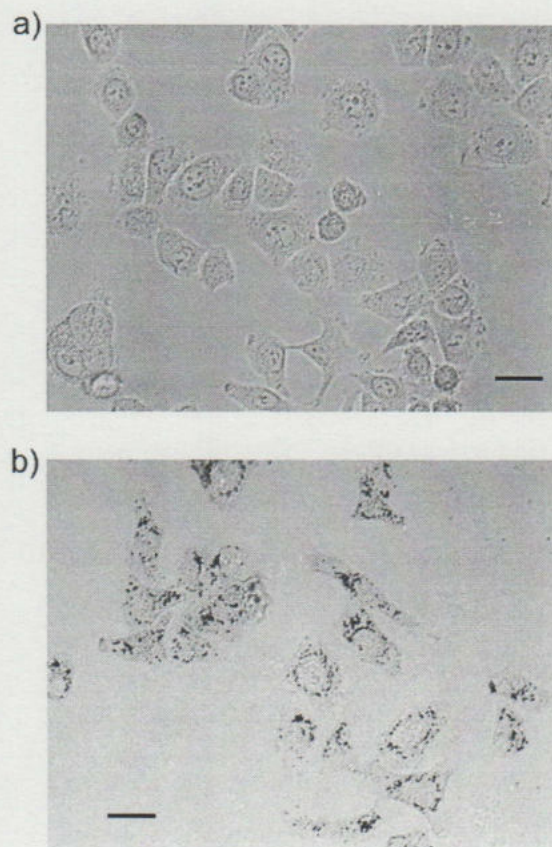
Figure 5.8. Comparison of B-HNPs uptaking by the cells a) SK-BR-3 cells not treated, b) SK-BR-3 cells treated with B-HNPs showing B-HNPs uptaking by the cells.

5.3.4.   Monitoring of Intracellular Doxorubicin Release

Doxorubicin is an anthracycline antibiotic, and a potent chemotherapeutic agent that has been used for over 30 years to treat a wide spectrum of human malignancies, especially breast cancer and lymphoma. Since the chemical structure of doxorubicin contain aromatic ring, thus it give some enhanced Raman signals when immobilized on gold surface. Doxorubicin can be released from the AuNPs surfaces by the action of intracellular glutathione. Glutathione (GSH) is the most abundant thiol species in the cell cytoplasm with a concentration range of 1 to 10 mM, and has been used as an in-situ releasing reagent in living cells due to its reducing capability in the biochemical processes. We studied the release property of doxorubicin from AuNPs surfaces outside cells in presence of different concentration of glutathione using SERS. Figure 5.9 shows the GSH concentration dependent doxorubicin release from the AuNPs surfaces outside cells. The decrease in intensity at 1275 cm-1Raman band of doxorubicin indicates the release of doxorubicin from the AuNPs surfaces. The result shows that doxorubicin release is high in the presence of 5-12 mM GSH concentration.

174
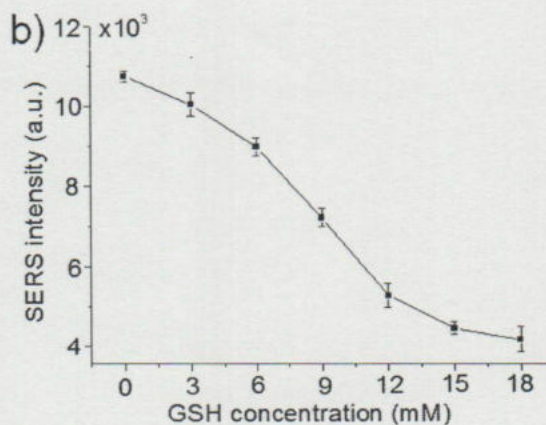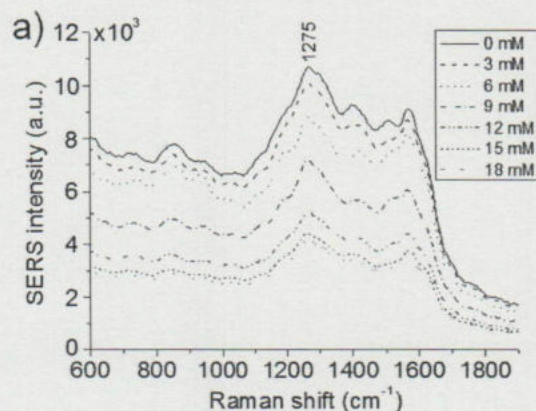
Figure 5.9. GSH concentration dependent doxorubicin release from the AuNP surface a) SERS spectra of doxorubicin showing decreasing in peak intensity at 1275 cm^{-1} Raman band due to increase of GSH concentration. b) Line grapg showing decrease in peak intensity of doxorubicin due to increase in GSH concentration. Error bars indicate standard deviation of three independent experiments.

175

Figure 5.10. Time dependent doxorubicin release from the AuNP surface a) SERS spectra of doxorubicin showing decreasing in peak intensity at 1275 cm^{-1} Raman band in presence of GSH due to elapsed time. b) Line graph showing decrease in peak intensity of doxorubicin due to elapsed time. Error bars indicate standard deviation of three independent experiments.
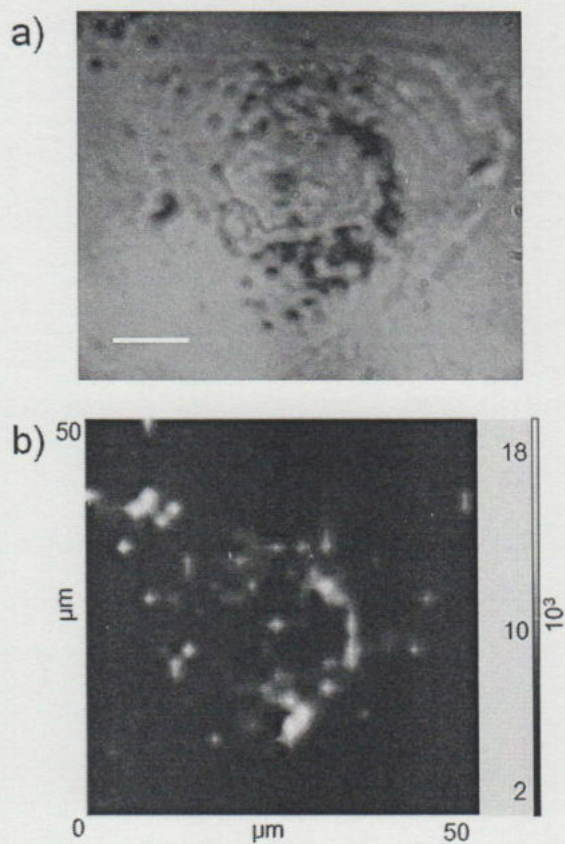
Figure 5.11. Time dependent monitoring of doxorubicin release inside the cells. a) Bright field image of a SK-BR-3 cell treated with B-HNPs. b) SERS map image of the cell in a). Scale bar 10 μm.

We also studied the time dependent doxorubicin release from the AuNPs surfaces outside cells in the presence 10 mM GSH using SERS. Figure 5.10 shows the time dependent doxorubicin release from the AuNPs surfaces outside cells. The result shows that doxorubicin release is high within 1 hour of GSH treatment.
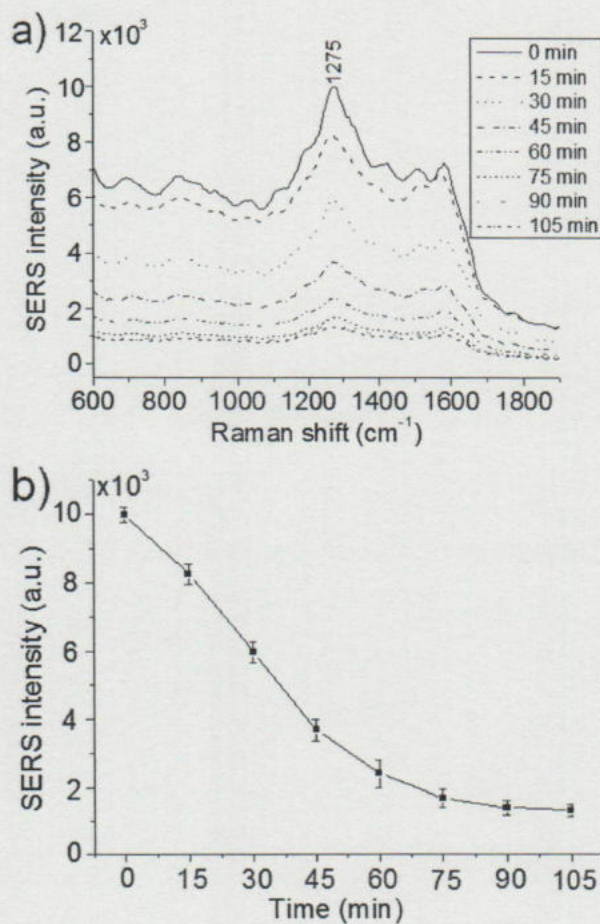
We studied the time dependent doxorubicin release inside live SK-BR-3 cells using SERS. Before measuring SERS we treated the mixed cultured cells with fully functionalized biohybrid nanoparticles. After two hours of treatment we removed the particles containing media and added fresh media.

Figure 5.11-12 shows the time dependent doxorubicin release from the AuNPs surfaces inside cells. We measured SERS spectra from the cell every four hour interval after two hours of nanoparticles treatment. The result shows that most of the doxorubicin is released from the AuNPs surfaces within 12 hours of particles treatment, followed by decreasing in concentration and release rate. But the doxorubicin release rate inside cells is comparatively low than doxorubicin release rate outside cells (Figure 5.10, 5.12). Figure 5.10 shows that in presence of 10 μM GSH most of the doxorubicin is released from the AuNPs surfaces within one hour. The lower release rate inside cells may be due to low concentration of GSH. In another

178

experiment we added 5 mM GSH-OEt to the cell medium after two hours of nanoparticles treatment, and SERS spectra were measured every 15 minutes interval few minutes after GSH-OEt treatment. The result is presented in Figure 5.13. The result shows that after adding 5 mM additional GSH-OEt to the cells the doxorubicin release rate is increased and most of the doxorubicin is released within one hour of GSH-OEt treatment.
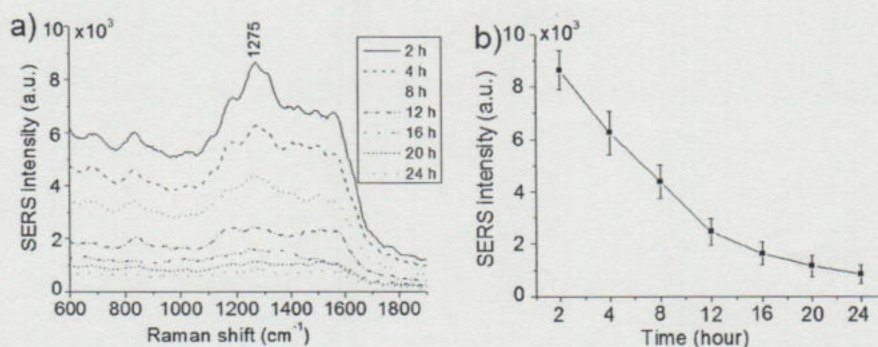
Figure 5.12. Time dependent doxorubicin release from the AuNP surface inside cells. a) SERS spectra of the cells showing decrease in peak intensity at 1275 cm^{-1} Raman band due to elapsed time. b) Line grapg showing time dependent decrease of peak intensity at 1275 cm^{-1} Raman band due to elapsed time. Error bars indicate standard deviation of three independent experiments.

179

Figure 5.13. Time dependent doxorubicin release from the AuNP surface inside cells after addition of 5 mM external GSH. a) Bright field image of a SK-BR-3 cell treated with B-HNPs. Blue dashed line is the scanning area. b) SERS map image of the cell in a). c) SERS spectra of the cell showing decrease in peak intensity at 1275 cm^{-1} Raman band in presence of additional GSH due to elapsed time. d) Line graph showing time dependent decrease of peak intensity at 1275 cm^{-1} Raman band due to elapsed time.

5.3.5. Cell Cytotoxicity Assay

To study the cytotoxicity of the conjugated nanoparticles we conducted MTT assay. Before measuring we treated the cells with fully functionalized BNPs. We used 1 μM doxorubicin to prepare the conjugated nanoparticles. After two hours of treatment the particle treated media was removed and fresh media was added. The MTT assay was conducted every 4 hours interval after naoparticles treatment to the cells. The result is presented in Figure 5.14. The result shows cell mortality increased with time elapsed, 9.53% cells died within 8 hours of particle treatment and 60.52% cells died within 24 hours of treatment. This may be due to active nanoparticles uptaking by the cells, and this result support the SERS result of time dependent intracellular doxorubicin release. On the other hand the conjugated nanoparticles containing AuNPs/TAT/PEG/antibody do not cause any significant cells mortality (Figure 5.15).
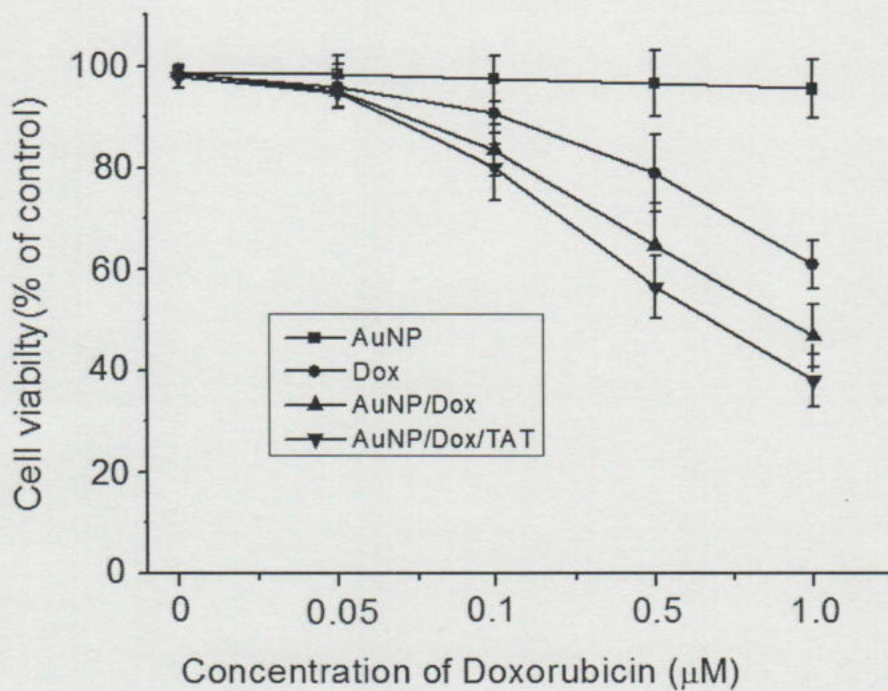
Figure 5.14. Cell cytotoxicity assay of bare AuNPs, doxorubicin, doxorubicin conjugated AuNPs, and AuNPs conjugated with doxorubicin and TAT. Error bar indicates standard deviation of three independent experiments.
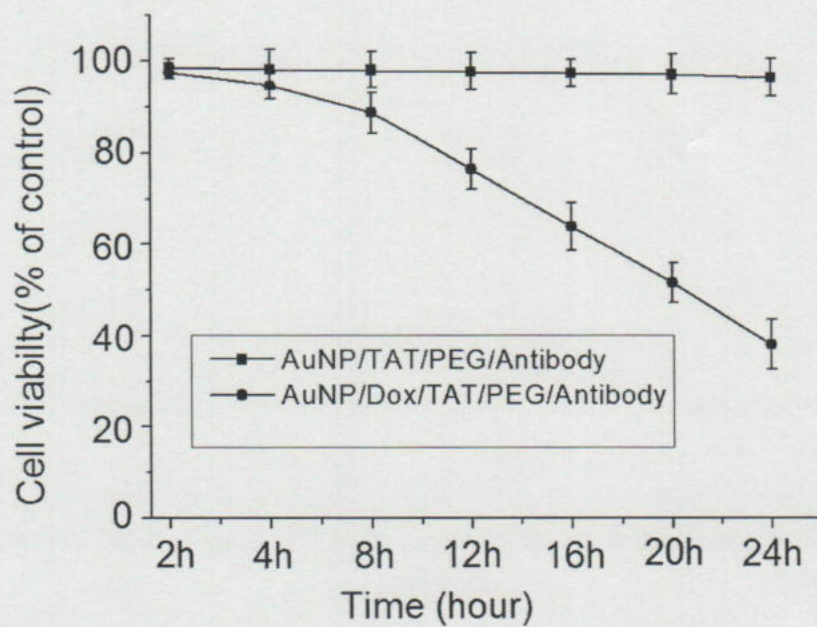
Figure 5.15. Cell cytotoxicity assay of the B-HNPs. Line graphs showing cell cytotoxicity of B-HNPs a) not containing doxorubicin. b) B-HNPs containing doxorubicin. Error bar indicates standard deviation of three independent experiments.

5.4. Conclusion

In conclusion, our conjugated nanoparticles were efficient in specific targeting and increase in uptaking by the cells. The increased uptaking was due to immobilization of CPP to the AuNPs, and specific targeting was due to immobilization of the marker specific antibody. As a result of increased uptaking, cell cytotoxicity was also increased. By using the biohybrid nanoparticles we successfully monitored the release of doxorubicin anticancer drug from AuNPs surfaces inside targeted cells with SERS method. Our newly developed conjugated nanopaticles can be used for specific targeting to any cells for targeted therapy, and can be used for monitoring of release behavior of any SERS active drug molecules inside living cells.

investigated by surface-enhanced Raman scattering. *Analytical Chemistry. 84,* 2172-217.

[5.6]   Duncan, B., Kim, C., & Rotello, V. M. (2010). Gold nanoparticle platforms as drug and biomolecule delivery system. *Journal of Controlled Release 148,* 122-127.

[5.7]   Nativo, P., Prior, I. A.; & Brust, M. (2008). Uptake and intracellular fate of surface modified gold nanoparticles. *ACS Nano 2,* 1639-1644.

[5.8]   Madhusudan, A., Reddy, G. B., Venkatesham, M. Veerabhadram, G., Kumar, D. A., Natarajan, S., Yang, M.-Y., Hu, A. & Singh, S. S. (2014). Efficient pH dependent drug delivery to target cancer cells by gold nanoparticles capped with caeboxymethyl chitosan. *International Journal of Molecular Sciences. 15,* 8216-8234.

[5.9]   Tomuleasa, C., Soritao, O., Orza, A., Dudea, M., Petrushev, B., Mosteanu, O., Susman, S., Florea, A., Pall, E., Aldea, M., Kacso, G., Cristea, V., Berindan-Neagoe, I., & Irimie, A. (2012). Gold nanoparticlesconjugated with cisplatin/doxorubicin/capecitabine lower the chemoresistance of hepatocellular carcinoma-derived

cancer cells. *Journal of Gastrointestinal and Liver Diseases. 21,* 187-196.

[5.10]   Song, J., Zhou, J. & Duan, H. (2012). Self assembled plasmonic vesicles of SERS-encoded Amphiphilic gold nanoparticles for cancer cell targeting and traceable intracellular drug delivery. *Journal of American Chemical Society. 134,* 13458-13479.

[5.11]   Alexiou, C., Arnold, W., Klein, R. J., Parak, F. G., Hulin, P., Bergemann, C., Erhardt, W., Wagenpfeil, S., & Lube, A. S. (2000). Locoregional cancer treatment with magnetic drug targeting. *Cancer Research. 60,* 6641-6648.

[5.12]   Mulvey, J. J., Villa, C. H., McDevitt, M. R., Escorcia, F. E., Casey, E. & Scheinberg, D. A. (2013). Self-assembly of carbon nanotubes and antibodies on tumors for targeted amplified delivery. *Nature Nanotechnology 8,* 763-771.

[5.13]   Kim, M., Seo, J. H., Jeon, W. I., Kim, M.-Y., Cho, K., Lee, S. Y. & Joo S.-W. (2012). Real time monitoring of anticancer drug release *in vitro* and *in vivo* on totania nanoparticles triggered by external glutathione. *Talanta. 88,* 631-637.

187

[5.14]   Bhattacharya, R.; & Mukherjee, P. (2008). Biological properties of nacked metal nanoparticles. *Advanced drug Delivery review. 60,* 1289-1306.

[5.15]   Everts, M., Saini, V., Leddon, J., L., Kok, R. J., Stoff-Khalili, M., Preuss, M. A., Millican, C. L., Perkins, G., Brown, J. M., Bagaria, H., Nikles, D. E., Johnson, D.T., Zharov, V. P. & Curiel, D. T. (2006). Covalently linked gold nanoparticles to a viral vector: potential for combined photothermal and gene cancer therapy. *Nano Letters. 6,* 587-591.

[5.16]   Cheng, M. M.-C., Cuda, G., Bunimovich, Y. L., Gaspari, M., Heath, J. R., Hill, H. D., Mirkin, C. A., Nijdam, A. J., Terraciano, R., Thundat, T. & Ferrari, M. (2006). Nanotechnologies for biomolecular detection and medical diagnostics. *Current Opininion in Chemical Biology. 10,* 11-19.

[5.17]   Heo, D. N., Yang, D. H., Moon, H. J., Lee, J. B., Bae, M. S., Lee, S. C., Lee, W. J., Sun, I.- C. & Kwon, I. K. (2012). Gold nanoparticles surface-functionalized with paclitaxel drug and biotin receptor as theranostic agents for cancer therapy. *Biomaterials.33,* 856-866.

188

[5.18]   Azmi, B. (2011). Potential efficacy of cell penetrating peptides for nucleic acid and drug delivery. *Biochimica et Biophysica Acta. 1816,* 232-246.

[5.19]   Nguyen, C., T., Nguyen, J., T, Rutledge, S., Zhang, J., Wang, Chen & Walker G.,C. (2010). Detection of chronic lymphocytic leukemia cell surface markers using surface enhanced Raman scattering gold nanoparticles.*Cancer Letters. 292*, 91 -97.

[5.20]   Lee, C., J.,   Kang, J., S., Kim, M., S., Kwang, P., L. & Lee, M.m S. (2004). The study of doxorubicin and its complex with DNA by SERS UV-resonance Raman Spectroscopy. nanoparticles. *Bulletin of Korean Chemical Society. 25*, 1211 -1216.

Chapter 6

Conclusion and Recommendations

6.1. Conclusions

For increasing capture efficiency and detection of CTCs many recent report recommended for improved CTC isolation and detection technique, in order to analyze cancer prognosis. Since the number of CTCs is very few in blood, therefore, it is very difficult to efficient isolation of CTCs from blood. Thus for efficient isolation, various charcateristics of CTCs should be taken in consideration. In my op inion both size based filtration and affinity based isolation can improve the capture efficiency, but as much as more surface marker should be targeted for achieving the best result.

Since the fluorescence microscopy has photobleaching property, and fluorescent spectra overlap during addressing of multiple cell surface receptors, in that case Raman spectroscopy may overcome the limitations of fluorescence microscopy. Nanoparticle based surface-enhanced Raman spectroscopic tags are resistant to photobleaching, and can be applied to label

190

the multiple cell surface receptors simultaneously without affecting each other. In chapter 2, I introduced multifunctional Raman hybrid nanoparticles, that can efficiently isolate the CTCs from blood with improved capture efficiency, and that can be successfully used for *in situ* expression analysis of the surface markers.

Since the stem-like CTCs are the basic cause of cancer metastasis, chemoresistance and recurrence of the disease, therefore their isolation, characterization and distinguishing is very important. Since the rnumbers of SCTCs are extremely low in the blood, therefore capturing of the SCTCs using multiple antibody may be a unique method of SCTCs detection. Furthermore, due to limitation of fluorescence microscopy for multiplex labelling of cells, SERS may be the best alternative for distinguishing SCTCs from CTCs. In chapter 3 I successfully distinguished SCTCs from the CTCS based on their surface marker expression level using SERS technique. Multifunctional SNTs were fabricated for multiplex labelling of the SCTCs and CTCs. By using the multifunctional SNTs the SCTCs and the CTCs were captured successfully and different surface marker expression level were detected simultaneously. Therefore, this newly developed technique may be a promising tool for efficient capturing and accurate in situ

191

analysis of the espression level of the the SCTCs and CTCs, and distinguishing them based on it. It can also be applied for multiple labelling of many targeted surface proteins of any cells at a time.

The miRNA are the emerging biomarkers of many diseases including cancers. In chapter 4, I introduced synthesis of a new hybrid nanoparticle (MiNPs), which consist of AuNPs, 4- MBA and complementary half miR200c that can be applied for *in situ* analysis of miR200c expression without affecting cellular viability. Among the three kinds of cells SK-BR-3 expresses highest quantity of miR200c, MCF-7 moderate and breast SCC express least quantity. We studied doxorubicin's cytotoxicity to three cell lines. Among them SK-BR-3 cells show highest cytotoxixity, MCF-7 moderate and breast SCC lowest. This result indicates that, miR200c expression is directly proportional to the doxorubicin's cytotoxicity.

In case of chemotherapy, targeted drug delivery is important to keep the healthy cells unaffected. In chapter 5, I synthesized a biohybrid conjugated nanoparticle (B-HNP) which is efficient in specific targeting and increase in uptaking by the cells. The increased uptaking was due to immobilization of CPP to the AuNPs, and specific targeting was due to immobilization of the marker specific antibody. As a result of increased uptaking, cell cytotoxicity

192

was also increased. By using the biohybrid nanoparticles I successfully monitored the release of doxorubicin anticancer drug from AuNPs surfaces inside targeted cells with SERS method. Our newly developed conjugated nanopaticles can be used for specific targeting to any cells for targeted therapy, and can be used for monitoring of release behavior of any SERS active drug molecules inside living cells.

6.1.1. Characterization of Breast CTCs

Multifunctional Raman hybrid nanoparticles (R-HNPs) can efficiently isolate the CTCs from blood with improved capture efficiency, and that can be successfully used for *in situ* expression analysis of the surface markers.

6.1.2. Distinguishing Breast SCTCs from Breast CTCs

Multifunctional SERS nanotags (SNTs) can successfully distinguish breast SCTCs from CTCs based on expression analysis of the surface markers

6.1.3. Detection of Intracellular Biomarker

MicroRNA modidied hybrid nanoparticles MiNPs) can successfully detect the expression of intracellular biomarker miR200c.

193

6.1.4. Targeted Drug Delivery

Anticancer drug modified biohybrid nanoparticles (B-HNPs) can successfully target the cancer cells and can improve uptaking efficiency, and can successfully work in monitoring of time dependent drug release

6.2.   Perspective and Recommendation for Further Study

6.2.1.   Targetting the Stem-like Cancer Cells

Nowadays cancer has become a common disease and a first or second most common cause of death worldwide. Despite the better understanding of the biology of cancer cells, eradication of cancer is stiil challenging. There has been increasing evidence that, cancer cells are heterogenous with respect to proliferation and differentiation. In several malignancies the initiation capacity and maintenance of cancer growth reside in a small population of cells, known as stem like cancer cells (SCCs). Stem-like circulating tumor cells (SCTCs) are a subpopulation of CTCs shares certain properties similar to normal stem cells. In recent years Stem like cancer cells (SCCs) hypothesis has attracted great attention the field of cancer biology. According to the concept, tumor consists of tumorigenic and non-

194

tumorigenic cells. The tumorigenic cells termed SCCs or tumor initiating cells (TICs), is able to self renew, and generate differentiated progenies to organige a hierarchial cell system in asimilar fashion to normal stem cells (Figure 6.1) [6.1]. Due to their stemness, the SCCs lead to the generation of more SCCs and ability to differentiate a varirty of cells that are found in malignancy. Additionally there is increasing evidence that SCCs pose a threat in the form of invasion that is resistant to current chemotherapy or radiotherapy. Furthermore, they could play a crucial role in distant metstasis.To increase the therapeutic efficacy targeting of SCCs are important. Hence, it is important to characterize the SCCs and distinguish them from tumor cells or CTCs.

Understanding the SCCs origin, molecular profile, and interaction with their microenvironment, these could be a paradigm shift in treatment of cancer.

6.2.2. Combined Targeted Chemotherapy and Photothermal Therapy

Targeted drug delivery is very important in chemotherapy in order to increase therapeutic efficacy and to keep the healthy cells unaffected. In last few years scientists applied many approaches for efficient drug delivery. But
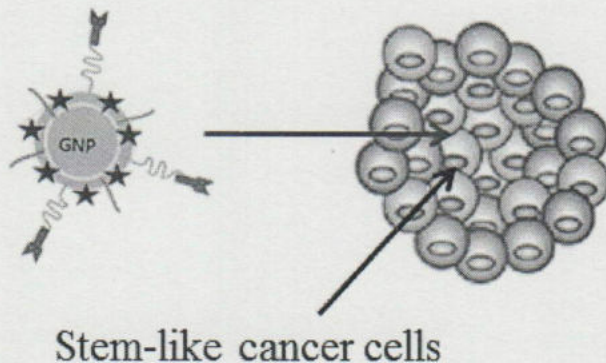
195

Stem-like cancer cells

Figure 6.1. Conjugated nanoparticles for targeted delivery to the stem-like cancer cells.

nanoparticles based delivery has extra benefit because, they are actively uptaken by the cells through endocytosis, and the nanoparticles can be used for photothermal therapy. By using the biohybrid nanoparticles it is possible to successfully deliver anticancer drug to the target organ.
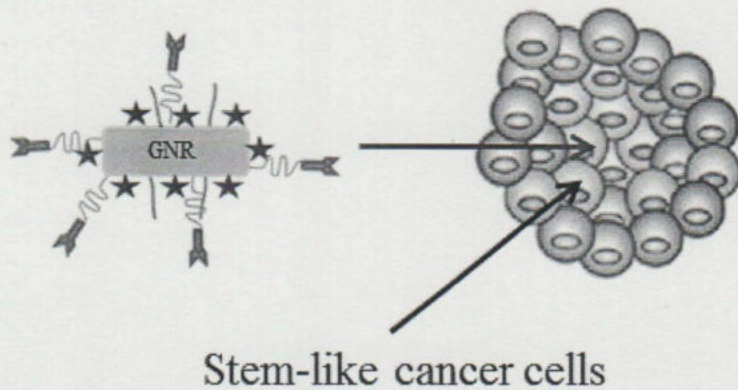
Stem-like cancer cells

Figure 6.2. Conjugated nanoparticles for combined targeted chemotherapy and photothermal therapy to the stem-like cancer cells.

6.3. References

[6.1]   Das, S., Srikanth, M. & Kessler, J., A. (2008). Cancer stem cells and glioma. *Nature Clical Practice Neurology. 4,* 427-435.

Vita

Biographical Data

Name   : Md. Khaled Hossain

Date of Birth   : 24 July, 1973

Place of Birth   : Nilphamari, Bangladesh.

Address   : Interdisciplinary Program of Integrated Biotechnology, Sogang University, Seoul, Korea.

Educational Background

1994~1998   : DVM from Bangladesh Agricultural University

1999~2000   : M.S. in Microbiology, Department of Microbiology and Hygiene, Bangladesh Agricultural University, Mymensingh.

2011~Present : Ph. D., Interdisciplinary Program of Integrated Biotechnology, Sogang University, Seoul, Korea.

Professioinal Experience

2000~2003   : Veterinary Surgeon, Department of Livestock Services, Bangladesh.

2003~2004   : Lecturer, Department of Microbiology, Dinajpur Govt. Veterinary College, Dinajpur, Bangladesh.

2004~2008   : Assistant Professor, Department of Microbiology, Dinajpur Govt. Veterinary College, Dinajpur, Bangladesh.

2008~2012   : Assistant Professor, Department of Microbiology, Hajee Mohammad Danesh Sci. & Tech. Univ., Dinajpur, Bangladesh.

2012~to date : Associate Professor, Department of Microbiology, Hajee Mohammad Danesh Sci. & Tech. Univ., Dinajpur, Bangladesh.

Achievements

List of Publications

1. **Md. Khaled Hossain**, Hyeon-Yeol Cho, and Jeong-Woo Choi, 'Gold nanopatterned substrate for characterization and distinguishing of breast cancer cell subtypes based on SERS', *Journal of Nanoscience and Nanotechnology, Submitted.*

2. **Md. Khaled Hossain**, Hyeon-Yeol Cho, Kyeon-Jun Kim and Jeong-Woo Choi, 'Silver Nanostar Patterned Substrate for Label-free Characterization of Breast Cancer Cells based on Surface-Enhanced Raman Spectroscopy'. *Science of Advanced Materials, Accepted.*

3. **Md. Khaled Hossain**, Hyeon-Yeol Cho, and Jeong-Woo Choi, 'Efficient Isolation and *In-situ* Characterization of Circulating Tumor Cells using Hybrid Nanoparticles based on Surface-Enhanced Raman Spectroscopy'. *In preparation.*

4. **Md. Khaled Hossain**, Hyeon-Yeol Cho, and Jeong-Woo Choi,

'Distinguishing Breast Stem-like Cancer Cells from Breast Circulating Tumor Cells based on Surface-Enhanced Raman Spectroscopy'. *In preparation.*

5. **Md. Khaled Hossain**, Kyeong-Jun Kim, Hyeon-Yeol Cho, and Jeong-Woo Choi, 'Detection of miR200c Expression in Breast Cancer Cells and Breast Stem-like Cancer Cells based on Surface -Enhanced Raman Spectroscopy'. *In preparation.*

6. **Md. Khaled Hossain**, Hyeon-Yeol Cho, and Jeong-Woo Choi, '*In situ* Monitoring of Doxorubicin Release inside Targeted Cancer Cells using Surface-Enhanced-Enhanced Raman Spectroscopy'. *In preparation.*